

POLITECNICO DI MILANO

Scuola di Ingegneria Civile, Ambientale e Territoriale
Corso di Laurea in Ingegneria Civile – Indirizzo New Structures



**NUMERICAL MODELLING VS ON-SITE
TESTING OF AN ARCH-SUSPENDED
FOOTBRIDGE**

Supervisor:

Prof.ssa Maria Gabriella MULAS

Co-Supervisor:

Prof.ssa Anna BANAS

Gdansk University Of Technology Poland

Tesi di Laurea Magistrale di

Nunzio Marrone

94520

Academic Year 2021/2022

INDEX

INDEX OF FIGURES	IX
INDEX OF TABLES	XV
INTRODUCTION	XX
1 Human induced Vibration	1
1.1 GAIT ANALYSIS	2
1.2 GROUND REACTION FORCES	5
1.3 FORCE MODELLING	10
<i>1.3.1 Deterministic force models.....</i>	<i>10</i>
<i>1.3.2 Probabilistic force models.....</i>	<i>13</i>
<i>1.3.3 Frequency-domain force models.....</i>	<i>14</i>
<i>1.3.4 Vibration of the structure</i>	<i>15</i>
<i>1.3.5 Human -Structure interaction</i>	<i>16</i>
1.4 CASE STUDY: THE SOLFERINO BRIDGE	18
2 THE STRUCTURE AT STUDY	23
2.1 POSITION OF THE STRUCTURE	24

2.2	GEOMETRY AND MATERIAL PROPERTIES	26
2.3	EXPERIMENTAL DATA	32
2.3.1	<i>Static Tests</i>	32
2.3.2	<i>Dynamic Tests</i>	36
2.3.3	<i>Methods to determine Experimental Mode Shapes</i>	38
2.3.4	<i>Data Processing and Modal Identification</i>	40
2.3.5	<i>Results of experimental modal identification</i>	41
3	STRUCTURAL MODELLING.....	43
3.1	ANSYS SOFTWARE	44
3.1.1	<i>Model's element</i>	45
3.2	MODELLING ASSUMPTIONS.....	48
3.3	FIRST MODEL.....	49
3.4	SECOND MODEL.....	56
3.5	THIRD MODEL.....	61
3.6	VALIDATION OF THE MODEL.....	72
4	HIVOSS GUIDELINE	75
4.1	HIVOSS STEP-PROCEDURE.....	76
4.2	EVALUATION OF NATURAL FREQUENCIES	77
4.3	CRITICAL RANGE OF NATURAL FREQUENCIES	77
4.4	ASSESSMENT OF DESIGN SITUATION: TRAFFIC CLASSES AND COMFORT CLASSES	78
4.5	ASSESSMENT OF STRUCTURAL DAMPING.....	79
4.6	DETERMINATION OF MAXIMUM ACCELERATION	80
4.7	HARMONIC LOAD MODEL.....	81
4.8	APPLICATION OF THE LOAD MODEL.....	82
4.9	CHECK OF CRITERIA FOR LOCK-IN.....	84
4.10	CHECK OF COMFORT LEVEL	85
5	DYNAMIC ANALYSES	86
5.1	RUNNING PEDESTRIAN INDUCED LOAD.....	87
5.2	REALRUN1	89
5.3	SETRA MODELING FOR RUNNING PEDESTRIAN	91
5.4	WALKING PEDESTRIANS' ANALYSIS: HIVOSS.....	95
5.4.1	<i>Harmonic analysis for walking pedestrians: results</i>	98

5.5	RUNNING PEDESTRIAN' ANALYSIS: HIVOSS	103
5.5.1	<i>Harmonic analysis for running pedestrian: results</i>	104
5.6	RUNNING HUMAN'S ANALYSIS: REALRUN1.....	106
5.6.1	<i>Transient analysis: Setra sinus model results</i>	107
5.6.2	<i>Transient analysis: Setra Fourier model results</i>	110
5.6.3	<i>Transient analysis: Sinus model results for 6 pedestrians</i>	113
6	CONCLUSIONS	116
	BIBLIOGRAPHY	119
	APPENDIX A	125
	APPENDIX B	130
	SAMPLE OF ONE ANSYS INPUT FILE	131

INDEX OF FIGURES

Figure 1.1: Gate Cycle phases [12].....	4
Figure 1.2: Sub-phases [13].....	4
Figure 1.3: Space parameters [14]	5
Figure 1.4,Representation of Ground Reaction Forces: a) Medial-Lateral, b) Anterior Posterior and c) Vertical components [15]	6
Figure 1.5: Plate measurements of GRFs [3].....	7
Figure 1.6: Relationship of a) time of support and b) time of swing with walking velocity [3].....	7
Figure 1.7:Vertical component of GRF for males and females as a function of velocity and normalized with respect to body weight [4].....	8
Figure 1.8: Vertical components of GRFs for both feet and two different velocities [16].....	9
Figure 1.9: Normalized distributions of DLFs up to the third harmonic [17]	13
Figure 1.10: Mass-Spring-Damper model to model human structure interaction [21]	16
Figure 1.11: Millennium Bridge	18
Figure 1.12: Solferino Bridge	19
Figure 1.13: Solferino Bridge's cross-section	19

Figure 1.14: Solferino Bridge's cross-section scheme [2]	20
Figure 1.15: Tuned Mass Damper Scheme.....	21
Figure 1.16 Acceleration response of the Solferino Footbridge during testing: a) low walk speed; b) higher walk speed. [29]	21
Figure 2.1: Position of the footbridge in red.....	24
Figure 2.2: Above: footbridge overpassing University Route in Bydgoszcz; below: lateral view with overall dimensions. [5].....	25
Figure 2.3: Deck cross-section.....	26
Figure 2.4: Development of the arch	27
Figure 2.5: Arch cross-section	27
Figure 2.6: Geometry of the concrete blocks B1 and B2.....	28
Figure 2.7: Rod-arch anchoring	29
Figure 2.8: Rode-deck anchoring.....	29
Figure 2.9: Geometry and relevant points of the footbridge on x-z plane.....	31
Figure 2.10: Geometry and relevant points of the footbridge on x-y plane.....	31
Figure 2.11: Plan view highlighting in green section 1-1 and 3-3.....	33
Figure 2.12: Measurement points for displacement (green), acceleration (pink), support settlement (blue)	34
Figure 2.13: Position of the water containers.	34
Figure 2.14: Comparison between theoretical (blue) and experimental (red) displacements.....	35
Figure 2.15: Dynamic tests a) walk b) run c) jump [5].....	38
Figure 2.16: Quantum HBM 840a	38
Figure 2.17:Dynamic measurement scheme [5]	38
Figure 2.18: FRFs used in PP method [5].....	39
Figure 2.19: Time history of acceleration and normalized FFT amplitude for the arch footbridge above the University Route in Bydgoszcz at point a1z excited by (a) synchronous run of a group of nine persons, (b) impulse. [5]	40

Figure 2.20: Modal shape obtained from the experimental the experimental campaign: a) Vertical Modal shape; b) Vertical Modal Shape; c) Torsional Modal Shape; d) Vertical Modal Shape.	42
Figure 3.1: BEAM188 Geometry [36].....	45
Figure 3.2: LINK180 Geometry [36].....	46
Figure 3.3: SHELL181 Geometry [36].....	46
Figure 3.4: MPC184 Geometry [36].....	47
Figure 3.5: SOLID185 Geometry [36]	47
Figure 3.6: COMBIN14 Geometry [36]	48
Figure 3.7: Deck cross-section.....	50
Figure 3.8: Steel arch cross-section	50
Figure 3.9: ANSYS model.....	51
Figure 3.10: ANSYS FEM model with the real shapes of the elements	51
Figure 3.11: Reinforced concrete material model	52
Figure 3.12: Steel material model.....	52
Figure 3.13: Comparison of modal shapes (field test—blue; FEM third model—orange)	56
Figure 3.14: Ansys Second Model.....	57
Figure 3.15: ANSYS FEM Second Model with the real shapes of the elements.	57
Figure 3.16: Discretization of the deck cross-section in the second model.....	57
Figure 3.17: Comparison of modal shapes (field test—blue; FEM third model—orange)	61
Figure 3.18: Vertical constraints positioning.....	62
Figure 3.19: Angles of the hanger in space system	62
Figure 3.20: Generation of pile stiffness k in coordinate direction [38].....	64
Figure 3.21: Stiffness and damping parameters of vertical response [38].....	65
Figure 3.22: Ansys Third Model.....	67
Figure 3.23: ANSYS FEM Third Model with the real shapes of the elements	67

Figure 3.24: Comparison of modal shapes (field test—blue; FEM third model—orange).	74
Figure 4.1 Design steps according to HiVoSS guidelines [7]	76
Figure 4.2 Traffic classes defined in HiVoSS, depending on pedestrians' density [7]	78
Figure 4.3: Comfort classes depending on the maximum acceleration [7]	79
Figure 4.4: Values of structural damping proposed by HiVoSS [7].....	80
Figure 4.5: 1 Proposed methods for the computation of maximum acceleration [7]	80
Figure 4.6: The equivalent number of synchronized pedestrians n' is a part of the total number of pedestrians n on the loaded surface [7].....	81
Figure 4.7: Example of load application for the walking pedestrians load case [7]..	83
Figure 4.8: Graphics for the computation of the Ψ reduction coefficient [7].....	83
Figure 4.9: Graphic for the computation of the Ψ reduction coefficient for the running pedestrians load case [7].....	84
Figure 5.1: Time history of GRF vertical component for a walking pedestrian [40]	87
Figure 5.2: Vertical components of GRFs for both feet and two different gaits [41]. On the left the case of the running pedestrian: no double support phase and no more M shape of the load.....	88
Figure 5.3: Graphical representations of the role of shape functions: the vertical load induced from the pedestrian is transformed into nodal forces and bending moments [39].....	90
Figure 5.4: Flow-chart for the generation of RealRun1 [39].....	90
Figure 5.5: Change in the period of contact according to frequency [6]	92
Figure 5.6: Running: impact factor according to the relative period of contact [6] ..	92
Figure 5.7: Time history of the running pedestrian induced load according to the SETRA sinus load model using a mass of 81.5 Kg, a running speed of 2.2 m/s. ²	93
Figure 5.8: Amplitude of the various harmonics [6]	94
Figure 5.9: Time history of the running pedestrian induced load according to the SETRA Fourier series load model	94

Figure 5.10: Analysed modal shape of the footbridge in a); applied distributed load for the case of the walking pedestrians in accordance with modal shape displacement b). 98

Figure 5.11: Position of nodes for which results have been extracted and reported here..... 100

Figure 5.12: Resonance curves of a) amplitude, b) real part and c) imaginary part of vertical displacements for node 2 (x=10 m) for the case of walking pedestrians at a frequency $f=2.3$ Hz. 100

Figure 5.13: Vertical accelerations at selected nodes along the footbridge for TC1 102

Figure 5.14: Vertical accelerations at selected nodes along the footbridge for TC2 102

Figure 5.15: Resonance curves of a) amplitude, b) real part and c) imaginary part of vertical displacements for node 2 (x=10m) for the case of running pedestrian..... 104

Figure 5.16: Vertical acceleration at selected nodes along the footbridge 105

Figure 5.17: Vertical acceleration at selected nodes along the footbridge for transient analysis..... 108

Figure 5.18: Vertical acceleration m/s^2 of node 1-bis (left) and of node 2 (right) during time 0-24s 109

Figure 5.19: Vertical acceleration m/s^2 of node 3 (left) and 4 (right) during time 0-24s 109

Figure 5.20: Vertical acceleration m/s^2 of node 5 (left) and 6 (right) during time 0-24s 109

Figure 5.21: Vertical acceleration m/s^2 of node 7 (left) and 8 (right) during time 0-24s 110

Figure 5.22: Vertical acceleration at selected nodes along the footbridge for transient analysis of 6 running pedestriana..... 111

Figure 5.23: Vertical acceleration m/s^2 of node 1-bis (left) and 2 (right) during time 0-24s..... 112

Figure 5.24: Vertical acceleration m/s^2 of node 3 (left) and 4 (right) during time 0-24s..... 112

Figure 5.25: Vertical acceleration m/s^2 of node 5 (left) and 6 (right) during time 0-24s..... 112

Figure 5.26: Vertical acceleration m/s^2 of node 7 (left) and 8 (right) during time 0-24s..... 112

Figure 5.27: Vertical acceleration m/s^2 of node 1-bis (left) and 2 (right) during time 0-24s..... 114

Figure 5.28: Vertical acceleration m/s^2 of node 3 (left) and 4 (right) during time 0-24s..... 114

Figure 5.29: Vertical acceleration m/s^2 of node 5 (left) and 6 (right) during time 0-24s..... 115

Figure 5.30: Vertical acceleration m/s^2 of node 7 (left) and 8 (right) during time 0-24s..... 115

INDEX OF TABLES

Table 1.1: DLFs for single person force models after different authors.....	12
Table 1.2: Comparison between calculated and identified frequencies in different conditions [29]	22
Table 2.1: WGS84 coordinate of the footbridge.....	24
Table 2.2: Properties of the concrete	26
Table 2.3: Properties of the steel	27
Table 2.4: Properties of the materials for concrete blocks	28
Table 2.5: Galvanized steel.....	29
Table 2.6: Relevant points of the arch	30
Table 2.7: Relevant points of the deck	31
Table 2.8 maximum accelerations recorded during the tests [5]	37
Table 2.9: Experimental modal shape obtained with vibration inductor	41
Table 2.10: Experimental modal shape obtained with impulse caused by container impact.....	41
Table 2.11:Frequancies of the experimental modal shape.....	42
Table 3.1: Modal Shapes of first model results with Lanczos method.....	52

Table 3.2: Correlation between experimental and FEM model modal parameters of the Footbridge	56
Table 3.3: Modal Shapes of second model result with Lanczos method.....	58
Table 3.4: Correlation between experimental and FEM model modal parameters of the Footbridge	60
Table 3.5: Reaction force of the roller constraints F_z , axial component in the hanger N and Uniform Thermal Loads ΔT	63
Table 3.6: Stiffness and damping parameters for horizontal response of pile for homogenous soil profile and parabolic soil profile [38].....	66
Table 3.7: Values of the spring for pile-soil interaction	66
Table 3.8: Modal Shapes of third model result with Lanczos method	67
Table 3.9: Correlation between experimental and FEM model modal parameters of the Footbridge	71
Table 3.10: Correlation between experimental and third FEM model modal parameters of the Footbridge	73
Table 5.1: Parameters for the computation of the modulus of the distributed load according to Hivoss guidelines for the case of walking pedestrians TC1.	96
Table 5.2: Parameters for the computation of the modulus of the distributed load according to Hivoss guidelines for the case of walking pedestrians TC2.	97
Table 5.3: Max displacement and acceleration at selected nodes for TC1	101
Table 5.4: Max displacement and acceleration at selected nodes for TC2.....	101
Table 5.5: Parameters for the computation of the modulus of the concentrated load according to Hivoss guidelines for the case of ne running pedestrian.....	104
Table 5.6: Max displacements and accelerations at selected nodes	105
Table 5.7: First contact point between the running pedestrian and the footbridge..	106
Table 5.8: Values of Newmark’s parameters.....	107
Table 5.9: Max displacement and acceleration at selected nodes.....	107
Table 5.10: Max displacement and acceleration on selected nodes.....	110

Table 5.11: Numerical values of vertical displacement and acceleration on selected points.....	113
Table 5.12: Experimental extreme values of acceleration [m/s ²] for walking and running pedestrians [5]	113

ABSTRACT

This thesis analyses the dynamic behaviour of a footbridge under the action of walking and running pedestrians. The arch-suspended footbridge (located in Bydgoszcz, Poland) is 32m long, with a not uniform spacing of the hangers, leaving a free span of 10m at one of the two sides. The footbridge was the object of a previous experimental campaign, leading to the identification of modal properties and to measuring the response to moving pedestrians and other types of loads. The first objective of this thesis was the development of a finite element (FE) model of the footbridge built within the framework of ANSYS APDL code. With a process of model updating, the final model is able to simulate the identified natural frequencies with an error lower than 5%. Modal shape correlation, in terms of MAC index, produces excellent results. As a second step, the FE model validated against the experimental results has been adopted to simulate the footbridge response to both static and dynamic load conditions. Vibration response was recorded under various conditions, including human-induced load, impulse load, and vibration exciter-induced excitations.

From the numerical point of view, in this thesis a successful simulation was performed for static tests. The assessment of serviceability conditions under walking pedestrian was performed according Hivoss guidelines, for the two lower traffic classes TC1 and TC2, since one of the natural frequencies of the footbridge falls within the critical range. The results show an exceedance of comfort limits restricted to the 10m long span. Moreover, given the availability of tests with running pedestrians, a transient analysis was performed adopting SETRA modelling. Two cases are considered, for one and six running pedestrians. The second case produces a very high level of vibration, due to the perfect synchronization of runners adopted in the analysis. Both analyses point out the critical response of the 10m long span.

SOMMARIO

Questa tesi analizza il comportamento dinamico di una passerella sotto l'azione di pedoni che camminano e corrono. La passerella (situata a Bydgoszcz, Polonia) è lunga 32 m, con una spaziatura non uniforme dei tiranti, lasciando una luce di 10 m su uno dei due lati. La passerella in esame è stata oggetto di una precedente campagna sperimentale, che ha portato all'identificazione delle proprietà modali e alla misurazione della risposta per pedoni in movimento e altri tipi di carichi. Il primo obiettivo di questa tesi è stato lo sviluppo di un modello agli elementi finiti (FE) nell'ambito del codice ANSYS APDL. Il modello finale, tramite una serie di aggiornamenti, è in grado di simulare le frequenze naturali individuate con un errore inferiore al 5%. La correlazione della forma modale, in termini di indice MAC, produce ottimi risultati.

In una seconda fase, il modello FE validato rispetto ai risultati sperimentali è stato adottato per simulare la risposta della passerella a condizioni di carico sia statiche che dinamiche. La risposta alle vibrazioni è stata registrata in varie condizioni, tra cui il carico indotto dall'uomo, il carico impulsivo e le eccitazioni indotte dall'eccitatore di vibrazioni.

Dal punto di vista numerico, in questa tesi è stata eseguita con successo una simulazione per prove statiche. La valutazione delle condizioni di comfort per le interazioni con i pedoni è stata eseguita secondo le linee guida Hivoss, per le due classi di traffico inferiori TC1 e TC2, in quanto una delle frequenze naturali della passerella rientra nell'intervallo critico. I risultati mostrano un superamento dei limiti di comfort con particolare riferimento alla campata di 10 m. Inoltre, data la presenza di test con pedoni in corsa, è stata eseguita un'analisi transitoria adottando la modellazione SETRA. Vengono considerati due casi il primo con un pedone e il secondo con sei. Si nota che nel secondo caso si genera un livello di vibrazione molto elevato, dovuto alla perfetta sincronizzazione dei pedoni adottata nell'analisi. Entrambe le analisi evidenziano la risposta critica della campata lunga 10 m.

INTRODUCTION

This thesis analyses the dynamic behaviour of an arch-suspended footbridge under the action of walking and running pedestrians. All along the second half of the last century, the search for new architectural solutions in the civil engineering field brought to the construction of increasingly slender structures. Footbridges, due to their environmental impact, have been the object of this evolution, which today are able to cover high span. The scientific community begin to raise concerns about the issue after the well-known cases of the Millennium Bridge [1] in London and of Passerelle Solférino [2] in Paris, driven by the aim to prevent or anticipate the need for vibration control measures that could account for a significant portion of the overall construction budget. In conditions of high pedestrian traffic, these two footbridges have highlighted excessive vibrations leading the scientific community to investigate the phenomenon of pedestrian-structure interaction. The high complexity of these studies is given by a gait that varies in time and space. Moreover, the mechanics of human gait is such that two steps, even consecutive ones, are not identically repeated. In order to develop models to characterize the human-induced loads, the academic community of civil engineering explored the field of biomechanics [3] [4]. Thanks to these studies, several mathematical models of Ground Reaction Forces (GRFs) have been proposed for the application in the civil engineering field. Deterministic and stochastic models were proposed to reproduce in the more accurate possible way the gait cycle. Moreover, the problem requires also the precise determination of the structure's properties. Mass, stiffness and, above all, damping characteristics highly affect the structure response this is because they play a role in the determination of natural frequencies of the structure.

The objective of this Master thesis is to study a 32 m length arch-suspended footbridge, with a not uniform spacing of the hangers, leaving a free span of 10m at one of the two sides. Experimental data [5] are given in order to implement a FE model that is strictly related to the experimental modal shapes and to evaluate several analyses for walking and running pedestrians load case. The FE model is validated against the experimental results and adopted to analyse the footbridge response to walking and running pedestrians, according to Hyvoss [6].and SETRA [7] prescriptions.

This Master thesis is subdivided according to the following scheme:

- CHAPTER 1: describes the physics underlying the issue of vibrations caused by people. Then, referencing the most recent research, all factors and phenomena that contributed to the development of the vibrations problem are explored. The reader encounters the following information in the following order: a description of the characteristics of human-induced loads and their mathematical modelling, a description of the key structural factors influencing the dynamic response to this type of loads, a description of the human-induced load models, and a description of potential effects of human-structure interaction. The essential works in the subject of gait analysis are then introduced, including descriptions of the Millennium Bridge and of the Passerelle Solférino case studies.
- CHAPTER 2 presents the footbridge at study. Key aspects as the geometry and materials properties provided and all the dynamic and static stests performed in the experimental campaign that led to experimental modal shapes.
- CHAPTER 3 describes the procedure for the creation of the FE model using the Ansys Mechanical APDL software, the assumptions at the base of modelling and the model updating necessary to match the experimental modal shapes.
- CHAPTER 4 presents the HiVoSS [6] guidelines for design and check of footbridges during the design phase.

- CHAPTER 5 first describes the outcomes of employing the HiVoSS prescriptions, the models of walking and running pedestrians suggested by SETRA [7] and the adoption of these mathematical model in a Matlab code. The Matlab code that generates a text file readable by Ansys is briefly described. After two analyses for a single pedestrian, the Matlab code is implemented for 6 synchronized running pedestrians.
- CHAPTER 6 contains the main conclusions drawn from the work.

1 Human induced Vibration

Chapter 1 is referred to the description of human induced vibrations. Before presenting analysis of the structure object of the work, the physics behind the problem of human induced vibration is described. Thus, in this chapter, after the description all the components and phenomena that contribute to create the vibration problem such as human-induced loads, structure characteristics and human-structure interaction effects, a study case is presented.

1.1 Gait analysis

When a pedestrian is in movement, during its normal walking produces dynamic forces. In [8], a design standard substituted by more recent guidelines but fundamental for definitions, dynamic forces are defined as “forces varying so quickly that they give rise to vibrations”. As for the vibration source, in the same work, a distinction is made. The vibration source can be inside or outside the building and human excitations are classified as part of the former group. Gait analysis is the branch of biomechanics studying the human motion from the mechanical point of view [9]. In [9] the human motion is analysed in terms of mechanical principles. Minimization of the loss of mechanical energy in the motion of the center of body mass explains why all humans walk in the same way: pelvic rotation, pelvic tilt, knee flexion and plantarflexion and dorsiflexion of the supporting foot have the objective, working all together, to reduce the vertical displacement of the center of mass of the human body. To fully understand the human gait, it is necessary to introduce the following definition: “The gait cycle is the period of time between any two nominally identical events in the walking process” [10]. One important distinction must be done between the term gait and walking. Gait is more general than walking, that only refers to the gait used at low speeds. We refer to gait as a cycle the sum of processes that repeat at each step during human movement. Even if the assumption that all cycles are equal is not always and completely true, it is accepted to make possible analysis of the phenomenon. Moreover, a gait cycle refers to only one side of the body and the assumption of symmetrical behaviour holds true, too. The beginning of the cycle is conventionally chosen as the moment in which one of the two feet hits the ground. A walking gait cycle is divided in two main phases:

Introduction

- *Stance phase*: known as the support or contact phase, it is the moment when the foot is on the ground. It begins when the heel hits the ground and finishes when the toe leaves the ground (62% of the gait cycle).
- *Swing phase*: it represents the interval of time between the end of a stance phase and the beginning of the following (38% of the gait cycle). It denotes the time interval in which the foot does not touch the ground.

Both are fractionated in sub-phases (Figure 1.2): 5 for the stance and 3 for the swing phase. The nomenclature of the sub-phases is defined by Perry et al. [11]. Their names give an idea of what happens, while percentage refers to their normalized duration with respect to the gait duration:

- *Stance*
 1. *Initial contact* (IC 0%);
 2. *Loading response* (LR 0-10%);
 3. *Mid-stance* (MSt 10-30%);
 4. *Terminal stance* (TSt 30-50%);
 5. *Pre-swing* (PSw 50-62%);
- *Swing*
 1. *Initial swing* (ISw 62-70%);
 2. *Mid-swing* (MSw 70-85%);
 3. *Terminal swing* (TSw 85-100%);

Introduction

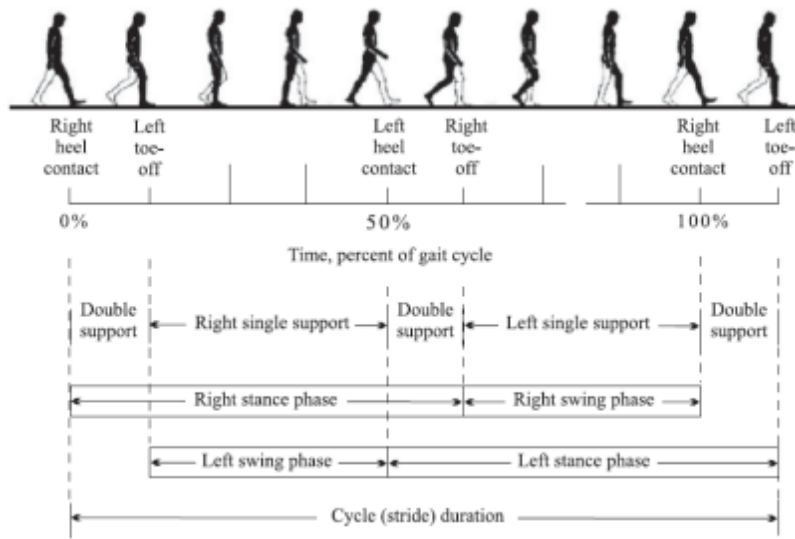


Figure 1.1: Gate Cycle phases [12]

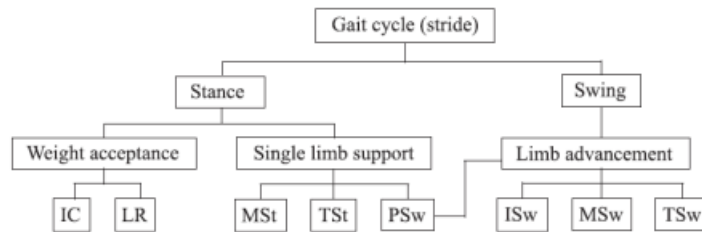


Figure 1.2: Sub-phases [13]

Different parameters exist, related to time and space, characterizing the human gait allowing to make definitions of walking, jogging or running. If the time duration is the interval over which the gait is realized, the stride, or cycle frequency, also known as cadence, is its reciprocal. The walking speed is the distance covered during the time to make a cycle, obtained also as the product of a given stride frequency times the distance. Thus, the walking speed can be modified in two ways: varying the stride frequency or the distance.

Space parameters (Figure 1.3) are:

- *stride length*, the distance measured between a heel strike and the successive in the direction of advancement.

- *step width*, is the distance between the two parallel lines passing through the mid-points of heels in the direction of progression.

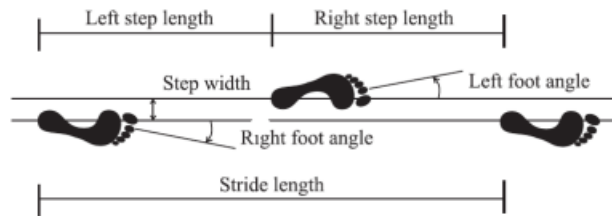


Figure 1.3: Space parameters [14]

1.2 Ground Reaction Forces

Ground reaction forces (GRFs) represent the response of the ground to the loading induced by the movement of humans over a surface. As every kind of forces in space, they have three components: vertical, medial lateral and anterior posterior components (Figure 1.4). During the stance phase, when the foot is in touch with the ground, forces are undoubtedly generated. Five sub-phases of the stance phase have already been identified. The divide is significant for more reasons than only gait analysis, as each of these phases corresponds to a different step of the burden transfer process. The idea of a straightforward human load transfer to the ground can be viewed as an impulse. In practice, the stance phase lasts for less than 1 second. However, even though it may seem counterintuitive, during each sub-phase of the stance the load has a particular way to be transferred. For example, going more in detail in the analysis of the vertical component, right after the heel strike, when “foot and leg act like shock absorbers” [11], the body weight is suddenly transferred to the ground. After this first moment, because of the movement of the other leg, and the consequent variation of the body’s center of mass position, a decrease in the reaction force can be appreciated. Finally, in the heel off phase, at the instant in which the foot start to detach from the ground, a new increase of the reaction appears that reaches its maximum when the heel of the

other foot touches the ground. Then, the force decreases until the entire foot lifts off reporting the reaction to zero. Each of these instants has been characterized by distinct points, also known as force parameters, $(F_i - T_i)$ in force vs. time diagrams. Considering the three components of the force, there are nine points characterizing ground reaction forces, varying as a function of individuals, speed and other boundary conditions.

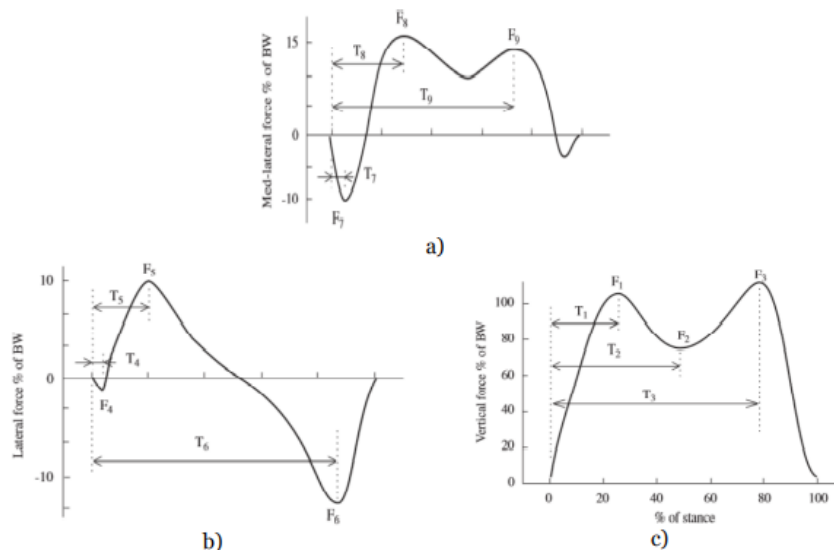


Figure 1.4, Representation of Ground Reaction Forces: a) Medial-Lateral, b) Anterior Posterior and c) Vertical components [15]

One important work was done by Andriacchi et al. [3]. They were the first to measure all the three components of GRFs through a force plate for a single footstep. Looking for indicators of limb diseases in the gait analysis, they analysed 17 normal subjects in two different occasions and 16 subjects with knee pathologies 3 and 6 months after operation. The method of the experiment is rigorously described in the paper. The fundamental results they found are related to the range of variation of the above defined 9 force parameters $(F_i - T_i)$ as a function of the walking speed with simple relationships ($F_1, F_2, F_3, F_4, F_5, F_6, F_7$ vary linearly with velocity). In Figure 1.5 a change of notation with respect to the above definition is noticed.

Introduction

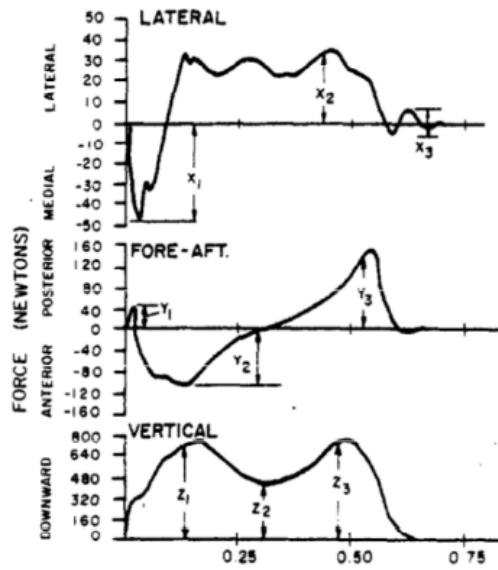


Figure 1.5: Plate measurements of GRFs [3]

In addition, they proved that “time of swing and time of support were found to be inversely proportional to walking speeds... As a subject increased his walking speed, a decrease in both time of swing and time of support was observed” (Figure 1.6)

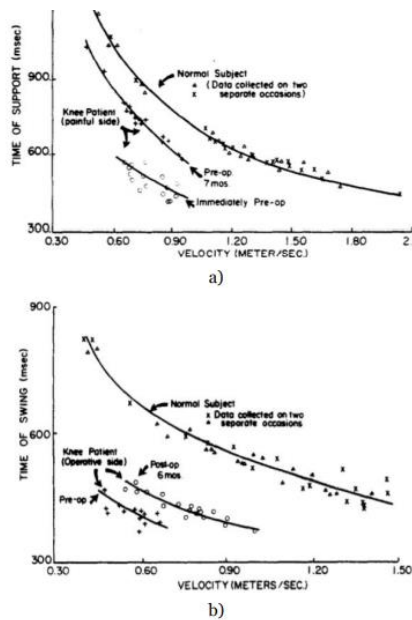


Figure 1.6: Relationship of a) time of support and b) time of swing with walking velocity

[3]

Unfortunately, the disadvantage of this study was that it was limited to a small statistic sample. A larger significant work was done by Keller et al. [4]. Their idea was to study the variation of GRFs amplitude as a function of speed, to answer the questions about the possibility to cause injuries when passing from fast walking to slow jogging and running. They found that, even if small, there is a difference in the vertical component of the GRFs between males and females. They reported their time histories separately for males and females (Figure 1.7).

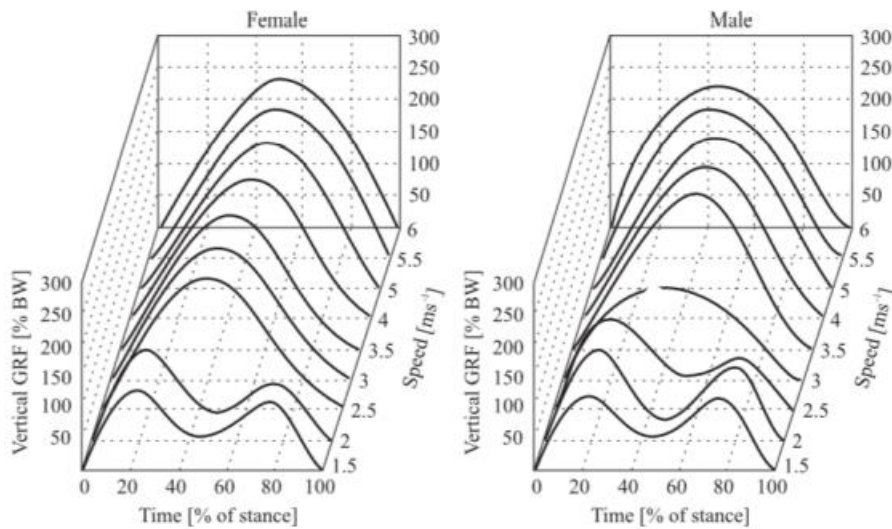


Figure 1.7: Vertical component of GRF for males and females as a function of velocity and normalized with respect to body weight [4]

They derived, through a linear regression, expressions to compute amplitude of peaks as a function of speed in the interval $1.5 < v < 3.5$ m/s:

- Males $F_z = 0.598v + 0.249$
- Females $F_z = 0.631v + 0.159$

For speeds above 3,5 m/s, F_z is approximately constant and equal to 2.5 times the body weight.

The analysis was carried out on GRFs produced during the gait cycle for only one foot. In real gait cycle there is interval, called double support phase, in which both feet are in contact with the ground (20% of entire duration). To evaluate the relationship between the double support phase duration and the gait speed, Galbraith and Barton

Introduction

[16] reported some important test results for three subjects “moving at rates ranging from very slow (sneak) to very fast (run) over three types of surfaces in footwear varying from high heels to stocking feet”. They concluded that no substantial influence was recorded because of the different ground and footwear types. In addition, they drawn two more important conclusions. First, as in the work by Keller et al. [4], they obtained that moving from low speeds to higher values, the vertical component of the GRFs has only one peak instead of two. Second, they measured duration of double support phases and plotted results for one normal walking speed and one running speed, proving that the double support phase has a duration linked to the speed and it does not exist anymore for running speed (Figure 1.8).

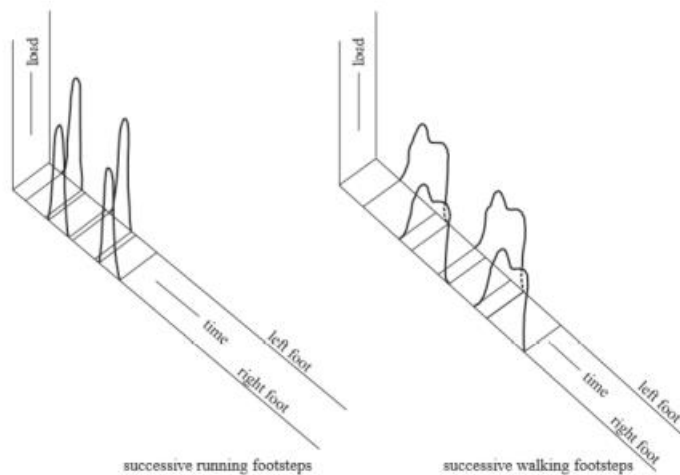


Figure 1.8: Vertical components of GRFs for both feet and two different velocities [16]

1.3 Force modelling

The greatest source of vibration for footbridges is human interaction, hence it is appropriate to model the force created in analytic form. Studies today appear to be less concerned with vibrations created by a single walker than they are with vibrations caused by groups of pedestrians, which are still poorly defined since they are significantly influenced by several difficult-to-generalize phenomena, such as synchronization. [17]. In this paragraph, the models present in literature for the representation of force modelling are mainly divided into two typologies: models in the time domain and models in the frequency domain. Despite the first typology is mostly used, both are rather complex because the forces are variable both in time and space and, depending on numerous parameters, have high randomness.

- *Time-domain force models*: they are based on the assumptions that both feet produce the same effects and repeat periodically. They are classified in:
 1. *Deterministic force models*, whose aim is to try to model each type of human activity in every situation.
 2. *Probabilistic force models*, that consider the great randomness of the whole process and want to model probability distribution functions of random variables influencing it.
- *Frequency-domain force models*, assume that human walking is a narrow-band process.

1.3.1 Deterministic force models

According to the assumption that human induced loads are periodic forces, they can be represented in the time domain by a Fourier series in the following form:

$$F_p(t) = G + \sum_{i=1}^n G \alpha_i (2\pi i f_p t - \varphi_i)$$

Where:

- G is the person's weight [N], usually assumed equal to 700 N;

- α_i are the Fourier's coefficients of the i -th harmonic, usually identified as dynamic load factors (DLFs);
- f_p is the step frequency [Hz];
- φ_i is the phase shift with respect to the i -th harmonic;
- n is the total number of the contributing harmonics.

Given that activity rates are measurable and phase shifts can be determined randomly, the most important parameters are DLFs. It has been found that DLFs depends on the rate activity as well as on the person's velocity and contributing harmonics. Živanović et al. [17] reported results of different authors (Table 1.1).

Table 1.1: DLFs for single person force models after different authors

Autor	DLF	Comment	type of activity and its direction
Blanchard et al.	$\alpha_1 = 0,257$	DFL is lessen for 4 Hz e 5 Hz	Walking-vertical
Bachmann & Ammann	$\alpha_1 = 0,4 - 0,5$ $\alpha_2 = \alpha_3 = 0,1$	Between 2,0 Hz and 2,4 Hz At 2,0 Hz	Walking-vertical
	$\alpha_1 = 0,37 \alpha_2 = 0,10 \alpha_3 = 0,12$ $\alpha_4 = 0,04 \alpha_5 = 0,08$	At 2,0 Hz	Walking-vertical
	$\alpha_1 = 0,39 \alpha_2 = 0,01 \alpha_3 = 0,043$ $\alpha_4 = 0,012 \alpha_5 = 0,015$ $\alpha_{1/2} = 0,37 \alpha_{1/1} = 0,204$ $\alpha_{3/2} = 0,026 \alpha_2 = 0,083$	At 2,0 Hz	Walking-vertical
Schulze	$\alpha_{5/2} = 0,024$	At 2,0 Hz	Walking-vertical
Rainer et al.	$\alpha_1, \alpha_2, \alpha_3$ e α_4	DLF frequency dependent	Walking-vertical
	$\alpha_1 = 0,4/0,5, \alpha_2 = \alpha_3 = 0,1/-$ $\alpha_1 = \alpha_3 = 0,1$ $\alpha_{1/2} = 0,1, \alpha_{1/1} = 0,2, \alpha_2 = 0,1$	Between 2,0 Hz and 2,4 Hz At 2,0 Hz At 2,0 Hz	Walking-vertical Walking-vertical Walking-vertical
Bachmann et al.	$\alpha_1 = 1,6 \alpha_2 = 0,7 \alpha_3 = 0,2$ $\alpha_1 = 0,37(f - 0,95) \leq 0,5$ $\alpha_2 = 0,054 + 0,0044f$ $\alpha_3 = 0,026 + 0,0050f$ $\alpha_4 = 0,010 + 0,0051f$	Between 2,0 Hz and 3,0 Hz	Running-vertical
Young		These are mean values for DLFs	Walking-vertical
	$\alpha_1 = 1,8/1,7, \alpha_2 = 1,3/1,1, \alpha_3 = 0,7/0,5$ $\alpha_1 = 1,9/1,8, \alpha_2 = 1,6/1,3, \alpha_3 = 1,1/0,8$ $\alpha_1 = 0,17/0,38, \alpha_2 = 0,10/0,12 \alpha_3 = 0,04/0,02$ $\alpha_1 = 0,5$	Jumps 2,0/3,0 Hz High Jumps 2,0/3,0 Hz	Vertical-Jump Vertical-Jump
Batchmann et al-		At 1,6/2,4 Hz At 0,06 Hz	Vertical-Jump Swinging
Yaou et al	$\alpha_1 = 0,7, \alpha_2 = 0,25$	Jumping on a flexible platform with n. f. of 2 Hz	Vertical-jump

1.3.2 Probabilistic force models

The probabilistic force models continue to be predicated on the notion that periodic human-induced loads exist. The distinction is that they were created with the intent to mimic the high degree of randomness found in human stride. One important example of force modelling with a probabilistic approach is provided by Živanović et al. [17], to consider DLFs as random variables and represent them through their normalized distribution (Figure 1.9: Normalized distributions of DLFs up to the third harmonic).

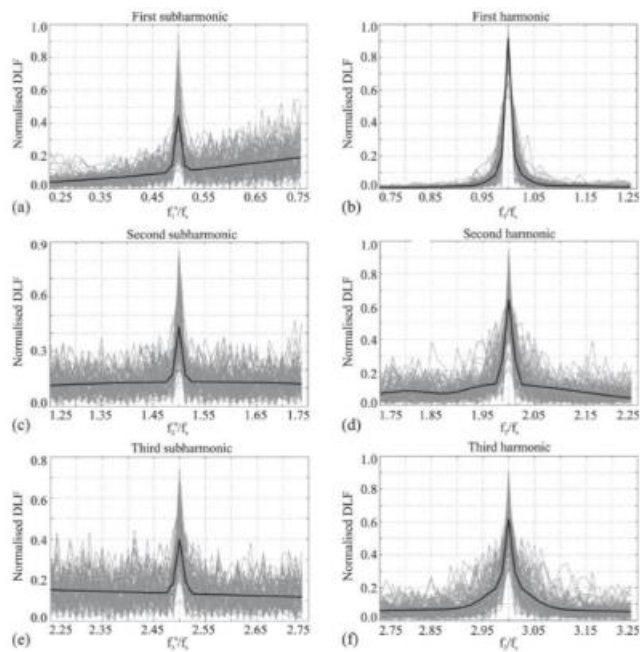


Figure 1.9: Normalized distributions of DLFs up to the third harmonic [17]

1.3.3 Frequency-domain force models

The force model described in the previous paragraph has been developed from the results obtained in the frequency-domain analysis by Brownjohn et al. [18], reached after several studies done in this field opened by Eriksson [19]. He first produced the ASD of a walking force. Brownjohn et al. established a frequency-domain force model to represent a group of imperfect pedestrians with a varying degree of correlation or synchronization. They proposed to estimate the ASD of the structure reaction as follows, using a coherence function, under the presumption that the spatial distribution of this load may be comparable to the wind action:

$$S_x(f) = \psi_x^2 |H(f)| S_{p,1}(f) \int_0^L \int_0^L \psi_{z1} \psi_{z2} coh(f, z_1, z_2) dz_1 dz_2$$

Where:

- $S_{p,1}(f)$ is the ASD of walking loads per unit length for the fundamental harmonic.
- N , W and L are the number and weight of pedestrians and the span length.
- $|H(f)|$ is the frequency response function for acceleration.
- ψ_{z1} are mode shape ordinates related to the location of two pedestrians on the bridge at distances z_1 .
- $0 < coh(f, z_1, z_2) < 1$ is the function expressing the degree of correlation between pedestrians;

The complexity of method makes it not easily usable. That is the reason why time-domain force models are more applied in serviceability assessment of footbridges.

1.3.4 Vibration of the structure

To obtain the dynamic response of a multi degrees of freedom system, as in the case of a FE model, the software will compute the solution of the following equations of motion:

$M\ddot{x}(t) + C\dot{x}(t) + Kx(t) = f(t)$	
---	--

where \mathbf{M} , \mathbf{C} , and \mathbf{K} are the structural matrices of mass, damping and stiffness respectively, while $\mathbf{x}(t)$, $\dot{\mathbf{x}}(t)$, $\ddot{\mathbf{x}}(t)$ are displacements, velocities and accelerations vectors. $\mathbf{f}(t)$ is the forces vector.

Geometry and material characteristics are used to calculate the mass and stiffness matrices. However, even with complete knowledge of the structure, there is some computation error. However, there are ways to make final element models better so that they produce conclusions that are consistent with experimental data. However, because there are no experimental data available at this point in the design process, they are not applicable. The most common criteria are the MAC (Modal Assurance Criterion) and COMAC (Coordinate Modal Assurance Criterion). The damping matrix represents the energy dissipation in the equation of motion, and its derivation can be the most complex aspect to play with when doing a dynamic analysis. Assuming that the damping matrix is uncoupled by the same coordinate transformation that uncouples mass and stiffness matrix, a system of decoupled equations is obtained, each associated to a value of modal damping ratio. In this case, the number of equations to solve is much smaller since the structure response depends on a limited number of modes. Higher modes effect can be neglected [20].

1.3.5 Human -Structure interaction

The phenomenon originating the excessive level of vibration in both Solferino and Millennium footbridge is named lock-in. This phenomenon can be defined as the one in which the pedestrian “synchronizes his footfall rate to the frequency of the swaying platform” [1]. Today, it is widely acknowledged that there is some sort of human-structure interaction during footbridge vibrations as a result of the numerous research conducted on the well-known cases of Solferino and Millennium Footbridges. Throughout the design phase, its consequences cannot be ignored. There are two crucial elements that demand examination. First, the movement and presence of people alter the footbridge's natural frequencies and damping characteristics. Second, the degree of synchronization among pedestrians or between pedestrians and structure is directly linked to the crowd density. Humans behave like extra dampers on the structure: damping is more efficient in the joint human-structure system with respect to the case of the empty structure. For example, to account for this issue other than for the change in the structure stiffness, Lai and Mulas [21] modeled the pedestrian as a MSD (Mass-Spring-Damper) system to obtain the bridge numerical response (Figure 1.10).

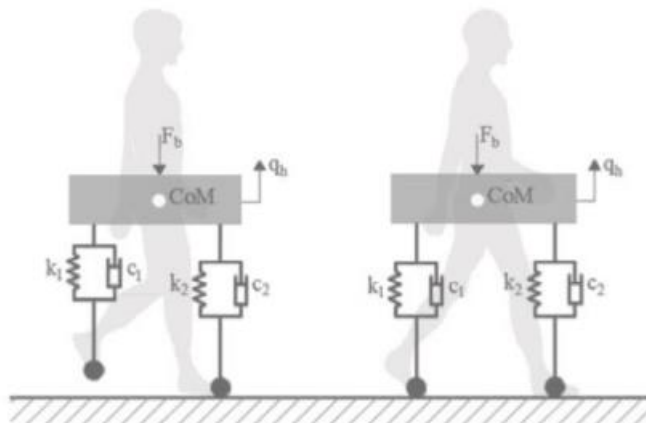


Figure 1.10: Mass-Spring-Damper model to model human structure interaction [21]

The lock-in phenomenon could be caused by lateral or vertical synchronization. After video evaluations, during the opening of Millennium Bridge, Dallard et al. [22] estimated that lateral acceleration was $0.20 - 0.25 g$ while displacements had an amplitude of up to $7 cm$ in the lateral direction. They proposed that, after synchronization, the dynamic force produced by pedestrians (t) was proportional to the deck lateral velocity (t):

$F(t) = kv(t)$	
----------------	--

Where k is a proportionality constant estimated to be equal to $300 Ns/m$ for the Millennium Bridge. This shows that human induced loads should be modelled differently before and after the lock-in occurrence. Another parameter to estimate the possibility for the lateral lock-in to occur is the critical number of people crossing the bridge:

$N_L = \frac{8\pi cfM}{k}$	
----------------------------	--

In this equation c is the modal damping ratio, f is the lateral frequency of the bridge, M is the corresponding modal mass and k was already defined [9]. The problem is that a collection of k values to determine the proper value for a given bridge does not exist yet. Regarding the vertical synchronization issue, two solutions must be mentioned. The first is predicated on the notion that the design should be completed by requiring that the reaction acceleration created after synchronization must be below a particular threshold. In [23], as reported by Živanović et al. [17], it was proposed that the acceleration response of the structure ag must be computed as a function of the probability of synchronization (ag), the number of people on the structure N and the response acceleration for a single pedestrian $a1rz$ in vertical direction. The second approach is based on principles typical of the wind engineering and was proposed by McRobie and Morgenthal [24]. The serviceability of a pedestrian footbridge could be assessed by evaluation of the vertical Pedestrian Scruton Number:

$vPSN = k_1k_2m$	
------------------	--

Where $k_1 = \xi/0.005$, $k_2 = 0.6/n$ and m are factors representing the influence of the damping ratio, of the crowd density, that could be different from the typical value of

0,6 *persons/m²*, and of the mass per unit deck area for an equivalent simply supported beam having constant cross section. Unfortunately, values of the Scruton number as a function of frequencies are not accessible for footbridge design, mostly due to two factors. First off, there is no database of pedestrian Scruton Numbers and the technique is very new. Second, because footbridges frequently vibrate laterally, it has been unable to assess the values of the pedestrian Scruton numbers on a broad scale.

1.4 Case study: The Solferino Bridge

In the civil society, the vibration of footbridges is a phenomenon attracting attention only in correspondence of well-known vibrations problems. Among the most important, it is possible to find the cases of the London Millennium Bridge (Figure 1.11) and of the Paris Solferino Footbridge (Figure 1.12). The scientific community began to examine the issue of human-induced vibration in a systematic manner after the opening of the Millennium Bridge. There is a lot of literature on this structure's dynamic behaviour. Images of lateral oscillations caused by the crowd crossing the structure during the public opening (10th June 2000) went all around the world. Some important works analysing reasons and causes of the structure behaviour were done by Dallard et al. ([1], [25] and [22]) and by Fitzpatrick et al ([26], [27]).



Figure 1.11: Millennium Bridge



Figure 1.12: Solferino Bridge

In this study, more emphasis is given to the other case. Literature about the Solferino Footbridge, today named Passerelle Léopold-Sédar-Senghor, is not wide as the previous case. Even the study case has the same level of importance.

The Jardin des Tuileries and the Orsay Museum are connected by the Solferino Footbridge, which spans the Seine River in Paris. The bridge was constructed between 1995 and 1999 by the Eiffel company, under the direction of architect Marc Mimram. The structure is composed of two couples of welded steel arches that support timber decks through coupled steel struts forming a V-shape in the bridge cross-section (Figure 1.13). The cross section of the struts is semi-elliptical, with thickness equal to 30 mm. The struts' length changes along the structure as well as their inclination.



Figure 1.13: Solferino Bridge's cross-section

This is a unique structure where two decks are above the central one and linked thanks to arch substructures (Figure 1.14).

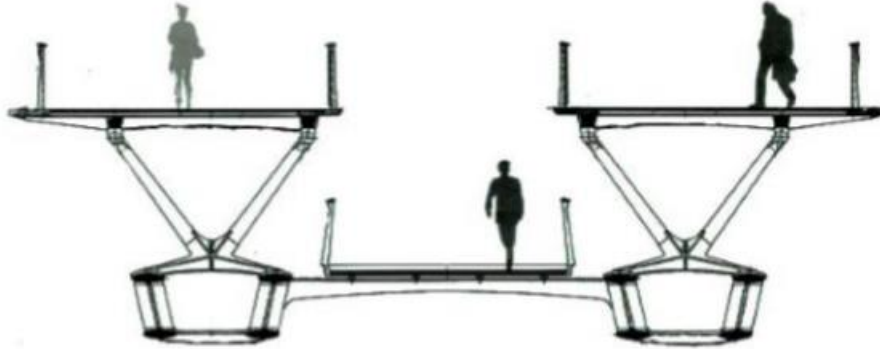


Figure 1.14: Solferino Bridge's cross-section scheme [2]

Similar to the Millennium Bridge, the Solferino Footbridge experienced unanticipated oscillations on the day of its official opening to the public on December 14, 1999. A few days later, the bridge was made inaccessible to the general public while investigations were conducted to determine how to lessen the structure's vibration. The objective was to obtain a good solution without the modification of the stiffness or of the mass of the bridge to maintain aesthetic principles. Only after almost one year, and the application of a TMD (Tuned Mass Damper Figure 1.15) system the footbridge returned to service, in November 2000. The cause of oscillations was a resonance phenomenon on the first lateral mode of vibration of the bridge, at a frequency around 0.8 Hz [28]. Two displacement tests for the deck were conducted, each with the same number of participants but speed walking. (Figure 1.16). Lower speeds and step frequencies that are closer to the bridge's fundamental lateral frequency result in larger accelerations.

Introduction

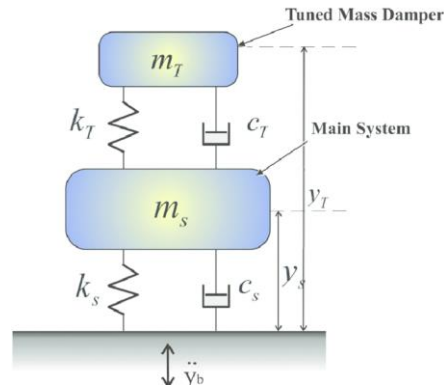


Figure 1.15: Tuned Mass Damper Scheme

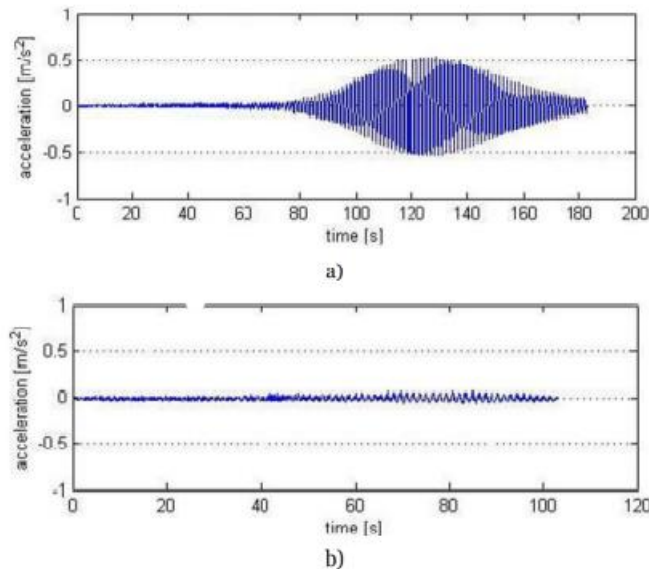


Figure 1.16 Acceleration response of the Solferino Footbridge during testing: a) low walk speed; b) higher walk speed. [29]

After [29], with a series of crowd test, “it was noticed that 140-160 pedestrians can initiate large levels of lateral accelerations making the footbridge uncomfortable”. In the same paper, the effect of the installation of a TMDs system on the natural frequencies of the structure is described. Table 1.2 presents the comparison between the situations before and after the installation of the system.

Table 1.2: Comparison between calculated and identified frequencies in different conditions [29]

Mode	Experimental (Hz)	Numerical (Hz)	Characteristics
1	0.71	0.811 ⁽⁰⁾ - 0.70 ⁽¹⁾	Symmetrical lateral bending (with torsion)
2	1.09	-	Non symmetrical torsion, 1 node, 2 lobes
3	1.12 ⁽²⁾	1.123 ⁽⁰⁾	Non symmetrical bending, central node, 2 lobes
4	1.55	1.386 ⁽⁰⁾	Non symmetrical torsion, central node (with lateral bending)
5	1.56	1.787 ⁽⁰⁾	Symmetrical bending, 1 lobe
6	1.70	1.527 ⁽⁰⁾ - 1.680 ⁽¹⁾	Non symmetrical torsion, central node, 2 lobes (with lateral bending)
7	1.95	1.971 ⁽⁰⁾	Non symmetrical torsion, 2 nodes, 3 lobes (with lateral bending)
8	2.01	2.076 ⁽⁰⁾ - 2.31 ⁽¹⁾	Symmetrical torsion, 2 nodes, 3 lobes (with lateral bending)
9	2.36 ⁽⁰⁾		Vertical bending of the access bridge, 1 lobe Torsion of the main footbridge
10	2.51 ⁽¹⁾ -2.60 ⁽⁰⁾	2.386 ⁽⁰⁾	Vertical bending of the access bridge, 1 lobe
11	-	2.722 ⁽⁰⁾	Non symmetrical lateral, 2 nodes, 3 lobes (with torsion of the access bridge)
12	2.88	2.784 ⁽⁰⁾	Symmetrical bending, 2 nodes, 3 lobes
13	3.02 - 2.92 ⁽¹⁾	2.928 ⁽⁰⁾	Torsion of the access bridge, 1 node
14	3.09	3.024 ⁽⁰⁾	Non symmetrical bending, 3 nodes, 4 lobes
15	-	3.204 ⁽⁰⁾	Symmetrical torsion, 3 nodes, 4 lobes
16	3.32	3.42 ⁽⁰⁾	Non symmetrical vertical bending, 1 node, 2 lobes (with movement of the side arches)
17	3.52	3.506 ⁽⁰⁾	Symmetrical bending, 2 nodes, 3 lobes (with lateral)
18	3.64 ⁽¹⁾	3.958 ⁽⁰⁾	Symmetrical bending, 1 lobe (with movement of the lateral arches)
19	3.74	3.385 ⁽⁰⁾	Symmetrical bending, 1 lobe (with movement of the side arches)
20	4.22	-	Symmetrical bending, 1 node, 2 lobes (with movement of the side arches)

In general, a number of variables that are still the focus of research influence the structural response. First, because of the high levels of inter- and intra-individual variability in human behaviour, human-induced load and vibration perception are both extremely complicated issues. For instance, they are affected by the walking surface's stiffness, movement speed, and environmental factors (for instance, being alone or within a sparse or a dense crowd). The behaviour of the structure is also crucial. On analytical or FE models, damping phenomena are not perfectly foreseeable and even less completely reproducible. Finally, a kind of human structure interaction may appear and change completely the behaviour of the structure because of the coupling between the bridge and the human body in terms of vibration.

2 THE STRUCTURE AT STUDY

Chapter 2 describes the structure analysed in this thesis. It is a footbridge built in Bydgoszcz, Poland. The structure is characterised by an unusual shape of steel arches, to whom a reinforced concrete deck is suspended by means of 14 hangers, 7 on each side. The steel arches rest on supporting blocks set on piles. The structure of the deck rests, independently of the arches, on reinforced concrete abutments. In the following, the structure is inserted in its geographical context then its characteristics are described.

2.1 Position of the structure

The structure is an existent footbridge located in Bydgoszcz (Figure 2.1 and Table 2.1) near the University route (Figure 2.2). This route connects the Northern and Southern settlements of the city: Bielawy and Skrzetusko with Wolności Hill. A pedestrian bridge over the road route provides a scenic accent to the route. The footbridge was projected by T. Stefanowski and the realization was carried on by “TRANSPROJEKT GDANSKI sp. z.o.o.”.

Table 2.1: WGS84 coordinate of the footbridge

Latitude	Longitude
53.117098	18.016966



Figure 2.1: Position of the footbridge in red

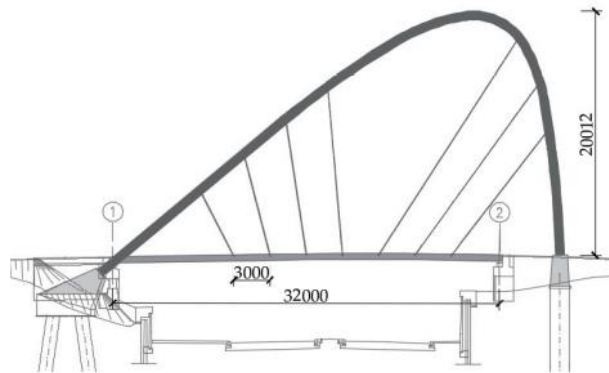


Figure 2.2: Above: footbridge overpassing University Route in Bydgoszcz; below: lateral view with overall dimensions. [5]

Bydgoszcz is a city in northern Poland, straddling the meeting of the River Vistula with its left-bank tributary, the Brda. With a city population of 339,053 and an urban agglomeration with more than 470,000 inhabitants, Bydgoszcz is the eighth-largest city in Poland. It is the seat of Bydgoszcz County and the co-capital, with Toruń, of the Kuyavian-Pomeranian Voivodeship.

The city is part of the Bydgoszcz–Toruń metropolitan area, which totals over 850,000 inhabitants. Bydgoszcz is the seat of Casimir the Great University, University of Technology and Life Sciences and a conservatory, as well as the Medical College of Nicolaus Copernicus University in Toruń. It also hosts the Pomeranian Philharmonic concert hall, the Opera Nova opera house, and Bydgoszcz Airport. Being between the

Vistula and Oder (Odra in Polish) rivers, and by the Bydgoszcz Canal, the city is connected via the Noteć, Warta, Elbe and German canals with the Rhine, a river linked to the Mediterranean and Black Seas by canals and flowing into the North Sea.

2.2 Geometry and material properties

The footbridge is a structure with an unusual shape in which a reinforced concrete deck is suspended by means of 14 hangers. The total length of the deck is 32 m and the cross-section is formed by a concrete C40/50 (Table 2.2) plate of 180 mm and by a sidewalk pavement of epoxy-polyurethane of 6 mm (Figure 2.3). There are two steel banisters located at 1.5 m from the centre of the cross-section.

Table 2.2: Properties of the concrete

C40/50		
F_{ck}	40	N/mm²
F_{cd}	26.7	N/mm²
f_{cm}	48	N/mm²
E	3522	N/mm²
Density	2300	kg/m³

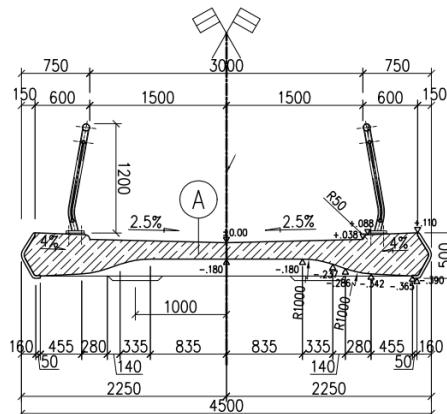


Figure 2.3: Deck cross-section

The arches are made of S335J2+N (Table 2.3), have a total length of 38.8 m and the highest point is 20 m, above the deck starting with a distance between the middle-axes of 10.2 m (B1) that slowly reduces along the length up to 0.5 m (B2) (Figure 2.4). The

arch cross-section is made of welded steel sheet and the arch is subdivided in segments with varying width from 40 to 30 mm (Figure 2.5). Both ends of the arch are anchored to concrete supports through bolted plate, as described in appendix A.

Table 2.3: Properties of the steel

S335J2+N		
f_{yk}	355	N/mm²
f_{tk}	510	N/mm²
E	220000	N/mm²
Density	7850	kg/mc

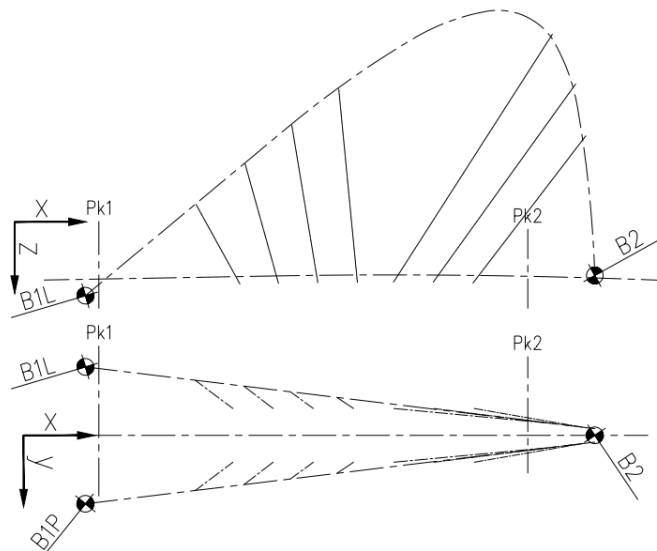


Figure 2.4: Development of the arch

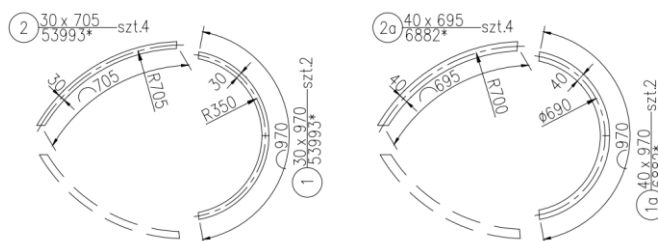


Figure 2.5: Arch cross-section

Reinforced concrete supports of the arches are made of C50/60 and A-IIIN B500SP for steel reinforcements (Table 2.4). The B1 point of anchoring is inclined of 40° while the B2 point only of 2° (Figure 2.6).

Table 2.4: Properties of the materials for concrete blocks

CLS 40/50		
fck	50	N/mm²
fcd	33.3	N/mm²
fcm	68	N/mm²
E	3727	N/mm²
Density	2300	kN/mc

A-IIIN B500SP		
f_{yk}	500	N/mm²
f_{tk}	750	N/mm²
E	220000	N/mm²
Density	7850	kg/mc

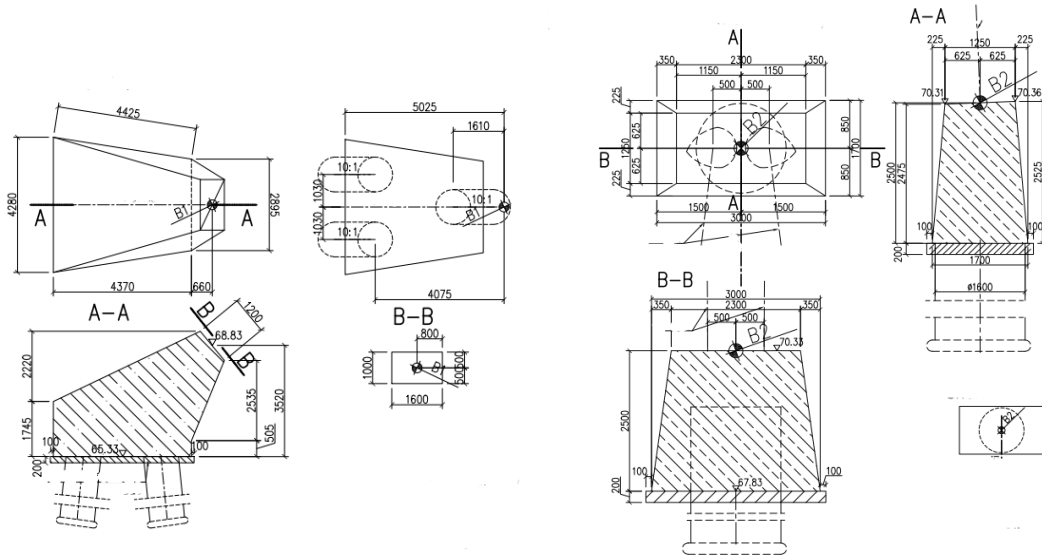


Figure 2.6: Geometry of the concrete blocks B1 and B2

Deck and arches are linked with seven rods with a diameter of 0.06 m, made of galvanized steel (Table 2.5). Anchoring to the arches is made with holed plates welded to the arch segments (Figure 2.7), while the anchoring between the deck and the rods is made using bolts directly fixed on the concrete plate (Figure 2.8). More details are given in appendix A.

Table 2.5: Galvanized steel

Galvanized steel		
f_{yk}	355	N/mm²
f_{tk}	510	N/mm²
E	220000	N/mm²
Density	7850	kg/mc

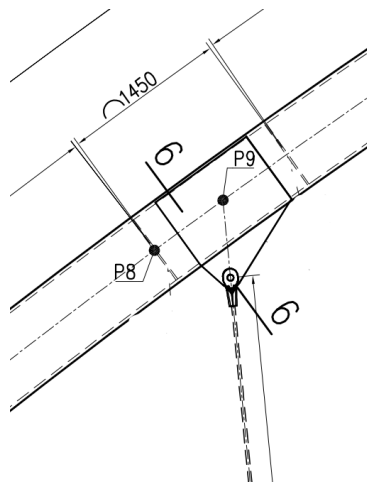


Figure 2.7: Rod-arch anchoring

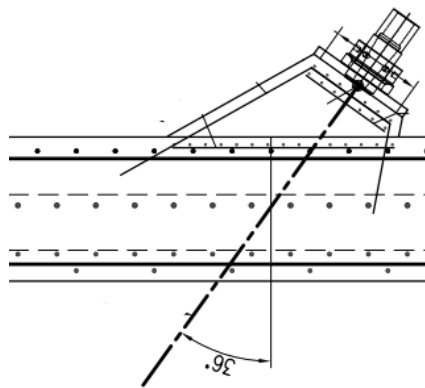


Figure 2.8: Rode-deck anchoring

The relevant points, adopted to describe the overall structural geometry of the bridge, are reported in excel for a better understanding of the geometry described in Figure 2.9 and Figure 2.10. The origin of the axis is located at the middle axis of the initial cross-section of the deck and relevant points are referred to the arches (Table 2.6), deck (Table 2.7) and hangers. In the reference system adopted, z is the vertical axis, x

is longitudinal and y transversal one. The nodes highlighted in red are located at the hangers anchoring.

Table 2.6: Relevant points of the arch

Nodes	x	y	z
1	0	±5100	0
2	5090	±4488	4201
3	8246	±4109	6806
4	10179	±3877	8401
5	11907	±3670	9827
6	15269	±3266	12602
7	15393	±3251	12704
8	18285	±2904	14958
9	18895	±2831	15405
10	21421	±2527	17152
11	24670	±2137	19175
12	25680	±2015	19721
13	26726	±1890	20195
14	27802	±1761	20596
15	28904	±1628	20920
16	30026	±1494	21167
17	31453	±1322	21240
18	32842	±1155	20907
19	34081	±1007	20194
20	34827	±917	19471
21	35067	±888	19159
22	35943	±783	17459
23	36564	±708	15770
24	36596	±705	15662
25	37015	±654	13796
26	37320	±618	11906
27	37866	±552	7572
28	38128	±521	4441
29	38273	±503	1518

Table 2.7: Relevant points of the deck

NODE	x	y	z
1	900	±2250	1518
2	10900	±2251	1518
3	13900	±2252	1518
4	16900	±2253	1518
5	19900	±2254	1518
6	22900	±2255	1518
7	25900	±2256	1518
8	28900	±2257	1518
9	32900	±2258	1518

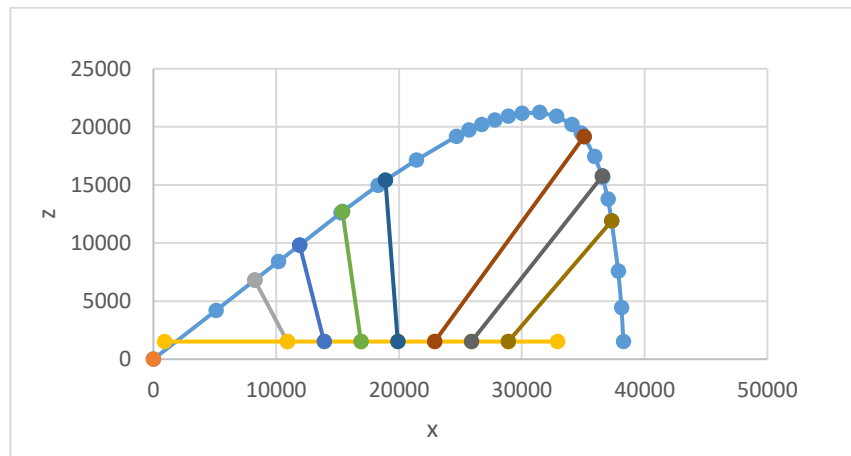


Figure 2.9: Geometry and relevant points of the footbridge on x-z plane

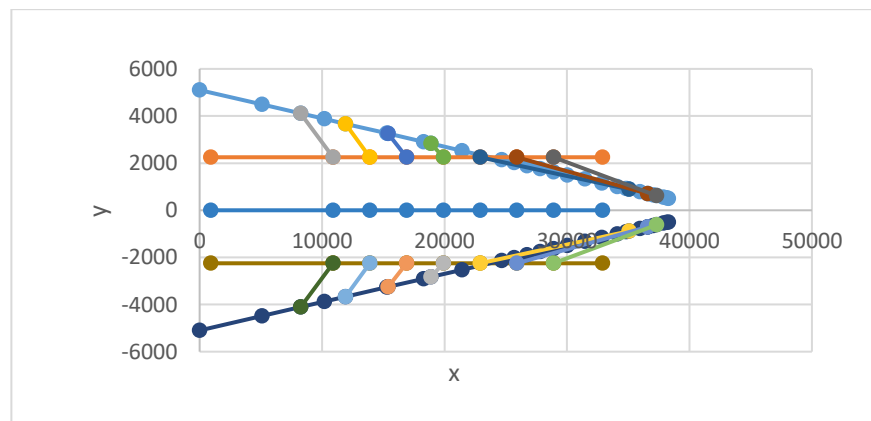


Figure 2.10: Geometry and relevant points of the footbridge on x-y plane

2.3 Experimental Data

Static and dynamic field tests were performed on the examined footbridges during an experimental campaign carried on by A. Banas [5] [30]. The displacement of the deck, settlement of the supports, and forces in the hangers were all measured during the static tests. The deck's vertical displacements, the increase in hanger strains, and the accelerations of the deck and of the steel arch were all measured as part of the dynamic testing.

2.3.1 Static Tests

Static tests of the footbridge included measurements of:

- vertical displacements - deflections of the span structure,
- settlement of supports.

For static measurements of vertical displacements - deflections of the span structure, 5 measuring cross-sections were adopted (Figure 2.11):

- cross-section 1-1 in the line of attachment of hangers no. 1,
- cross-section 2-2 in the line of attaching hangers no. 2,
- cross-section 3-3 in the clipping-in line of hangers no. 3,
- section 5-5 in the clipping-in line of hangers no. 5,
- section 6-6 in the clipping-in line of hangers no. 6.

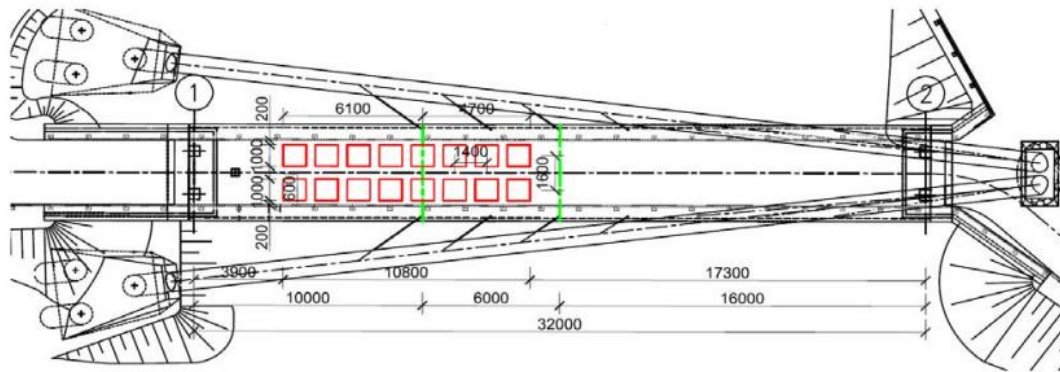


Figure 2.11: Plan view highlighting in green section 1-1 and 3-3

In the selected cross-sections, the following measurement points of vertical displacements - deflections of the load-bearing structure - were assumed, as denoted in Figure 2.12:

- u1/1 - extreme, left edge of the deck in the place of connecting hanger No. 1;
- u2/1 - extreme, right edge of the deck in the place of connecting hanger No. 1;
- u1/2 - extreme left edge of the deck in the clipping-in point of hanger no. 2;
- u2/2 - extreme right edge of the deck in the clipping-in point of hanger No. 2;
- u1/3 - extreme left edge of the deck in the clipping-in point of hanger No. 3;
- u2/3 - extreme right edge of the deck in the clipping-in point of hanger no. 3;
- u1/5 - extreme left edge of the deck in the place of clip-in hanger No. 5;
- u2/5 - extreme right edge of the deck in the clipping-in point of hanger no. 5;
- u1/6 - extreme left edge of the deck in the clipping-in point of hanger no. 6;
- u2/6 - extreme right edge of the deck in the clipping-in point of hanger no. 6.

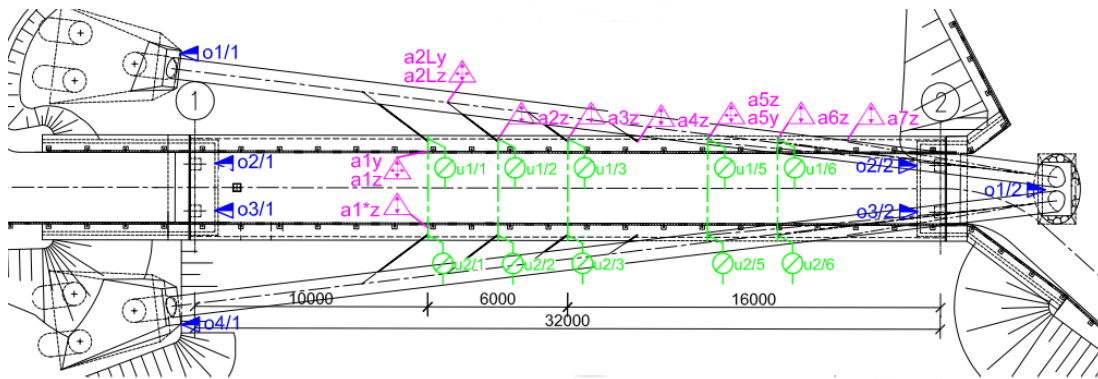


Figure 2.12: Measurement points for displacement (green), acceleration (pink), support settlement (blue)

As a part of the static tests, 1 setting (3 schemes) of the test load was realised. Setting U1 induced the maximum vertical displacement - deflection and the maximum increment of deformation/stress - normal force in hanger W1 of the span structure in gauge section 1-1.

To realise the U1 setting of the test load, a set of 16 water containers measuring 1.0×1.2 m, with a total weight of 10.5kN each, was adopted (Figure 2.13).

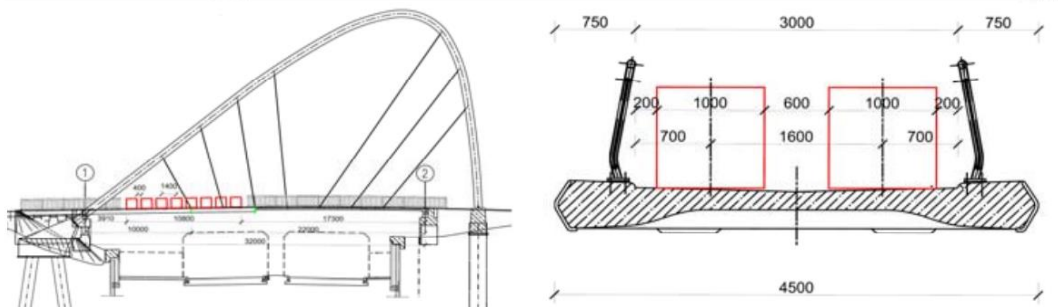


Figure 2.13: Position of the water containers.

Measuring apparatus, measuring method:

- vertical displacements - span deflections for static settings were measured and recorded using inductive sensors and specialised measuring equipment from Hottinger Baldwin Messtechnik GMBH;

- the expanded uncertainty of measurement for vertical displacements - deflections is $\pm (0.42\% \text{ of the measured value} + 0.07\text{mm})$, the uncertainty of measurement is stated as the standard uncertainty of measurement multiplied by the coverage factor $k=2$, which for a normal distribution corresponds to a coverage probability of approximately 95%.

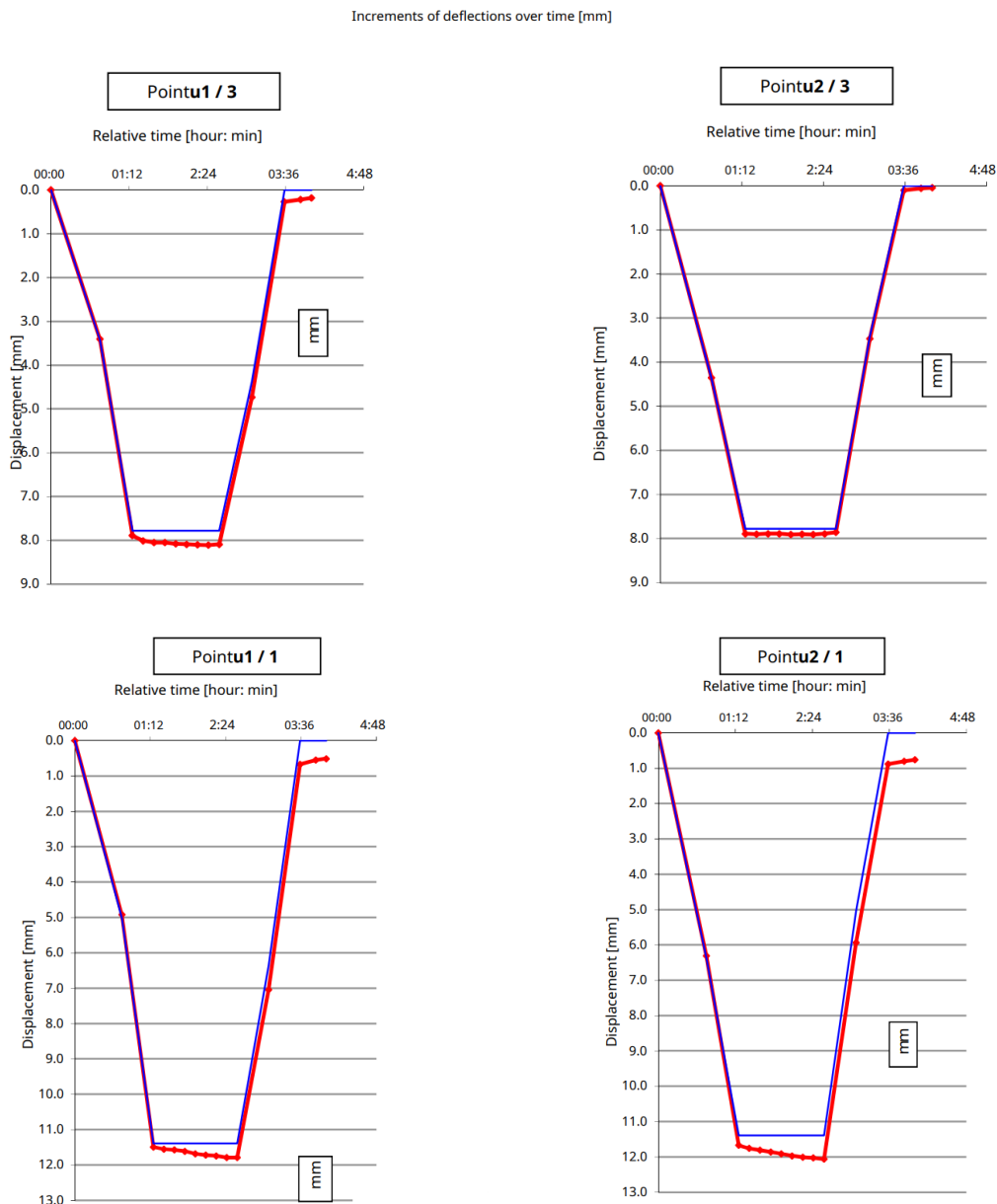


Figure 2.14: Comparison between theoretical (blue) and experimental (red) displacements.

The measurement of vertical displacements and strains/stresses has been performed in accordance with the procedures of the internal quality system according to EN ISO/IEC 17025. Figure 2.14 depicts the comparison, performed at the time of on-site testing, between analytical and experimental results in terms of vertical displacements for the cross-section 1-1 (above) and 3-3 (below).

2.3.2 Dynamic Tests

The most frequently used methods of excitation of vibrations of footbridges are dynamic tests based on the movement of a person or a group of people in the form of walking, running or jumping (Figure 2.15). They give an image of the behaviour of the structure under real operational load. During the tests carried out on the structure, many load scenarios were used: free and synchronous march, free and synchronous run, as well as jumps at specific points of the structure. During the tests, groups of pedestrians of various sizes were used. This made it possible to examine the impact of the increasing number of pedestrians on the values of the obtained accelerations (Table 2.8). Three-axial, micro-electro-mechanical capacitive accelerometers LIS344ALH manufactured by STMicroelectronics, were used to measure the acceleration of the structure. They consist of a seismic mass suspended on a spring, for which length depends on the level of acceleration. As a consequence, the electronic system contained in the accelerometer generates a voltage proportional to the capacitor's capacity. The LIS344ALH has a full-scale of $\pm 2 \text{ g} / \pm 6 \text{ g}$, and the device is capable of measuring accelerations over a maximum bandwidth of 1.8 kHz for all axes. The operating temperature is between $-40^{\circ}\text{C} \sim 85^{\circ}\text{C}$. The measurement data were recorded using the QUANTUM HBM 840a 8-channel measurement amplifier [5] (Figure 2.16). A standard laptop was connected to the measuring station and it was used for the data processing, visualization, and storage of the measurement results. During the tests, accelerometers were placed in such a way that one axis was perpendicular to the axis of the deck, the second axis was vertical, and the third one was longitudinal. In each case, the accelerometers were rigidly connected to the deck, either with concrete screws or with strong neodymium magnets and additionally compressed with the

clamp elements of the hanger’s anchor. The measurements of accelerations were also taken for a dynamic impact test and using a light vibration exciter. During the impulse tests, a container filled with water with dimensions of $1 \times 1 \times 1$ m was dropped from the height of ca. 6 cm on the footbridges deck. Also, the light vibration exciter was used, which generated a sweep signal with variable frequency in the range of 0–10 Hz. In each test, the measurement time was set in such a way that the suppression of free vibrations of the structure was allowed. The distribution of measurement points is shown in Figure 2.17. In this case, also eight platform accelerations were deployed, starting from the support axis of the structure through the attachment of all hangers. In total 38 dynamic tests were performed for the footbridge. The main measuring points were marked as B_a0z – B_a7z, respectively. Horizontal and vertical accelerations of the arch were also measured together with accelerations of the opposite side of the deck in the axis of hanger number 2. In addition, the horizontal acceleration of the deck at the attachment of hangers 2 and 5 was measured to assess the maximum horizontal acceleration during human-induced vibrations.

Table 2.8 maximum accelerations recorded during the tests [5]

N. of people	March		Run		Jump
	Sync.	Free	Sync.	Free	
Vertical accelerations [m/s ²]					
6	0.93	0.09	0.45	0.23	1.31
9	1.84	-	0.68	-	-
12	1.19	0.08	0.70	0.48	2.23
Horizontal accelerations [m/s ²]					
6	0.18	0.02	0.12	0.04	0.31
9	0.24	-	0.13	-	-
12	0.17	0.02	0.13	0.06	0.37



Figure 2.15: Dynamic tests a) walk b) run c) jump [5]



Figure 2.16: Quantum HBM 840a

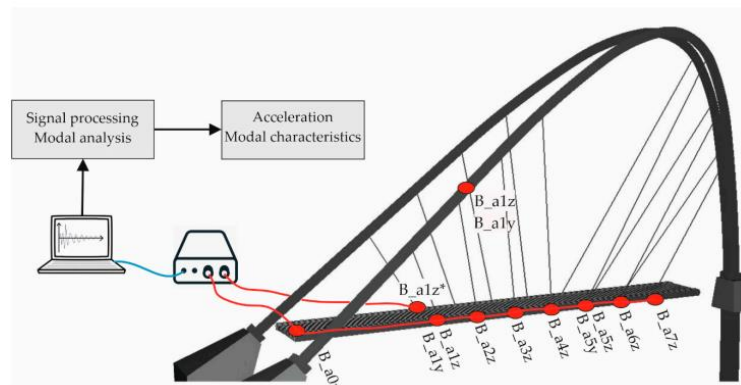


Figure 2.17: Dynamic measurement scheme [5]

2.3.3 Methods to determine Experimental Mode Shapes

The methods based on the classical input–output estimation of modal parameters are the well-known and widely used methods of modal analysis [31]. The peak picking (PP) method is one of the most accessible because of its simplicity and speed [32]. This method is based on the estimation of the frequency response function (FRF) in the frequency domain or the impulse response function (IRF) in the time domain. The experimental tests can be carried out under any excitation, including sinusoidal,

impulse, random, or pseudorandom. The excitation is usually applied at one point while the signals are measured at many points. The second method is to place the sensor at one key point of the structure and then force it at subsequent points. The algorithm of the method assumes subjecting each force signals and structure responses signals to the Fourier transform. Based on the obtained Fourier transform, the transform function $\mathbf{H}(\omega)$ is calculated. In order to receive one row of the matrix $\mathbf{H}(\omega)$, the measurement is taken for the signal of excitation in particular points of the structure; however, the responses are measured in one point. For the matrix column $\mathbf{H}(\omega)$, the signal of force is measured in one point, and the value of structure response is recorded from each measuring point. The determination of mode shapes is possible at any row or matrix column $\mathbf{H}(\omega)$. The measured signals used in the PP method may concern accelerations, velocities, or displacements. The type of signal determines three types of transition functions: accelerance, mobility, and receptance (Figure 2.18). The method's limitation is its use for structures that are lightly damped. For structures with very high damping or damping close to zero (infinite peak), the method does not give satisfactory results [33]. The modified PP method can also be used for the operational modal analysis (OMA). In this case, FRF is replaced with power spectrum densities (PDS) from the output. Comparing the results of PP method with the frequency domain decomposition (FDD) and stochastic subspace identification (SSI). Using this method, damping can be estimated by employing the half-power procedure [34].

FRF	Symbol	Signal
Receptance	$\mathbf{H}^r(\omega)$	$\frac{\text{Displacement}}{\text{Force}}$
Mobility	$\mathbf{H}^m(\omega)$	$\frac{\text{Velocity}}{\text{Force}}$
Accelerance	$\mathbf{H}^a(\omega)$	$\frac{\text{Acceleration}}{\text{Force}}$

Figure 2.18: FRFs used in PP method [5]

2.3.4 Data Processing and Modal Identification

Following a series of dynamic testing, the natural frequencies and damping ratios for each signal from the structure's free response were established [5]. The results of all tests were averaged to produce the final results. All time histories were filtered and the linear trend was eliminated, which allowed to get more accurate identification findings. In order to remove components from the signal that were beyond the scope of interest, a Butterworth fifth-order filter was used with a cut-off frequency below 0.5 Hz and above 20 Hz [35]. To check the correct operation of all sensors, signals measured during all tests were printed and checked for non-functioning or giving unreal or excessively noisy acceleration values. Figure 2.19 shows the representative acceleration time histories together with the corresponding normalized FFT amplitudes for the footbridge above the University Route in Bydgoszcz (point a1z). Vibrations were caused by the synchronous run of a group of nine persons, and the impulse was induced by dropping a container filled with water. In this case, it was possible to get some frequencies only using impulse excitation. Neither various type of the human-induced load, as well as the use of a light vibration exciter which generates excitation with a variable frequency, allowed these frequencies to be identified.

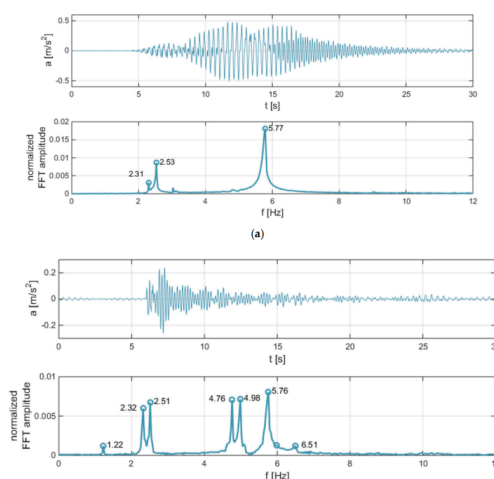


Figure 2.19: Time history of acceleration and normalized FFT amplitude for the arch footbridge above the University Route in Bydgoszcz at point a1z excited by (a) synchronous run of a group of nine persons, (b) impulse. [5]

2.3.5 Results of experimental modal identification

During the tests four modes were clearly identified using two different approaches (Table 2.9 and Table 2.10). On the base of this results, a series of FE model were elaborated in order to have a good match with the experimental modal shapes in terms of frequencies (Table 2.11) and modal displacements (Figure 2.20). The experimental shapes present the first two and the last mode related to vertical displacement of the deck while the third one identifies a torsional modal shape. More details are presented in the following chapter.

Table 2.9: Experimental modal shape obtained with vibration inductor

mode shape	1	2	3	4
length [m]	vector			
0	0	0	0	0
13	1	1	0.95719	0.29625
16	0.93168	0.8542	1	0.92968
19	0.6101	0.53763	0.72482	0.94892
22	0.24808	0.17429	0.4771	1
25	0.018829	-0.05387	0.20132	0.69529
28	-0.09786	-0.10513	0.12094	0.41027
32	0	0	0	0

Table 2.10: Experimental modal shape obtained with impulse caused by container impact

mode shape	1	2	3	4
length	vector			
0	0	0	0	0
10	-0.99076	1	-0.84038	-0.49265
13	-1	0.97263	-1	0.29558
16	-0.86641	0.7995	-0.95465	0.78036
19	-0.59382	0.54988	-0.75003	0.85034
22	-0.25538	0.21618	-0.51196	1
25	0.031439	-0.06792	-0.36093	0.61319
28	0.11923	-0.13504	-0.20989	0.3366
32	0	0	0	0

Table 2.11: Frequencies of the experimental modal shape

Mode	Frequency
	Field
1	2.31
2	2.52
3	4.99
4	5.73

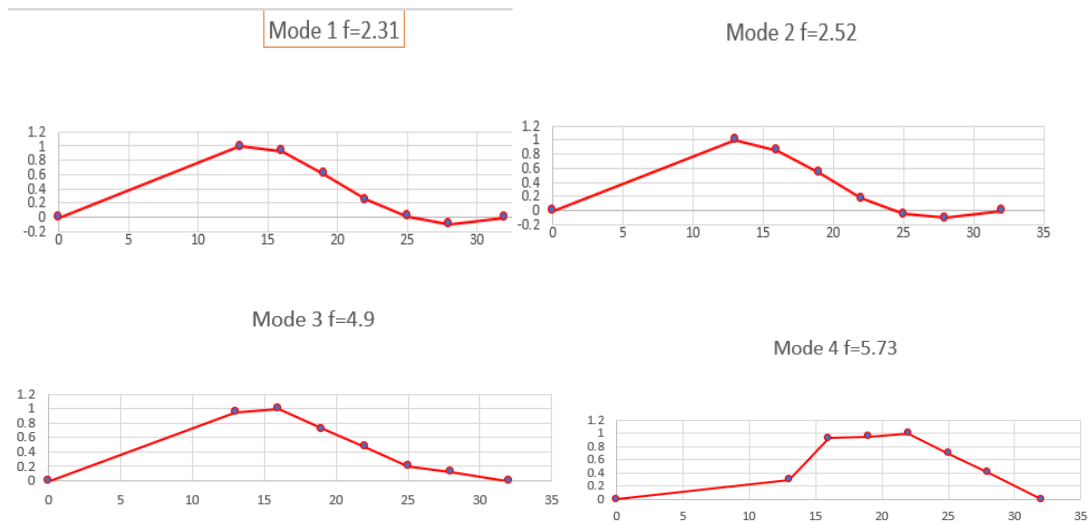


Figure 2.20: Modal shape obtained from the experimental the experimental campaign: a) Vertical Modal shape; b) Vertical Modal Shape; c) Torsional Modal Shape; d) Vertical Modal Shape.

3

STRUCTURAL MODELLING

Chapter 3 presents the modelling process of the structure described in CHAPTER 2. As already stated, the software used for this purpose is the educational version of Ansys Mechanical APDL (Ansys Parametric Design Language). After a brief description of the software, all the assumptions at the base of the FE modelling are presented referring to the footbridge features. Finally, differences among the proposed models and the analyses performed are discussed.

3.1 Ansys Software

A student license for the commercial software Ansys was used to analyse the structure described above. The following gives a quick overview of the software. Engineering software called Ansys uses the finite elements method as its foundation. It is a potent piece of software that may be used to address a variety of issues and is accessible through a variety of interfaces. There are interfaces, also called platforms, for impacts or explosions problems (Ansys Autodyne), fluid dynamics (Ansys Fluent, CFD, CFX), electronics (Ansys HFSS, Maxwell and Slwave) as well as for mechanics (Ansys Mechanical). They can be distributed all together with Ansys Multiphysics or Ansys Workbench. Different releases exist, updated periodically by the developer. This software can resolve any physical issue. It is possible to describe materials, boundary conditions, loads, and other concepts relatively simply. The Ansys software versions mentioned offer a highly straightforward and user-friendly user interface. In order to have a greater control over the model, it is possible to use a more complex version where the user can build the model, do analyses, and get results by writing directly the problem's source code in the initial approach with the program and in cases of modelling errors. This opportunity is given by the Ansys Mechanical APDL version of the software. APDL stands for Ansys Parametric Design Language. The driving idea of APDL is to model the problem writing a code in a text format file, following the rules given in the Help guide of the product. Once the model is ready, Ansys can read the file and perform analysis following the instructions written in the file. The analyst, when understands the way to use commands and to implement all parameters necessary to complete the FE model, can really appreciate the power of this very compact language that allows for making very difficult operations by simply writing one line of code (ex. in Appendix B).

3.1.1 Model's element

The elements used for creating a FE model of the structure are either bi and mono-dimensional. The principal ones are BEAM188, LINK180, SHELL181, SOLID185, COMBIN14 and MPC184 [36] [37].

- **BEAM188**

This element type present rigid section, shear stress output related to torsion and flexure and cubic shape functions. This element type is based on the Timoshenko theory, particularly recommended for beams from slender to relatively stubby dimensions. The element has six degrees of freedom per node. Input data are cross-section properties, material properties and three nodes. The end nodes (I and J) are mandatories, the third node (K) is used to define the orientation of the element around the axis going from node I to J (Figure 3.1);

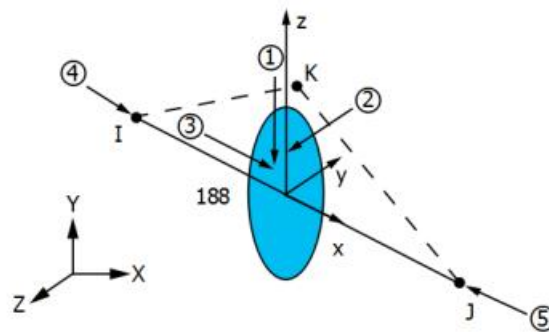


Figure 3.1: BEAM188 Geometry [36]

- **LINK180**

This element presents a rigid section. It is adopted to model trusses, sagging cables, links, springs and so on. It has three degrees of freedom per node, that describe nodal translation along x, y and z-axis. It is possible to model tension only behaviour. The element is defined through the following input data: two nodes (I and J), section properties and material properties (Figure 3.2).

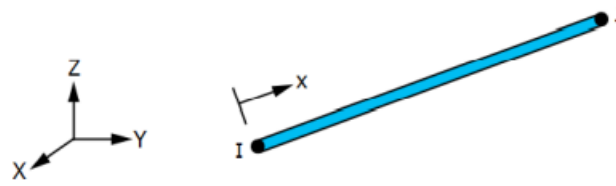


Figure 3.2: LINK180 Geometry [36]

- **SHELL181**

This type is bi-dimensional element mainly used for thin plates. It has six degrees of freedom (three translation x,y and z and three rotation, one for each axis). It is possible to coupling translational degrees of freedom with the following formula:

$U_{i,k} - U_{j,k} = 0 \quad k = x, y, z$	
---	--

i and j are referred to the node's number constrained and k is the direction.

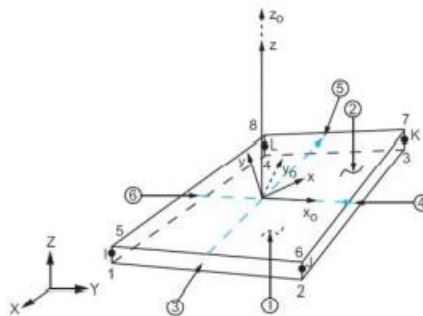


Figure 3.3: SHELL181 Geometry [36]

- **MPC184**

The MPC184 rigid link/beam element can be used to model a rigid constraint between two deformable bodies or as a rigid component used to transmit forces and moments in engineering applications. This element is well suited for linear, large rotation, and/or large strain nonlinear applications (Figure 3.4).

The kinematic constraints are imposed using one of the following two methods:

1. The **direct elimination method**, wherein the kinematic constraints are imposed by internally generated MPC (multipoint constraint) equations. The

degrees of freedom of a dependent node in the MPC equations are eliminated in favour of an independent node.

2. The **Lagrange multiplier method**, wherein the kinematic constraints are imposed using Lagrange multipliers. In this case, all the participating degrees of freedom are retained.

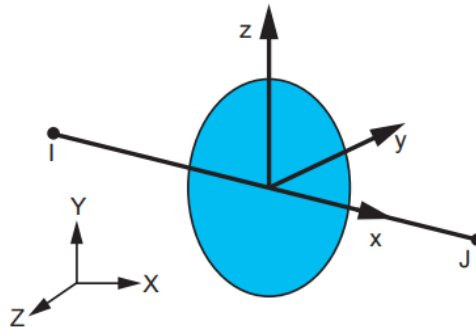


Figure 3.4: MPC184 Geometry [36]

- **SOLID185**

SOLID185 is used for 3-D modeling of solid structures. It is defined by eight nodes having three degrees of freedom at each node: translations in the nodal x, y, and z directions. The element has plasticity, hyperelasticity, stress stiffening, creep, large deflection, and large strain capabilities. It also has mixed formulation capability for simulating deformations of nearly incompressible elastoplastic materials, and fully incompressible hyperelastic materials (Figure 3.5).

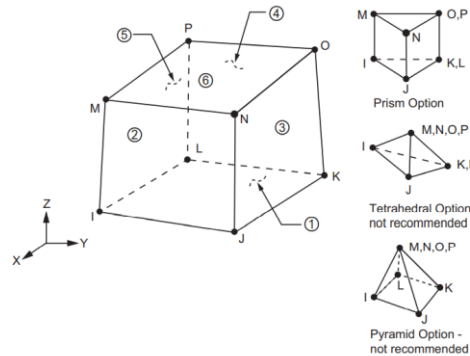


Figure 3.5: SOLID185 Geometry [36]

- **COMBIN14**

COMBIN14 (Figure 3.6) has longitudinal or torsional capability in 1-D, 2-D, or 3-D applications. The longitudinal spring-damper option is a uniaxial tension-compression element with up to three degrees of freedom at each node: translations in the nodal x, y, and z directions. No bending or torsion is considered. The torsional spring-damper option is a purely rotational element with three degrees of freedom at each node: rotations about the nodal x, y, and z axes. No bending or axial loads are considered [36].

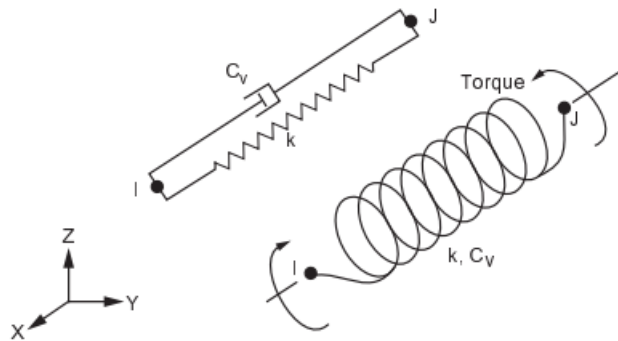


Figure 3.6: COMBIN14 Geometry [36]

3.2 Modelling assumptions

The assumptions at the base of the model derivation are presented in the following. The models are presented in order of increasing accuracy. The choice for setting origin of reference system and its characteristics were imposed. The right-handed reference system has vertical positive z-axis upwards, x and y-axis, in the plane of the deck, respectively parallel and transversal to the deck. The conversion of actual boundary conditions into numerical ones is a crucial step in the modelling process. Beginning with the simplest engineering problem, the ability to accurately express the boundary conditions will have a significant impact on the solution. Boundary conditions must be assigned on some nodes of the discretized structure. These are the supports of the deck connecting the structure with the ground.

3.3 First Model

The first model is made considering the deck as a beam element with rectangular section. In the real footbridge the deck section has a not-regular shape and is not compatible with ANSYS's model tools. To overcome at this difficulty, a rectangular section is modelled by imposing as a fixed value of the base of the section (4.5 m) and of the moment of inertia with respect to y axis. In the following the differences between the two sections are presented.

Real Section	
Area [mm ²]:	1282090.223
Perimeter [mm]:	9659.5726
Principal Moments in X-Y direction respect to the baricenter [mm ⁴]:	
I:	1.35E+10
J:	2.69E+12

Rectangular Section (Figure 3.7)			
Height[mm]:	330	Area[mm ²]:	1484175
Base[mm]:	4500		
Principal Moments in X-Y direction respect to the baricenter [mm ⁴]:			
I:		1.35E+10	
J:		2.50E+12	

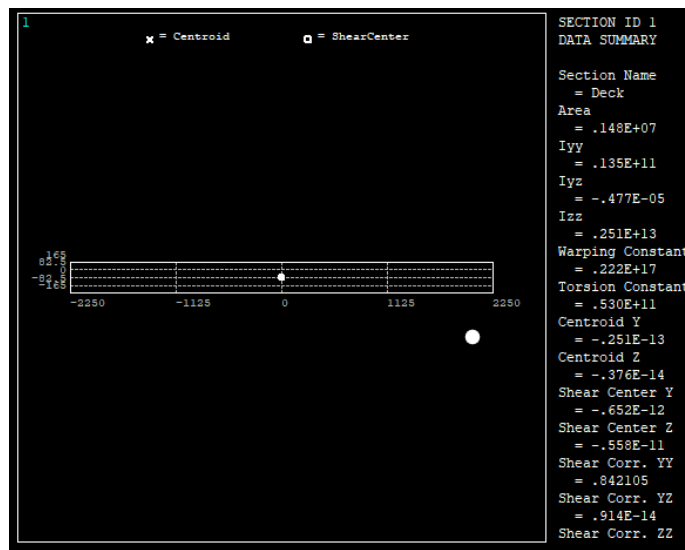


Figure 3.7: Deck cross-section

The difference of area between the comparable rectangular portion and the real one (15%) is the primary difference. To respect the entire mass of the actual construction, it is assumed that a lower density coefficient will be used. Also the arch is modelled with beam elements, all the nodes used for the model shape are the one reported on Chapter 2 “Geometry and material properties”. The steel arch cross-section (Figure 3.8) used on ANSYS is the real one, the approach used is to import it from Autocad, this is possible because has a simple shape respect to the deck’s one.

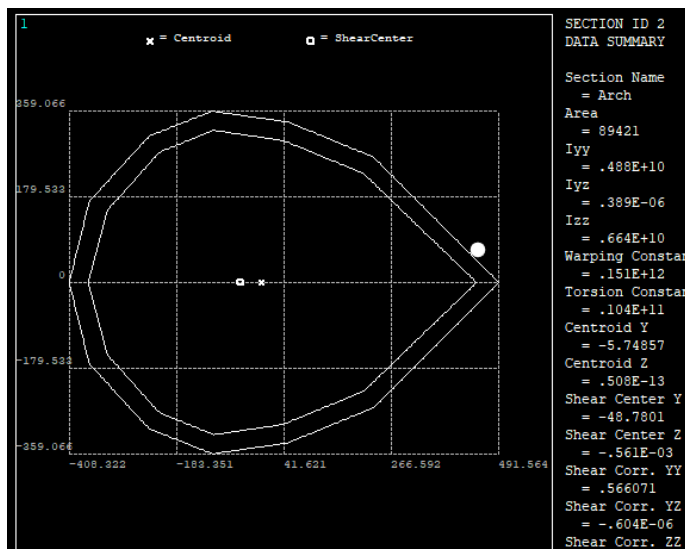


Figure 3.8: Steel arch cross-section

The rods, which have a circular area of 2826 mm², are the final elements to be modelled. The CERIG command [36], which couples degrees of freedom (rigid link RBE2) between independent nodes (of the beam element used to model the deck) to dependent nodes (at the link's ends), was implemented to connect the rod and deck. Using either the middle axis or a plot of actual cross section shapes, ANSYS can display elements, as visible in Figure 3.9 and Figure 3.10.

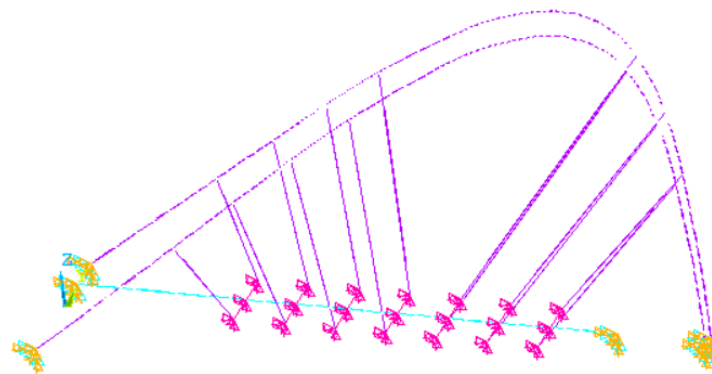


Figure 3.9: ANSYS model

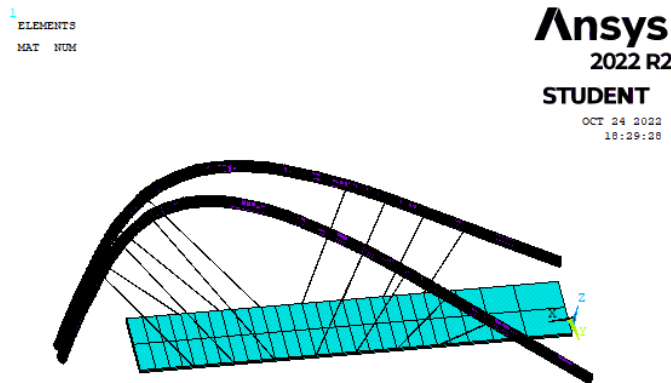


Figure 3.10: ANSYS FEM model with the real shapes of the elements

Two types of material model are defined, the first referred to deck and the second for the steel elements (see Figure 3.11 and Figure 3.12).

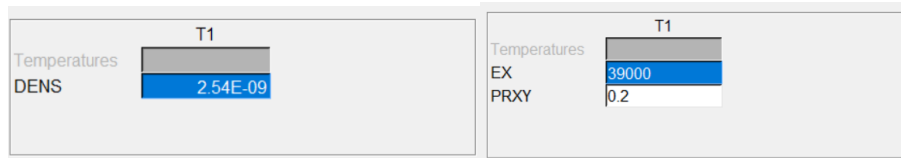


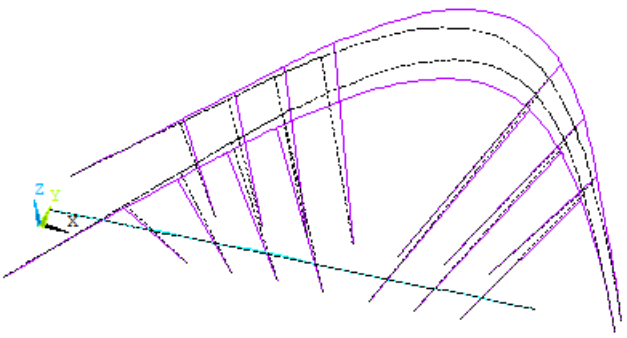
Figure 3.11: Reinforced concrete material model



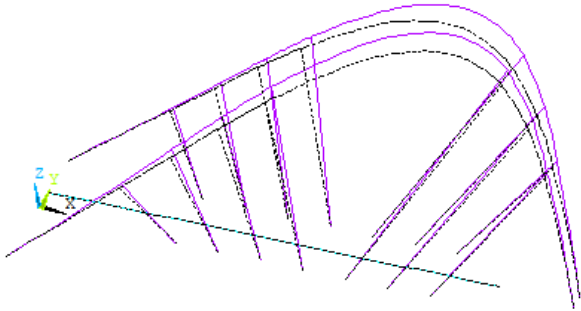
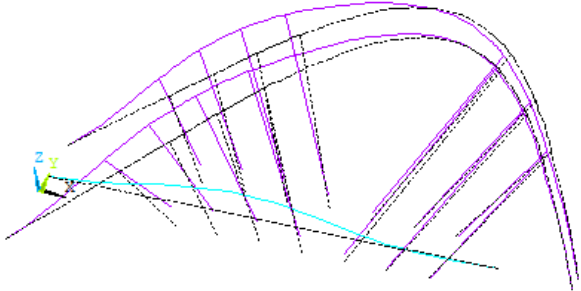
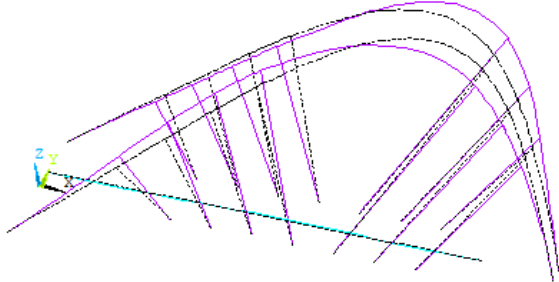
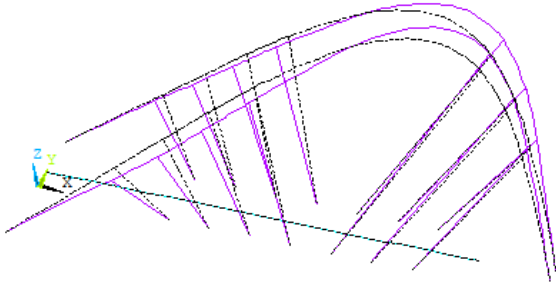
Figure 3.12: Steel material model

In the subsequent step modal analysis is performed, providing the dynamic properties of the structure, in terms of natural modes and frequencies. The Lanczos method was chosen to extract the pairs of eigenvectors and eigenvalues from the FEM model in both cases. Due to the geometry of the structures, all computed natural modes were marked with symbols and a number, which depended on the type of dominant vibration mode. The abbreviation “L”, “V” and “T” in brackets specify if the eigenmode is lateral, vertical or torsional, while “a” and “d” refers to arch and deck, respectively.

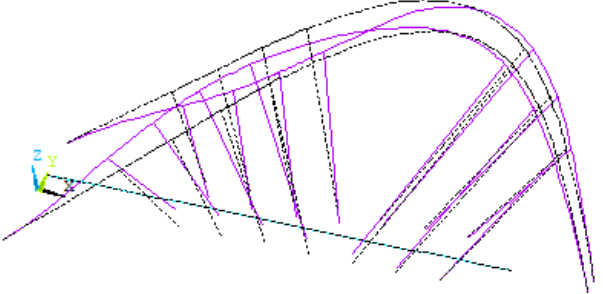
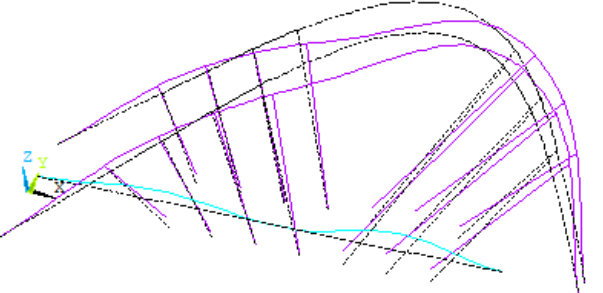
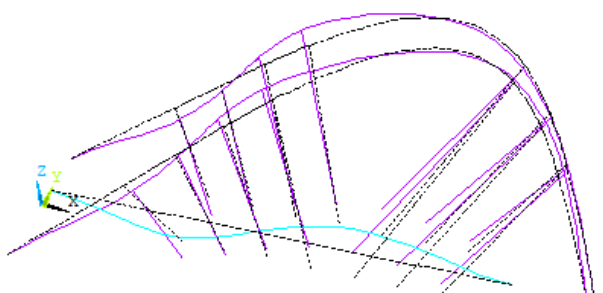
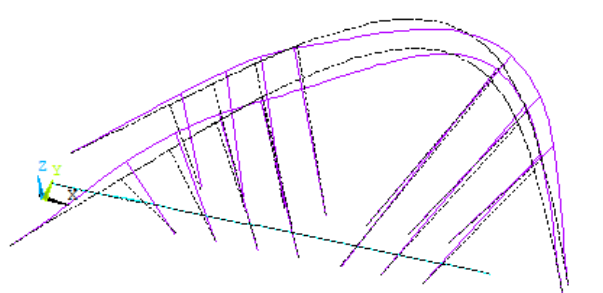
Table 3.1: Modal Shapes of first model results with Lanczos method

Mode	Frequency [Hz]	Modal Shape
La1	1.0558	

NUMERICAL MODELLING VS ON-SITE TESTING OF AN ARCH-SUSPENDED FOOTBRIDGE

La2	1.05	
Vd1	2.33	
La3	2.85	
La4	2.86	

NUMERICAL MODELLING VS ON-SITE TESTING OF AN ARCH-SUSPENDED FOOTBRIDGE

Td1	3.81	
Vd2	4.99	
Vd3	5.57	
La5	5.68	

NUMERICAL MODELLING VS ON-SITE TESTING OF AN ARCH-SUSPENDED FOOTBRIDGE

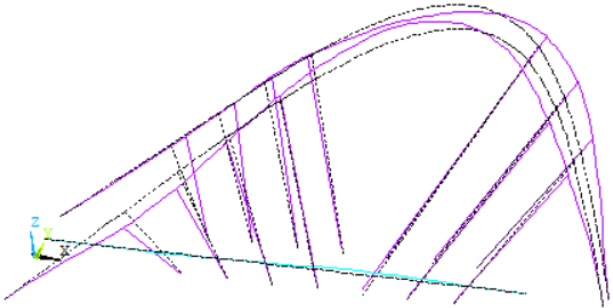
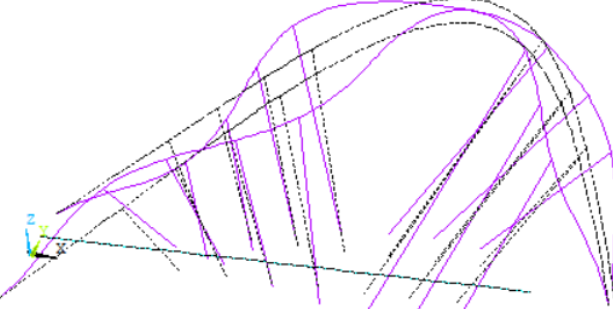
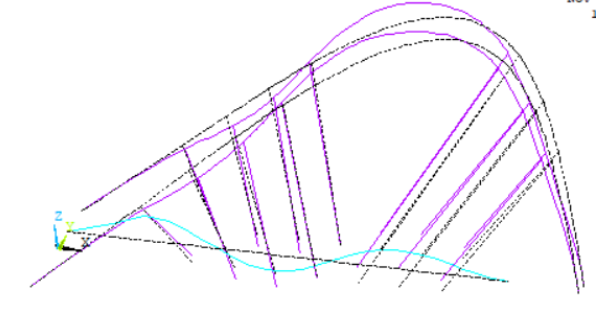
La6	6.22	 <p>17</p>
La7	6.23	 <p>1</p>
Vd4	8.28	 <p>NOV 1</p>

Table 3.2: Correlation between experimental and FEM model modal parameters of the Footbridge

Mode	Frequency [Hz]		Δf [%]
	Field	Fem	
Vd1	2.31	2.34	1.3
La4	2.52	2.86	13.49
Td	4.99	-	-
La5	5.73	6.22	8.5

Comparing the numerical frequencies (Figure 3.13) to the experimental ones (Table 3.2), it can be seen how the model should be improved. The beam model presents a stiffer behaviour for the arches. This aspect appears in lower frequency in La₄; in addition the model doesn't show the second torsional modal shape that appears in the experimental analysis.

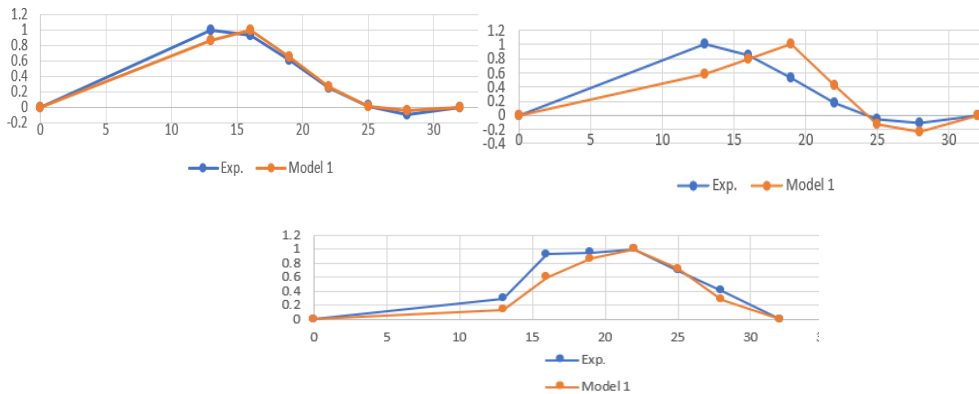


Figure 3.13: Comparison of modal shapes (field test—blue; FEM third model—orange)

3.4 Second Model

The second model (Figure 3.14 and Figure 3.15) differs from the first one for the deck modelling. Shell elements, having dimensions $750 \times 750 \text{ mm}^2$ describe the deck, whose thickness is equal to 400 or 180 mm depending on the position of the element. The cross-section is modelled in order to have same area, base and moment of inertia about the horizontal axis as the real one's (Figure 3.16). The rigid cross-section assumption used in the prior model can be dropped with the usage of shell elements.

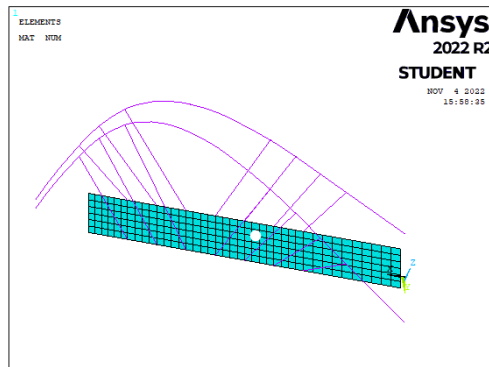


Figure 3.14: Ansys Second Model.

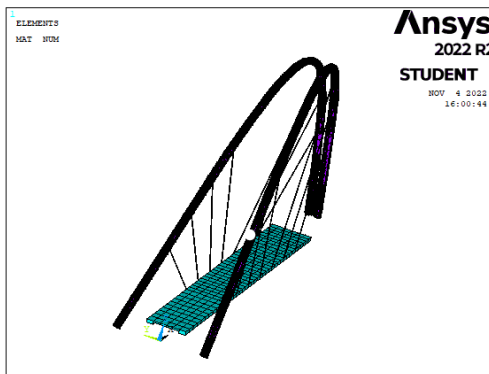


Figure 3.15: ANSYS FEM Second Model with the real shapes of the elements.

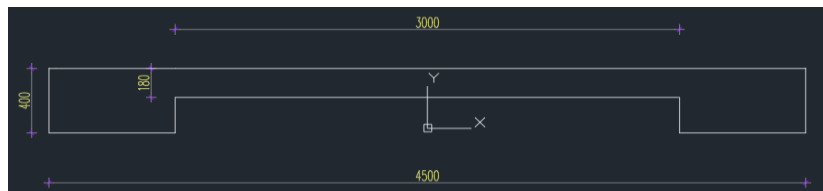
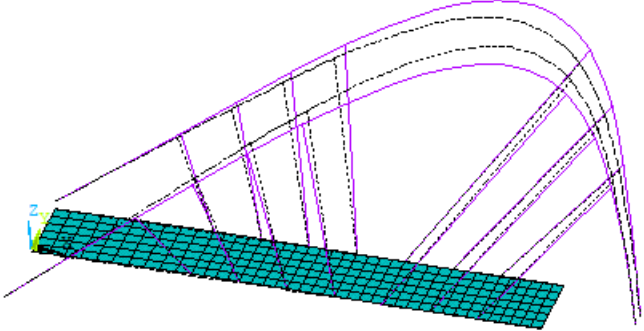
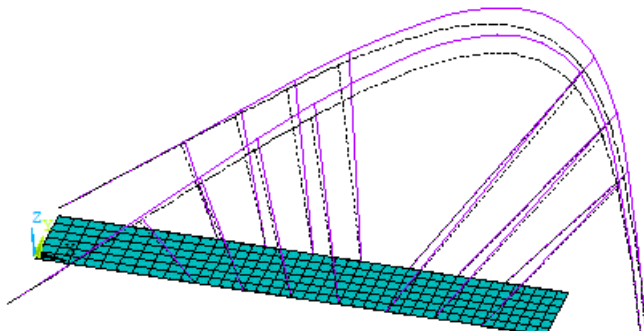
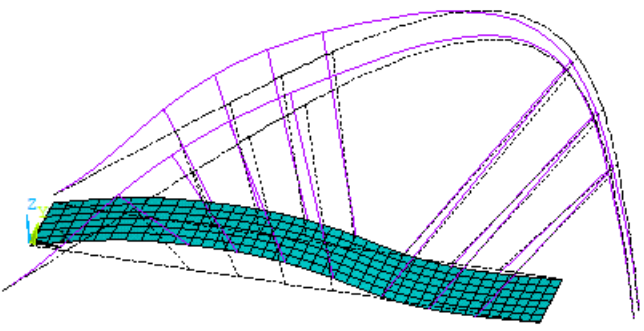


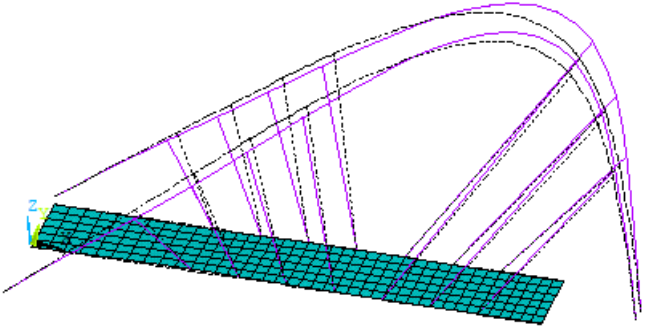
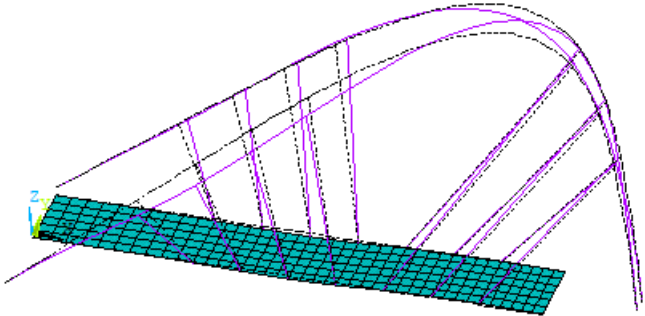
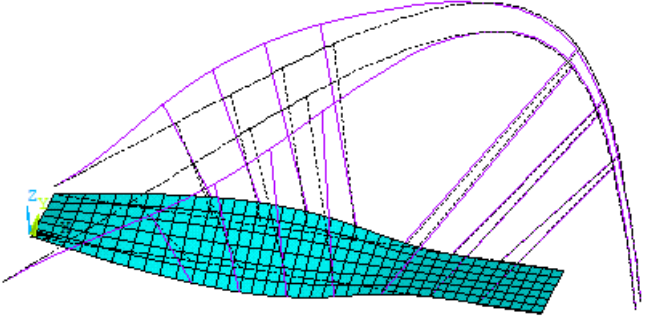
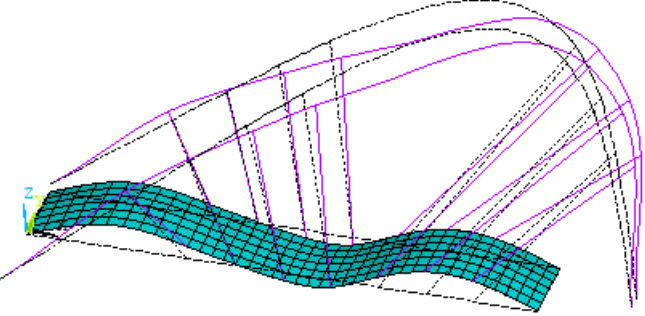
Figure 3.16: Discretization of the deck cross-section in the second model.

Modal analysis is performed with Lanczos method. Results are listed in the Table below.

Table 3.3: Modal Shapes of second model result with Lanczos method

Mode	Frequency [Hz]	Modal Shape
La1	1.0236	
La2	1.0303	
Vd1	2.3902	

NUMERICAL MODELLING VS ON-SITE TESTING OF AN ARCH-SUSPENDED FOOTBRIDGE

La3	2.7703	
La4	2.7718	
Td1	3.9032	
Vd2	4.6464	

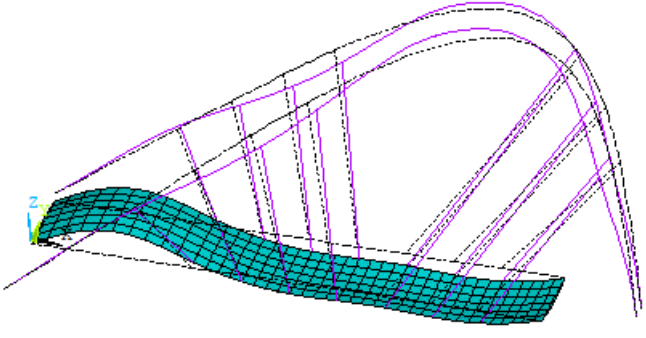
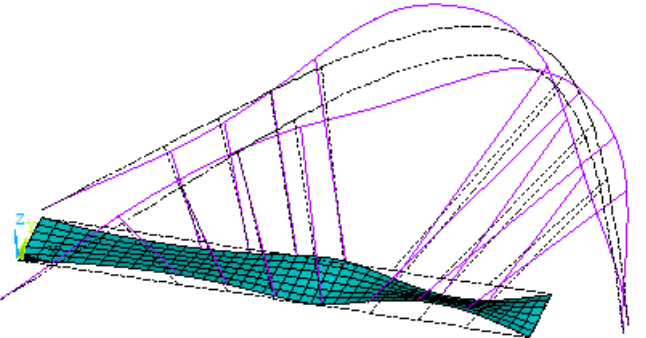
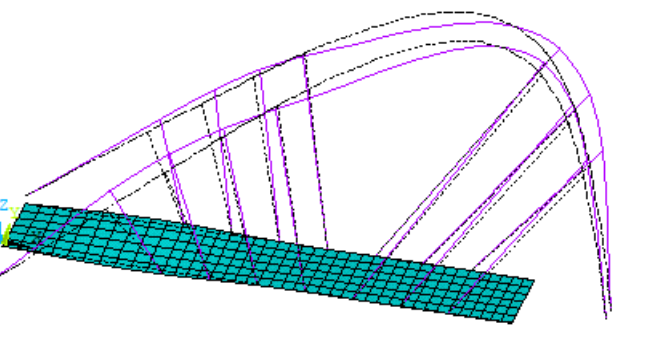
Vd3	5.2282	
Td2	5.9136	
La5	6.0297	

Table 3.4: Correlation between experimental and FEM model modal parameters of the Footbridge

Mode	Frequency [Hz]		Δf [%]
	Field	Fem	
Vd1	2.31	2.39	3.46
La4	2.52	2.77	9.9
Td1	4.99	3.9	21.8
La4	5.73	5.22	8.9

It can be seen in Table 3.4 that La4 have a better comparison with the experimental results (Figure 3.17), with the torsional modal shape now being apparent while the frequency error for the other two modes has increased. In addition, it is possible to see that the modal forms' frequencies rapidly rise, indicating that the model is still stiffer than the actual structure.

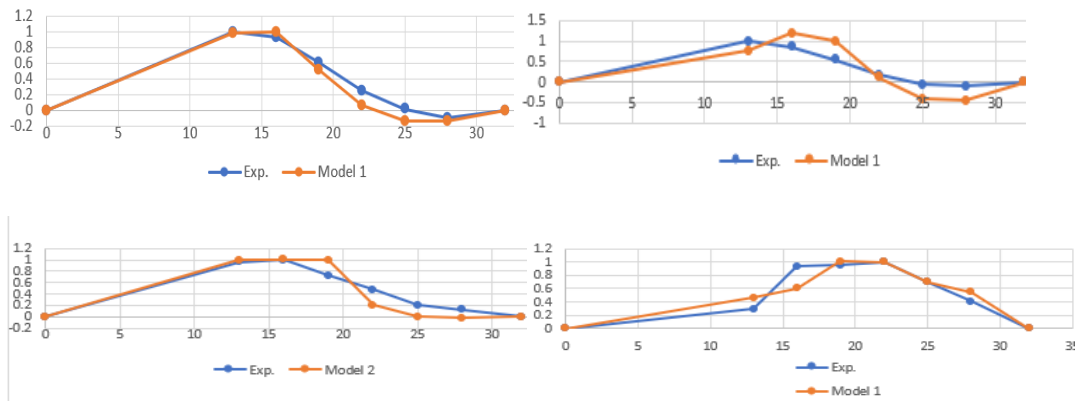


Figure 3.17: Comparison of modal shapes (field test—blue; FEM third model—orange)

3.5 Third Model

Three modifications were inserted to get a better assessment of the experimental modes, in order to estimate the soil-structure interaction through springs, the concrete blocks at the foot of the arches are introduced into the FE model and to replicate the pretension acting on cables, temperature loads are applied to rods to prevent static stresses. The concrete blocks have the dimensions seen in Chapter 2.2 and are linked to the arches with rigid link element on the upper surface to represent the fixed constraint.

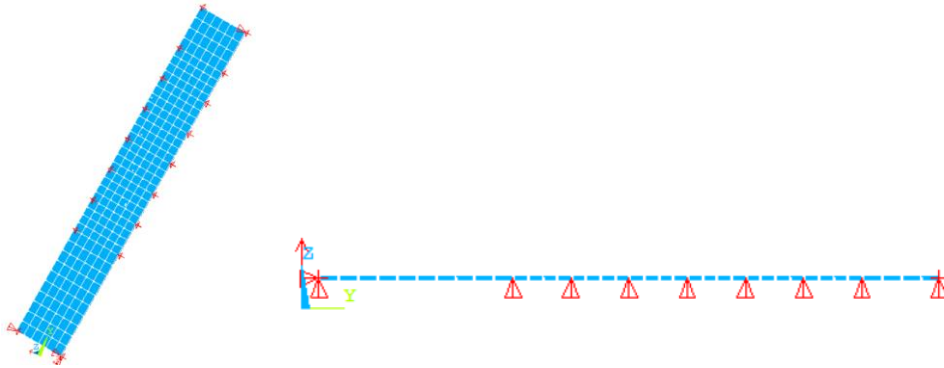


Figure 3.18: Vertical constraints positioning

A method that uses a uniform thermal load applied to the link elements to estimate the pretension in the hangers is adopted. This method consists in performing a static analysis on the deck (Figure 3.18) supported by rollers in the points of connection to hangers and obtain their F_z reactions (Table 3.5). The reactions F_z are considered as vertical component the axial force N in the hangers (Table 3.5); knowing the inclination of the hanger (Figure 3.19), it is possible to calculate the axial pretension force as:

$N_i = \frac{F_i}{\cos\alpha_i \cos\theta_i}$	
---	--

Where:

- F is the reaction force in the i -th rods point on the deck;
- α is the angle of the i -th rod respect to z -plane;
- θ is the angle of the i -th rod respect to y -plane.

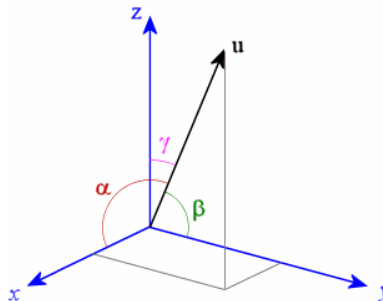


Figure 3.19: Angles of the hanger in space system

Collecting the axial reaction of rods, the uniform temperature load applied in each of them was estimated (Table 3.5) as:

$\Delta T_i = \frac{\Delta L_i}{\alpha}$	
--	--

Where:

- ΔL is the deformation due to the axial load;
- α is the coefficient of thermal expansion.

Table 3.5: Reaction force of the roller constraints F_z , axial component in the hanger N and Uniform Thermal Loads ΔT

Rod	Fz [N]	N [N]	L [mm]	ΔL [mm]	ΔT [C°]
LD1	137340	154140.3	6442	1.67	21.6
LD2	3518	3625.699	8725	5.00E-01	4.78
LD3	46680	47283.94	11826	9.42E-01	6.64E
LD4	42340	42500.74	13816	9.89E-01	5.97
LD5	43023	51434.45	21292	1.85	7.22
LD6	40403	50002.01	17459	1.47	7.02
LD7	54064	66908.61	12997	1.47	9.40

Comparing the results in Table 3.5 reveals that LD1 has a consistent thermal load that is significantly larger than the others. This is understandable given the hangers' placements and spacing, in addition LD1 supports a span of 10 meters

The blocks are based on piles that have a length of from 13 m to 16 m. For modelling the soil-pile interaction a continuum approach is used. This method was developed by several authors such as Tajimi (1969), Kobori et al. (1977) and Novak (1977). The prediction of the response of structures supported on piles requires the definition of stiffness and damping of piles (Figure 3.20). These parameters, frequency dependent, and involve properties of both soil and pile [38].

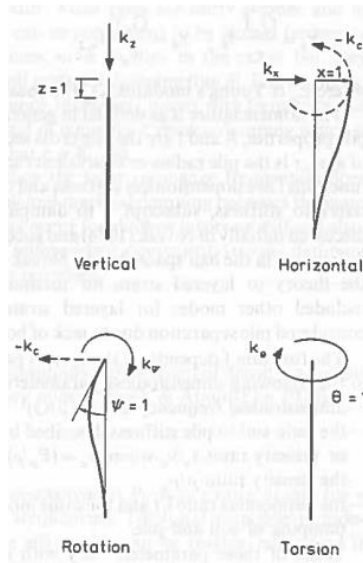


Figure 3.20: Generation of pile stiffness k in coordinate direction [38]

The equation of motion for soil/pile system can be written in terms of stiffness k_i and damping coefficients c_i . The following equations refers to a unit amplitude at the pile head in directions (z, x, ψ, θ):

- Vertical translation z :

$k_z = \frac{E_p A}{r} f_{z,1}$	$c_z = \frac{E_p A}{v_s} f_{z,2}$	
---------------------------------	-----------------------------------	--

- Horizontal translation x :

$k_x = \frac{E_p I}{r^3} f_{x,1}$	$c_x = \frac{E_p I}{r^2 v_s} f_{x,2}$	
-----------------------------------	---------------------------------------	--

- Rotation of pile in vertical plane ψ :

$k_\psi = \frac{E_p I}{r} f_{\psi,1}$	$c_\psi = \frac{E_p I}{v_s} f_{\psi,2}$	
---------------------------------------	---	--

- Torsion about longitudinal axis θ :

$k_\theta = \frac{G_p J}{r} f_{\theta,1}$	$c_\theta = \frac{G_p J}{v_s} f_{\theta,2}$	
---	---	--

Where:

- E_p is the young modulus of the pile;

- A is the cross-section area of the pile;
- r is the radius of the cross-section of the pile;
- v_s is the velocity of propagation of the pile material;
- G_p is the shear modulus of the pile;
- I is the moment of inertia of the pile cross-section;
- J is the polar moment of inertia of the cross-section.

Functions f are used to take into account the interaction with the soil and mainly depend on soil parameters such as Young's modulus of the soil, specific weight of the soil, Poisson's ratio of the soil, the distribution of the shear modulus G along the soil layers and the slenderness of the pile (Figure 3.21).

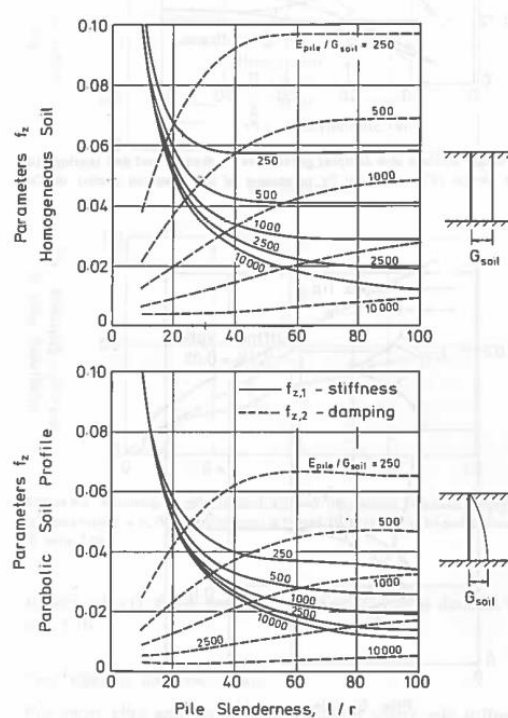


Figure 3.21: Stiffness and damping parameters of vertical response [38]

CPTU tests were performed in the experimental campaign and density indexes and plasticity indexes of the soil are collected (specific index are reported in appendix A). Starting from them soil properties are obtained, in particular the layer of soil shows a

shear modulus G around 30-40 MPa. Hence it was possible to use the homogenous distribution of the soil (Table 3.6), picking the values of f functions referred to $\frac{E_{pile}}{G_{soil}} = 1000$ and Poisson coefficient of 0.25 (Table 3.6). It is now possible to compute k_i and c_i coefficients used in Ansys for modelling spring-dumper elements (Table 3.7). Different approach is used for the inclined pile, using the PLV method it was possible to compute k_i and c_i referred to z, x, ψ and θ directions (e.g., the vertical stiffness for inclined pile is given by partial contribution of the axial stiffness k_z and partial contribution of the horizontal stiffness k_x).

Table 3.6: Stiffness and damping parameters for horizontal response of pile for homogenous soil profile and parabolic soil profile [38]



	ν	$\frac{E_{pile}}{G_{soil}}$	Stiffness parameters			Damping parameters				
			$f_{\phi,1}$	$f_{c,1}$	$f_{s,1}$	$f_{\phi,1}^*$	$f_{\phi,2}$	$f_{c,2}$	$f_{s,2}$	$f_{\phi,2}^*$
Homogeneous soil profile										
	0.25	10000	0.2135	-0.0217	0.0042	0.0021	0.1577	-0.0333	0.0107	0.0054
		2500	0.2998	-0.0429	0.0119	0.0061	0.2152	-0.0646	0.0297	0.0154
		1000	0.3741	-0.0668	0.0236	0.0123	0.2598	-0.0985	0.0579	0.0306
		500	0.4411	-0.0929	0.0395	0.0210	0.2953	-0.1337	0.0953	0.0514
	0.40	250	0.5186	-0.1281	0.0659	0.0358	0.3299	-0.1786	0.1556	0.0864
		10000	0.2207	-0.0232	0.0047	0.0024	0.1634	-0.0358	0.0119	0.0060
		2500	0.3097	-0.0459	0.0132	0.0068	0.2224	-0.0692	0.0329	0.0171
		1000	0.3860	-0.0714	0.0261	0.0136	0.2677	-0.1052	0.0641	0.0339
	0.25	10000	0.1800	-0.0144	0.0019	0.0008	0.1450	-0.0252	0.0060	0.0028
		2500	0.2452	-0.0267	0.0047	0.0020	0.2025	-0.0484	0.0159	0.0076
		1000	0.3000	-0.0400	0.0086	0.0037	0.2499	-0.0737	0.0303	0.0147
		500	0.3489	-0.0543	0.0136	0.0059	0.2910	-0.1008	0.0491	0.0241
	0.40	250	0.4049	-0.0734	0.0215	0.0094	0.3361	-0.1370	0.0793	0.0398
		10000	0.1857	-0.0153	0.0020	0.0009	0.1508	-0.0271	0.0067	0.0031
		2500	0.2529	-0.0284	0.0051	0.0022	0.2101	-0.0519	0.0177	0.0084
		1000	0.3094	-0.0426	0.0094	0.0041	0.2589	-0.0790	0.0336	0.0163
0.40	500	0.3596	-0.0577	0.0149	0.0065	0.3009	-0.1079	0.0544	0.0269	
	250	0.4170	-0.0780	0.0236	0.0103	0.3468	-0.1461	0.0880	0.0443	

Table 3.7: Values of the spring for pile-soil interaction

K_z	5.13609E+13
K_x	5.05048E+12
K_y	5.05048E+12
K_θ	5.13746E+13
K_ψ	3.28709E+13

The modelling of the concrete block and the values of the spring-dumper element are reported in Ansys FEM model Figure 3.22 and Figure 3.23.

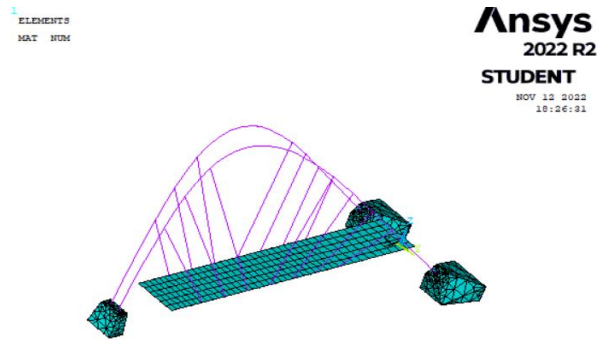


Figure 3.22: Ansys Third Model

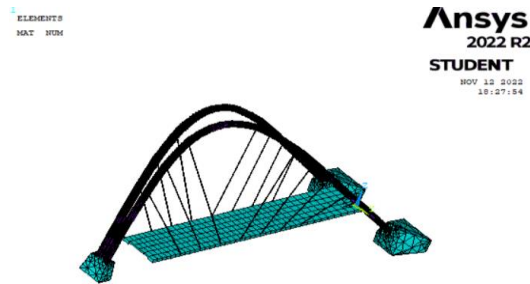


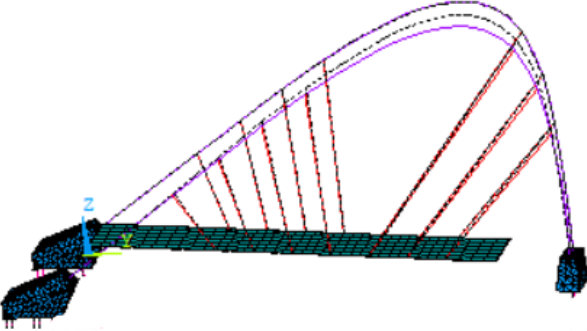
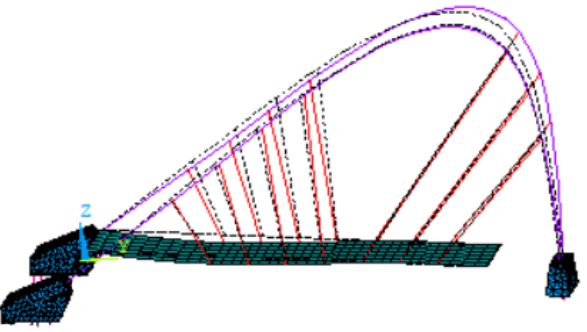
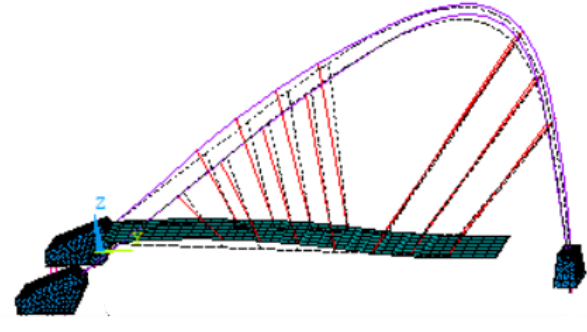
Figure 3.23: ANSYS FEM Third Model with the real shapes of the elements

Modal analysis with Lanczos method is performed:

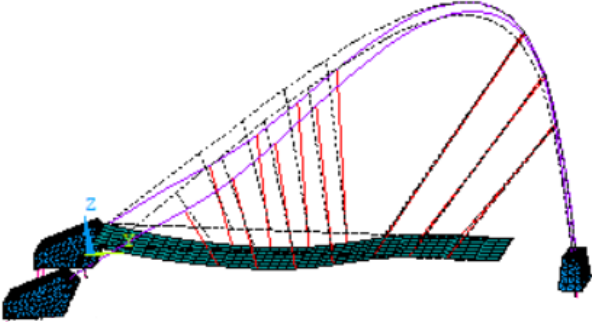
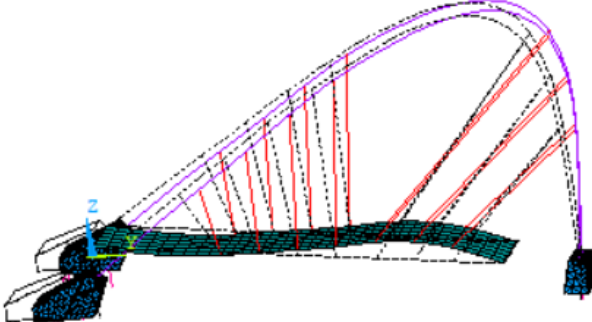
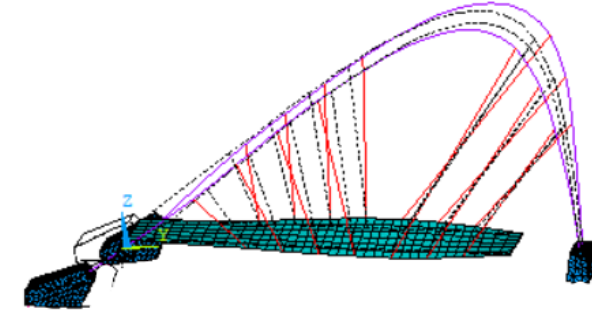
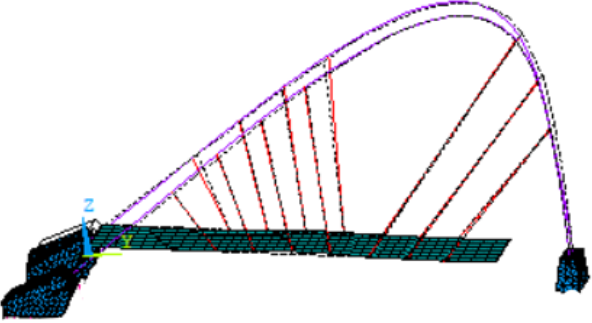
Table 3.8: Modal Shapes of third model result with Lanczos method

Mode	Frequency [Hz]	Modal Shape
La1	0.96	

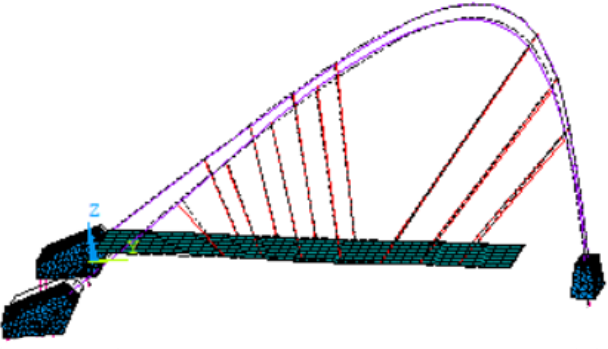
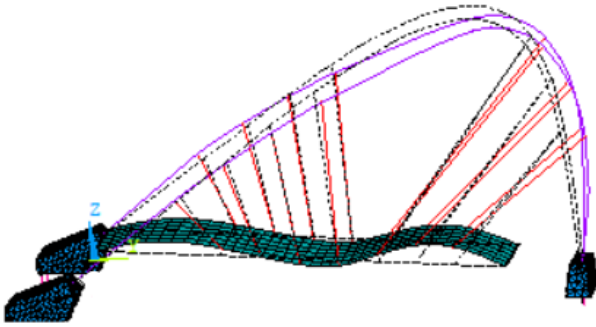
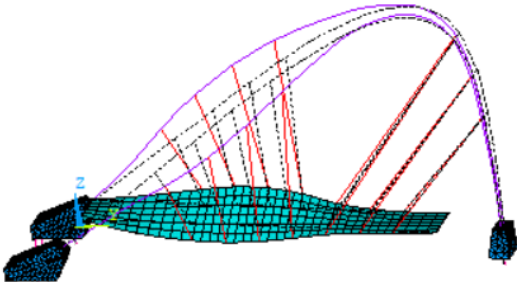
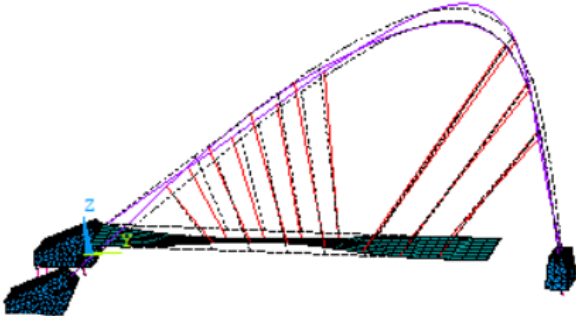
NUMERICAL MODELLING VS ON-SITE TESTING OF AN ARCH-SUSPENDED FOOTBRIDGE

La2	0.97	
Vd1	2.30	
La3	2.38	

NUMERICAL MODELLING VS ON-SITE TESTING OF AN ARCH-SUSPENDED FOOTBRIDGE

La4	2.56	
Vd2	3.25	
Td1	3.37	
Vd3	3.77	

NUMERICAL MODELLING VS ON-SITE TESTING OF AN ARCH-SUSPENDED FOOTBRIDGE

La5	3.78	
Vd4	4.72	
Td2	5.10	
Td3	5.15	

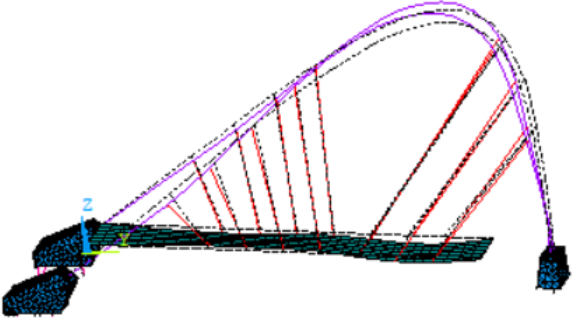
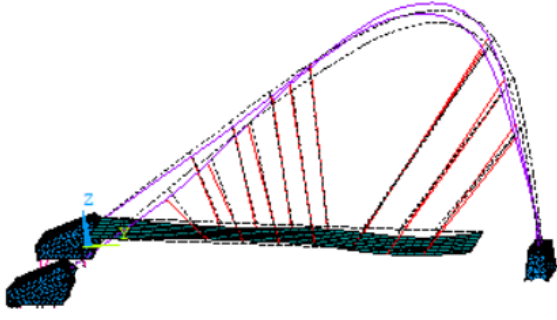
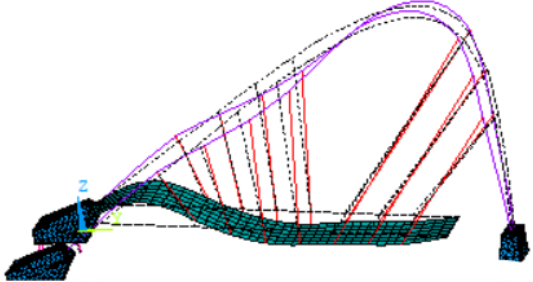
La5	5.42	
La6	5.42	
Vd5	5.98	

Table 3.9: Correlation between experimental and FEM model modal parameters of the Footbridge

Mode	Frequency [Hz]		Δf [%]
	Field	Fem	
Vd1	2.31	2.32	0.4329
La4	2.52	2.56	2.6
Td2	4.99	5.10	3.2
Vd5	5.73	5.98	4.3

The accuracy of the FE model improved, as shown in Table 3.9, exhibiting an error in each modal form frequency of less than 5%. Additionally, the torsional modal shape Td_2 was also detected.

3.6 Validation of the model

A representation of the fundamental dynamic properties of the structure is provided by the combination of modal pairs, or frequencies and modal shapes (Figure 3.24). The foundation for many more investigations, including the validation or update of numerical models, can be found in mode shapes. As a result, they either serve as the foundation for diagnostic analyses or allow for the assessment of the structure's state. The use of appropriate comparative techniques is necessary when conducting advanced analyses based on comparing dynamic characteristics discovered through experimental research of real structure and characteristics discovered through numerical analyses. One of the most significant problems is related to the 'pairing' mode shapes, both in terms of frequencies and mode shapes. This is especially true of more complex systems, which may have similar-looking modal shapes. The disparity in scale between the amplitude of the modal forms produced from the numerical model and experimental studies is another significant concern. Modal assurance criterion (MAC) is one of the most popular criteria, which is often used for comparing the mode shapes of natural modes.

$MAC_{ij} = \frac{ \Phi_{mi}^T \Phi_{aj} ^2}{(\Phi_{aj}^T \Phi_{aj})(\Phi_{mi}^T \Phi_{aj})}$	
---	--

where Φ_{aj} and Φ_{aj} are the experimental and numerical mode shape vector, respectively, and symbol T denotes the transposition. Only the mode shapes are compared by the criterion. Hence, it is also important to compare the natural frequencies in addition to the mode shapes. The resulting MAC matrix has elements with values ranging from zero (no match) to one (complete match). Together with the frequency comparison, this presentation enables us to choose the suitable modal pairs

from the experimental investigation and numerical analysis. It is assumed that the compatibility of mode shapes is high when the MAC value is greater than 0.90. The modal scale factor (MSF), which is the scaling factor for the mode shapes received from experimental tests in proportion to the parameter gained from numerical studies, was proposed along with the MAC criterion. The formula is used to express the coefficient.

$$MSF_i = \frac{\Phi_{aj}^T \Phi_{mi}}{\Phi_{mi}^T \Phi_{mi}}$$

The difference between experimental and numerical frequencies can be defined as:

$$f = \frac{f_a - f_m}{f_m} 100 [\%]$$

where f_m and f_a are the experimental and numerical frequencies in Table 3.10.

Table 3.10: Correlation between experimental and third FEM model modal parameters of the Footbridge

Mode	Frequency [Hz]		Δf [%]
	f_m	f_a	
Vd1	2.31	2.32	0.4329
La4	2.52	2.56	2.6
Td2	4.99	5.10	3.2
Vd5	5.73	5.98	4.3

After carefully examining the pre-existing circumstances of the second model, it was decided to add springs that account for pile-soil interaction, pretension effect through uniform thermal load mechanism, and concrete blocks to allow for relative displacements between the bases of the arches. In this manner, the FE model's accuracy improved, demonstrating an error in each modal form frequency of less than 5%. Additionally, the torsional modal shape Td_2 was ultimately detected and all the modal shapes match the experimental ones. (Figure 3.24).

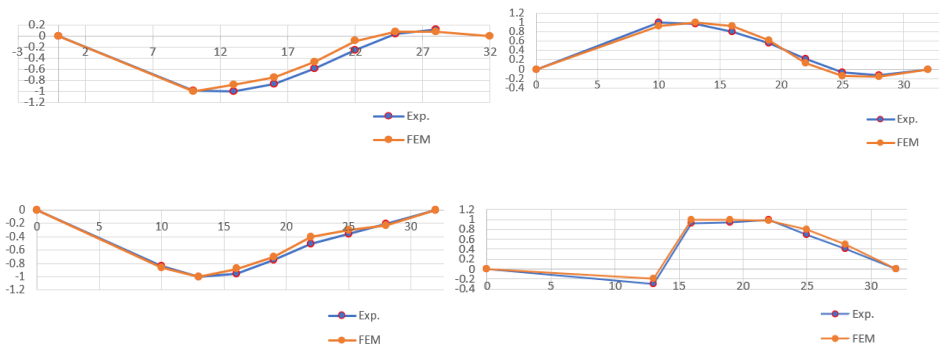


Figure 3.24: Comparison of modal shapes (field test—blue; FEM third model—orange).

This modelling update demonstrates that, for structures where an experimental campaign is conducted, employing the proper increasing implementation could result in a truly accurate model that allows for the execution of more tests. This approach saves time and is effective since it eliminates the need to plan further experimental campaigns. Additionally, a variety of solutions that can be used in real-world situations can be studied using the Model (i.e. installation of a TMDs system).

4 HIVOSS GUIDELINE

The HiVoSS [6] criteria for the design and inspection of footbridges are presented in this chapter. Even though HiVoSS stands for Human Induced Vibrations on Steel Structures, this paper serves as a useful manual for the design of footbridges composed of a variety of materials, including reinforced or pre-stressed concrete, timber spanning steel, and composite steel-concrete structures. This helpful tool was created to provide designers with clear answers who felt the need to pay more attention to the serviceability state of these types of structures regarding dynamic human induced loads in light of the Millennium Bridge and Passerelle Solférino cases. In fact, installing vibration mitigation technologies after the structure has been erected may result in a significant increase in the overall cost of construction.

4.1 Hivoss step-procedure

There are currently no applicable code regulations for the assessment of footbridges serviceability condition when there are pedestrians walking across them. The research project RFS-CR-03019, "Advanced Load Models for Synchronous Pedestrian Excitation and Optimized Design Guidelines for Steel Footbridges (SYNPEX)," which was funded by the Research Foundation for Coal and Steel, proposes design processes based on findings (RFCS) [6]. A flowchart of HiVoSS guidelines is presented in Figure 4.1 Design steps according to HiVoSS guidelines Figure 4.1.

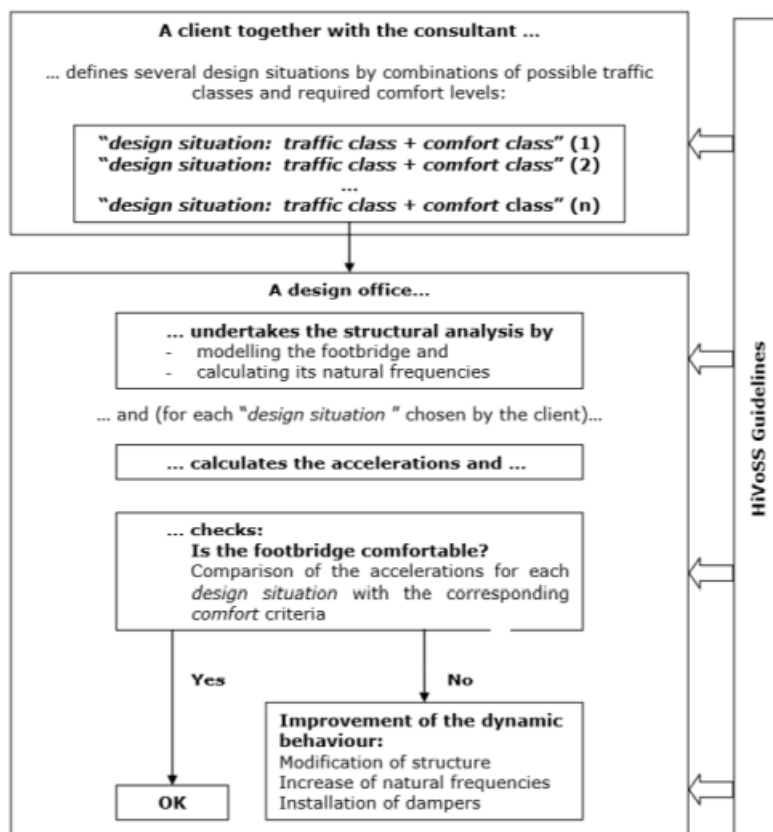


Figure 4.1 Design steps according to HiVoSS guidelines [6]

4.2 Evaluation of natural frequencies

The evaluation of natural frequencies during design can be done in two principal ways:

- By hand calculations;
- Through FE model;

It is generally acknowledged that even if manual calculations and streamlined techniques are effective tools, a precise calculation is necessary when the goal is to make sure that the footbridge's natural frequencies are outside a critical range. The model must, of course, be sufficiently accurate to accurately reflect the actual behaviour of the structure. After the footbridge is built, it is necessary to verify the material properties, the damping coefficient, and the interactions between the soil and the structure in order to validate the model and enable further tests.

4.3 Critical range of natural frequencies

According to HiVoSS recommendations, footbridges should have natural frequencies outside of a crucial range that changes depending on whether one looks at the vertical, antero-posterior, or medial-lateral orientation:

- For vertical and antero-posterior (also longitudinal) directions, the critical range is:

$1.25 \text{ Hz} \leq f_i \leq 2.3 \text{ Hz}$	
--	--

- For the medial-lateral direction (also lateral), the critical range is:

$0.5 \text{ Hz} \leq f_i \leq 1.2 \text{ Hz}$	
---	--

If the contribution of the second harmonic of the pedestrian load is taken into account, the interval for the antero-posterior direction (including longitudinal) may be increased

up to 4.6 Hz. Running pedestrians are not given a critical range for medial-lateral direction, but the critical range for vertical direction is adjusted as follows:

$1.9 \text{ Hz} \leq f_i \leq 3.5 \text{ Hz}$

4.4 Assessment of design situation: traffic classes and comfort classes

Since a specific level of comfort must always be guaranteed, design is always based on certain reference scenarios that can occur during the life cycle of the structure. Clearly, it is crucial to mimic actual traffic circumstances from the perspective of design. According to HiVoSS, design situations are defined through a combination of one of the 5 traffic classes given in Figure 4.2, and one of the 4 comfort classes listed in Figure 4.3.




Traffic Class	Density d (P = pedestrian)	Description	Characteristics
TC 1 ^{a)}	group of 15 P ; $d = 15 P / (B L)$	Very weak traffic	(B =width of deck; L =length of deck)
TC 2	$d = 0,2 P/m^2$	Weak traffic 	Comfortable and free walking Overtaking is possible Single pedestrians can freely choose pace
TC 3	$d = 0,5 P/m^2$	Dense traffic 	Still unrestricted walking Overtaking can intermittently be inhibited
TC 4	$d = 1,0 P/m^2$	Very dense traffic 	Freedom of movement is restricted Obstructed walking Overtaking is no longer possible
TC 5	$d = 1,5 P/m^2$	Exceptionally dense traffic	Unpleasant walking Crowding begins One can no longer freely choose pace

Figure 4.2 Traffic classes defined in HiVoSS, depending on pedestrians' density [6]

Comfort class	Degree of comfort	Vertical a_{limit}	Lateral a_{limit}
CL 1	Maximum	< 0,50 m/s ²	< 0,10 m/s ²
CL 2	Medium	0,50 – 1,00 m/s ²	0,10 – 0,30 m/s ²
CL 3	Minimum	1,00 – 2,50 m/s ²	0,30 – 0,80 m/s ²
CL 4	Unacceptable discomfort	> 2,50 m/s ²	> 0,80 m/s ²

Figure 4.3: Comfort classes depending on the maximum acceleration [6]

Traffic classes are established in terms of pedestrians' density while comfort classes in terms of footbridges acceleration.

Given the lifespan of the structure, it makes sense that the designer would select a comfort level that isn't extremely high for a scenario that might only occur once over the footbridge's lifetime. On the other hand, a higher level of comfort must be ensured for a circumstance that occurs frequently.

4.5 Assessment of structural damping

Damping is a very important parameter in the evaluation of amplitude of human induced oscillations and may depend on losses of energy due to material properties, all along the structure, and on local effects of bearings or vibration control systems. The majority of damping effects are created inside structural components, however non-structural components like railings and deck surface coverage can occasionally also play a significant impact.

Regrettably, none of the mechanisms results in dissipations that can be properly predicted during the design stage, and the accurate assessment of energy loss can only be done after the building of the footbridge.

Since civil engineering structures are usually light damped, it is customary and generally accepted to describe damping in terms of a linear model. In practice, forces that are linearly proportional to velocity are used to simulate damping effects in the viscous damping model.

To determine the damping coefficient to be used in the equations of motion, HiVoSS gives, in Figure 4.4, mean and average values of damping coefficient to use in service load cases for different footbridge construction materials.

Construction type	Damping ratio ξ
Reinforced concrete	5,0%
Prestressed concrete	2,0%
Steel, welded joints	2,0%
Steel, bolted joints	4,0%
Reinforced elastomers	7,0%

Figure 4.4: Values of structural damping proposed by HiVoSS [6]

4.6 Determination of maximum acceleration

The maximum acceleration that footbridge points can experience is the criterion required to assess a footbridge's comfort level. Acceleration is the factor that affects how footbridge users perceive the situation. Three distinct approaches to estimating the maximum acceleration are put forth in HiVoSS. One is a spectrum design method, while the other two are based on time domain analysis (Figure 4.5).

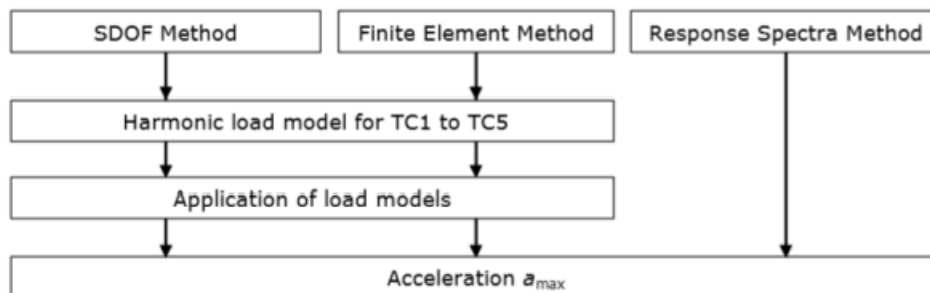


Figure 4.5: 1 Proposed methods for the computation of maximum acceleration [6]

For a SDOF system and FE methods, the determination of a_{max} is done through harmonic analysis. The third method relies on the application of an empirical formula “based on numerical time step simulations of various pedestrian streams on various

bridges geometries” with a Monte Carlo approach. But we'll concentrate on describing the FE approach that will be used with Ansys.

4.7 Harmonic load model

It was clear from CHAPTER 1 how many variables there are that affect human-induced loads and how challenging it is to model them. However, in HiVoSS, the human induced load is represented by a simple harmonic load in order to provide a design technique accounting for all the problem's characteristics while, at the same time, for the need of a simplified solution. The number of synchronized pedestrians on the structure is first introduced as a concept. It is noted that it is possible to spot an equivalent number of people n' walking in perfect synchronicity with one another inside a crowd of pedestrians made up of n people strolling in a random way.

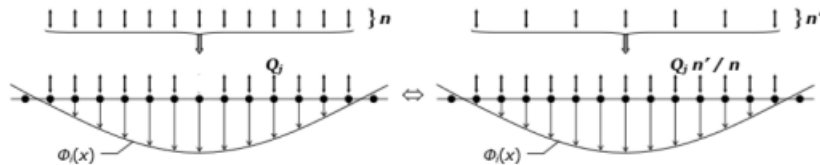


Figure 4.6:*The equivalent number of synchronized pedestrians n' is a part of the total number of pedestrians n on the loaded surface [6]*

It has been demonstrated that this load can be expressed as a deterministic load and that this is sufficient to assess the level of comfort of a footbridge in a very realistic way. After an analytical derivation for a straightforward situation, the background material attached to HiVoSS explains that n' was determined "by regression as a function of the damping ratio and the total number of pedestrians on the footbridge." As a function of the design traffic class, two expressions for this parameter are provided:

- Traffic classes from TC1 to TC3 and $d < 1.0 \text{ ped/m}^2$:

$n' = \frac{10.8\sqrt{\xi n}}{s}$	
-----------------------------------	--

- Traffic classes TC4 and TC5 and $d \geq 1.0 \text{ ped/m}^2$

$n' = \frac{1.85\sqrt{\xi n}}{s}$	
-----------------------------------	--

Where:

- n' is the equivalent number of synchronized pedestrians on the loaded surface;
- n is the number of pedestrian inside the stream;
- ξ is the damping coefficient;
- S is the loaded surface of the footbridge;
- d is the pedestrian density on the loaded surface.

4.8 Application of the load model

The harmonic load model mentioned in the preceding section is described as a cosinusoidal evenly distributed load that depends on time and one of the structure's eigenfrequencies:

$p(t) = P \cos(2\pi f_s t) n' \psi$	
-------------------------------------	--

Where:

- P is the component of the force due to a single pedestrian with a walking step frequency f_s ;
- f_s is the step frequency, which is assumed equal to the footbridge natural frequency under consideration;
- n' is the equivalent number of pedestrians on the loaded surface S ;
- S is the area of the loaded surface;
- Ψ is the reduction coefficient taking into account the probability that the footfall frequency approaches the critical range of natural frequencies under consideration.

It is necessary to apply the load in accordance with a clear logic. First, the load's positive direction must match the structure's researched deformed shape (such as the HiVoSS example in Figure 4.7), and second, the frequencies at which the verification

will be conducted must be carefully chosen. Analysing frequencies that would never be excited by a walking pedestrian would be pointless.

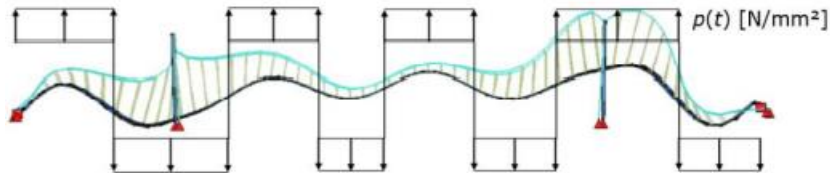


Figure 4.7: Example of load application for the walking pedestrians load case [6]

In order to ensure that the frequency under study is inside the critical interval described in section 4.3, the coefficient is therefore required. Its value is calculated using either the curve suggested for the case of vertical or longitudinal oscillations or the case of lateral ones in Figure 4.8.

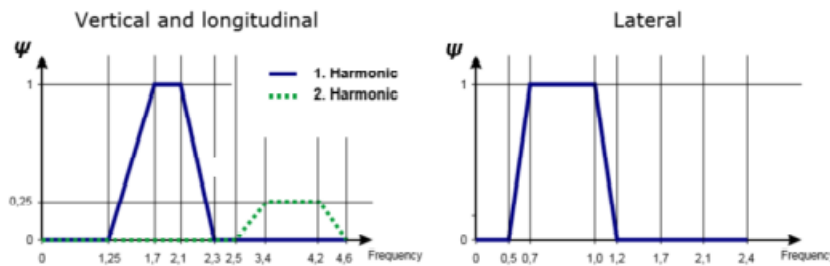


Figure 4.8: Graphics for the computation of the Ψ reduction coefficient [6]

Finally, the kind of the modal shape under consideration must be taken into account while selecting the P parameter. The load model that was just stated only takes into account a stream of people using footbridges to walk. The design load model for running pedestrians is only mentioned in Section 9 of the HiVoSS Background Document. Here, the number of running pedestrians crossing the footbridge tout court is equal to the comparable number of synchronized runners. The load model is still harmonic, but it differs from the situation with pedestrians walking since it now represents a concentrated load and needs to be applied to the node of the analysed modal shape with the greatest displacement. The relationship given below explains the model:

$p(t, v) = P \cos(2\pi f_s t) n' \psi$	
--	--

Where all symbols have the same meaning as in the case of the walking pedestrians load except n' , which in this case does not have a dimension, and where v is the runner's speed over the footbridge, which is by default set to zero. In this case, the interval of critical frequencies is different and verifications must be done only according to the vertical direction. The P parameter, in order to well represent this different kind of induced load, has always the value of 1250 N while the determination of the Ψ coefficient is based on Figure 4.9.

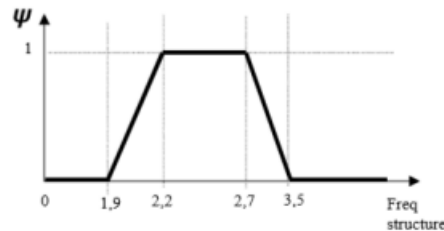


Figure 4.9: Graphic for the computation of the Ψ reduction coefficient for the running pedestrians load case [6]

4.9 check of criteria for lock-in

When the frequency of the excitation is close to one of the natural frequencies of the structure, the lock-in phenomena takes place. It results in the overall damping diminishing, causing the structure to respond suddenly with an enhanced reaction. The human body works as negative dampers when a footbridge vibrates slightly, introducing energy into the system and starting the lock-in phenomena. Although this is not the main emphasis of the work, two approaches are suggested to verify this issue in HiVoSS and its underlying material. The first is based on determining the bare minimum of individuals required to trigger the lock-in phenomena, while the second is based on figuring out the minimal rate of acceleration prior to the lock-in.

4.10 check of comfort level

After doing calculations and verifications, the designer's job is to determine if the values of accelerations adhere to the comfort class minimal requirements that were established during the design process.

If this does not happen, four possible solutions are proposed:

- Modification of the mass;
- Modification of the frequency;
- Modification of the structural damping,
- Addition of damping

It is always advised to take into account the possibility of installing damping devices on the footbridge from the design phase onward in order to avoid problems with space and adaptation on the existing structure, given the great variability affecting the structure and the pedestrians, even if the design shows a good behaviour of the structure. The guidelines include recommendations for controlling vibration response as well as some recommendations for measuring, testing, and evaluating the dynamic features of existing footbridges.

5 DYNAMIC ANALYSES

This section details both the results of employing the HiVoSS recommendations and the results of a method that takes into consideration the time variation of human-induced forces produced during running. So, after a summary of the work the approach is based on, the Matlab code built to produce a text file readable by Ansys is described. As the runner goes across the footbridge, the RealRun1 code [39] has been used to generate time-varying loads on mesh nodes and update their positions at each load step. However, according to Hivoss and as a result of the Matlab code, a preliminary check was made for the situation of a group walking pedestrian before results for the running human example were presented. It is confirmed that this load case, for the natural frequency lying in the HiVoSS interval of critical frequencies for walking pedestrians, induces relevant deck accelerations.

5.1 Running pedestrian induced load

A description of the load transmitted by walking people was given in CHAPTER 1. The main characteristics of the load, including a considerable inter- and intra-subject variability and its stochastic nature, were made clear through the analysis of various researches. Here, a few important details are pointed out. Three distinct components make up the walking pedestrian induced load, commonly referred to as Ground Reaction Force (GRF): vertical, longitudinal, and lateral. For biomechanical reasons, the determination of their time histories continues to be the subject of research today as it has been for the past few decades. The challenge lies in the difficulty to sample this type of loads without accounting for boundary constraints, which could be represented by the stiffness of plates or treadmills, shoes, interaction with other pedestrians, etc. However, a good agreement is typically established for the M-shaped vertical component of the GRF for walking pedestrians.

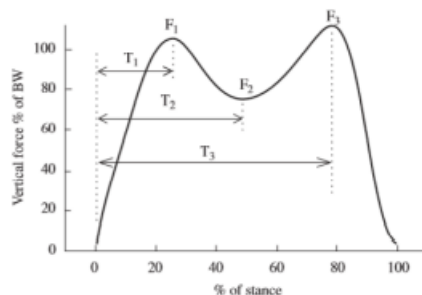


Figure 5.1: Time history of GRF vertical component for a walking pedestrian [40]

This unique shape is the result of how bodyweight and inertial loads are transferred to the ground during the gait cycle, as it was shown previously. Figure 5.1, however, only depicts the stress brought on by a single step. More research was done to find a possible relationship between the pedestrian's speed and the length of support phases because steps are taken in succession while walking and the so-called double support phase includes a period when both feet are on the ground. It was found that as speed increases, the double support phase gets shorter until it is eventually so brief that it no longer exists when the pedestrian begins to run. Additionally, it was found that the load's time history form was depending on speed. The difference between the vertical

components of the human-induced load when walking or running is made clear in Figure 5.2.

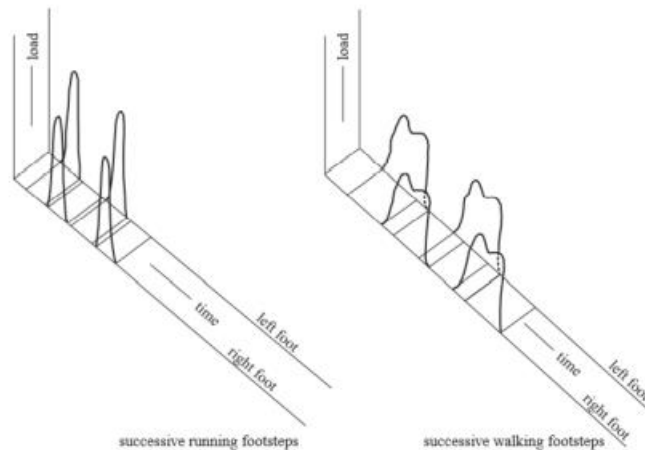


Figure 5.2: Vertical components of GRFs for both feet and two different gaits [41]. On the left the case of the running pedestrian: no double support phase and no more M shape of the load.

There hasn't been a need to examine GFRs of moving pedestrians up until recent times, which has resulted in a dearth of details and descriptions of this unique load. In actuality, following the cases of the Millennium Bridge and Passerelle Solférino, the academic community turned its attention to GRFs caused by walking pedestrians with the goal of finding design methods while simultaneously taking into account the challenge of modelling this stochastic load and the need for an easily implementable design method. The findings have been formulated as recommendations, such as HiVoSS, which is discussed in CHAPTER 4, and SETRA [7], "Technical guide for assessment of vibrational behaviour of footbridges under pedestrian loading," where the issue of running pedestrians is only cursorily addressed. However, in recent years, there has been a renewed interest in this issue. As competitions are being held in urban settings more frequently, footbridges must be comfortable enough to be used in these settings as well. As a result, research was carried out globally in an effort to develop a trustworthy design methodology that can satisfy the concerns of engineers.

5.2 RealRun1

The Matlab-written numerical code RealRun1 [39] creates a text file in accordance with the Ansys Mechanical APDL code guidelines for the execution of a transient analysis of a footbridge loaded by a moving pedestrian. The code generates nodal loads time histories that are produced by a single person moving across space, based on a load time history of any sort, such as the one shown in the preceding section. The algorithm was created on the fundamental assumption that the runner could proceed only along a rectilinear track parallel to the footbridge's axis, not necessarily coincident with one of the mesh lines along the y-direction. The most important conceptual steps at the base of the code can be synthesized in the following list:

1. Definition of fundamental variables:
 - Time duration to cross the footbridge;
 - Coefficients α e β of the Rayleigh damping;
 - Coordinates of the first contact point on the footbridge;
2. Reading of the load time history that must be post-processed;
3. Reading of the Ansys input file to store deck nodes and their coordinates;
4. Generation of the output load time history from the input load time history of the load as a function of the computed time to cross the footbridge and correction of oscillations of the load during the time in which cycles should represent the flying phase for models where negative values of load are possible;
5. Definition of coordinates of contact points along the trajectory and determination of coordinates of nodes over which the load will be transmitted at each load cycle;
6. Computation, for each load cycle, of nodal loads using shape functions to transform the runner induced pedestrian load. The shape functions transform the vertical load induced by the pedestrian in a generic point of the deck in vertical forces and bending moments in longitudinal and transversal direction,

acting on the nodes of the mesh grid surrounding the vertical load. Figure 5.3 describes the way the shape functions are exploited.

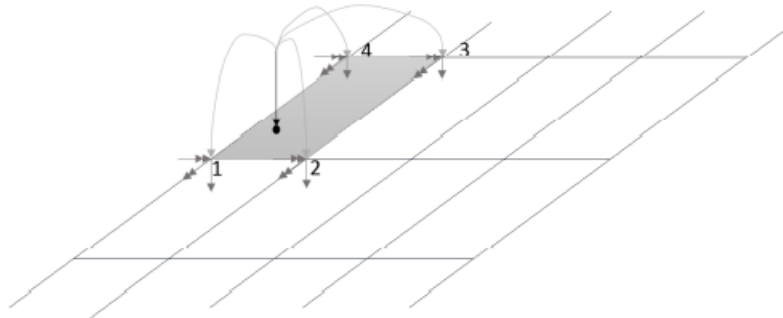


Figure 5.3: Graphical representations of the role of shape functions: the vertical load induced from the pedestrian is transformed into nodal forces and bending moments [39].

7. Generation of the text file readable by Ansys for the execution of a transient analysis under the varying nodal loads.

The flow chart for the generation of the code is presented in Figure 5.4.

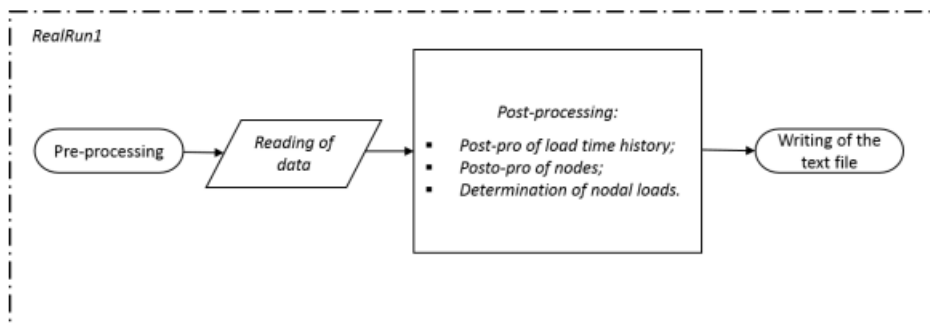


Figure 5.4: Flow-chart for the generation of RealRun1 [39].

5.3 Setra modeling for running pedestrian

The two models mentioned in the SETRA *Technical Guide for Footbridges Assessment of vibrational behaviour of footbridges under pedestrian loading* [7] are described here. The first of them uses positive sine function values to represent the force produced by the runner, while the second makes use of a Fourier series made up of three sine functions.

Running is characterized by a discontinuous contact with the ground, with the frequency f_m typically falling between 2 and 3.5 Hz, as stated in section 1.3.

The vertical component of the human-induced load is approximated, as with the first model outlined in SETRA, by a straightforward.

$F(t) = k_p G_0 \sin\left(\frac{\pi t}{t_p}\right) \text{ for } (j-1)T_m \leq t \leq (j-1)T_m + t_p$	
$F(t) = 0 \text{ for } (j-1)T_m + t_p \leq jT_m$	

Where:

- k_p the impact factor $k_p = \frac{F_{max}}{G_0}$
- j : the step number;
- F_{max} : the maximum load;
- G_0 : the weight of the pedestrian;
- t_p : the period of the contact;
- Tm : the period ($Tm = \frac{1}{fm}$), fm being the frequency of running

It should be observed that $= \frac{Tm}{2}$. This approximation of the period of contact t_p is an overestimation of the values measured experimentally, which are represented according to the frequency of running on the graph in Figure 5.5.

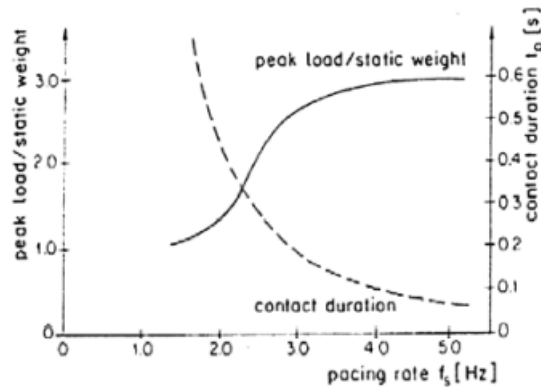


Figure 5.5: Change in the period of contact according to frequency [7]

As for the values of the impact factor k_p , these are inferred from Figure 5.6, according to the relative period of contact $\left(\frac{t_p}{T_m}\right)$.

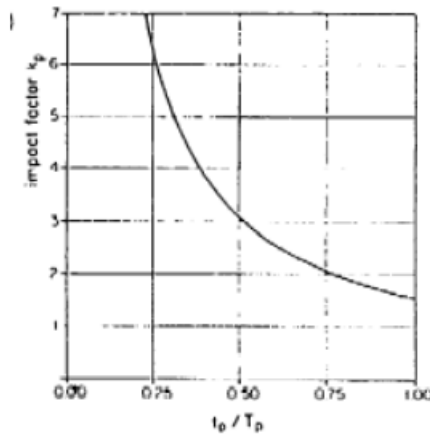


Figure 5.6: Running: impact factor according to the relative period of contact [7]

Figure 5.7 reports the load time history that was obtained using the sinusoidal pattern to model the run over the footbridge with reference to our study case, a pedestrian with a weight of 81.5 Kg, a running speed of 2.2 m/s and a step frequency of 2.3 Hz.

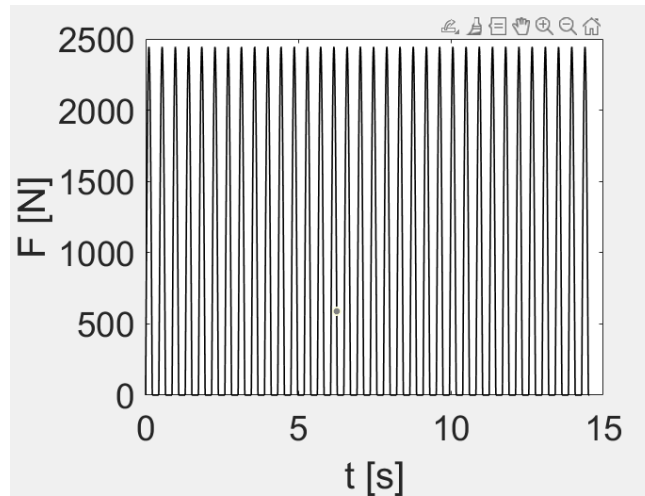


Figure 5.7: Time history of the running pedestrian induced load according to the SETRA sinus load model using a mass of 81.5 Kg, a running speed of 2.2 m/s.²

This is the easiest way to represent the force produced by a running pedestrian. In order to judge the quality of this modelling it would be necessary to compare results of a dynamic analysis performed using this modelling method with measurements collected on a real structure.

According to SETRA, a Fourier transform can be used to model the running pedestrian induced load. This has the advantage of not explicitly considering the impact factor k_P , which is difficult to be determined. Only the positive part of the transform is kept in order to account for the natural discontinuous contact when running, and it can be expressed using the previous notation:

$F(t) = G_0 + \sum_{i=1}^n G_i \sin(2\pi i f_m t) \quad \text{for } (j-1)T_m \leq t \leq \left(j - \frac{1}{2}\right)T_m + t_p$	
$F(t) = 0 \quad \text{for } \left(j - \frac{1}{2}\right)T_m + t_p \leq jT_m$	

In this case, the phase shifts are not considered relevant, and the first three harmonics' amplitudes are average values, with these coefficients being, strictly speaking, a function of the running frequency as k_P (Figure 5.8):

$G_1 = 1.6G_0$	$G_2 = 0.7G_0$	$G_3 = 0.2G_0$
----------------	----------------	----------------

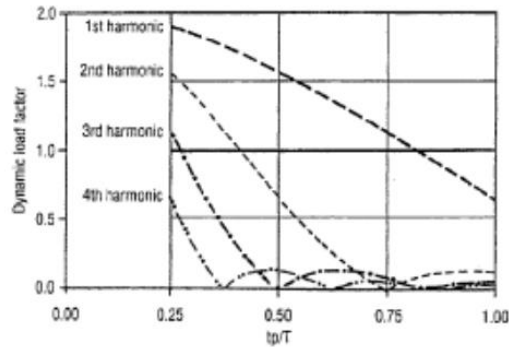


Figure 5.8: Amplitude of the various harmonics [7]

Again, taking into account the study case, the load time history obtained using this model resembles that produced using the sinusoidal model, a pedestrian with a weight of 81.5 Kg, a running speed of 2.2 m/s² and a step frequency of 2.3 Hz.

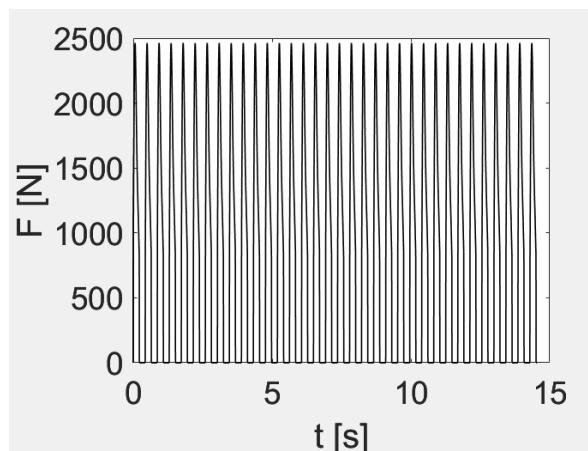


Figure 5.9: Time history of the running pedestrian induced load according to the SETRA Fourier series load model

When examining each load cycle in detail, it becomes clear that the signal is periodic here as well, but unlike the previous instance, the individual load cycles are slightly less pure sine-like in shape. In this way, the computed force should be more closely related to the load signal actually produced by a running pedestrian.

5.4 Walking pedestrians' analysis: Hivoss

To evaluate the level of comfort of a footbridge subjected to walking pedestrians-induced loads, in accordance with Hivoss rules and as previously indicated in Chapter 4 devoted to Hivoss Guideline, it is necessary to determine the following elements of the problem:

- Traffic Class or people density over the footbridge;
- Natural frequencies of the footbridge in the interval $1.25 \leq f_i \leq 2.5$ Hz, coincident with the interval of human walking frequencies;
- Damping coefficient;
- Prescribed comfort Class or maximum accepted acceleration;

The verification procedure prescribes “the application of the following harmonic load”:

$p(t) = P \cos(2\pi f_s t) n' \psi$	
-------------------------------------	--

uniformly distributed on the footbridge deck and applied with positive direction according to the considered modal deformed shape. Modulus of the distributed load is determined on the base of the geometry of the structure and of the following variables:

Where:

- P is the component of the force due to a single pedestrian with a walking step frequency f_s ;
- f_s is the step frequency, which is assumed equal to the footbridge natural frequency under consideration;
- n' is the equivalent number of pedestrians on the loaded surface S ;
- S is the area of the loaded surface;
- Ψ is the reduction coefficient taking into account the probability that the footfall frequency approaches the critical range of natural frequencies under consideration;

The length and width of the footbridge deck are $L = 32 \text{ m}$ and $B = 4.5 \text{ m}$. The TC1 and TC2 traffic class, corresponding to a very weak and weak traffic, were chosen. The reduction coefficient was determined for the third eigenfrequency of the structure, laying in the critical interval of frequencies.

Table 5.1: Parameters for the computation of the modulus of the distributed load according to Hivoss guidelines for the case of walking pedestrians TC1.

Parameter	Value	Note
$d \left[\frac{P}{m^2} \right]$	0.104	Traffic class 1 with $d = \frac{n}{BL}$ and $n=15$
$f_i = f_s$	2.31	Eigenfrequency in the critical interval
ξ [%]	0.6	Damping coefficient
$a_{max} \left[\frac{m}{s^2} \right]$	0.5	Comfort Class 1
P [N]	280	
$n \left[\frac{1}{m^2} \right]$	0.0187	$n' = \frac{10.8\sqrt{\xi n}}{S}$
S [m^2]	144	$S = BL$
Ψ [-]	0.68	Linear interpolation

Table 5.2: Parameters for the computation of the modulus of the distributed load according to Hivoss guidelines for the case of walking pedestrians TC2.

Parameter	Value	Note
$d[\frac{P}{m^2}]$	0.2	Traffic class 2
$f_i = f_s$	2.31	Eigenfrequency in the critical interval
ξ [%]	0.6	Damping coefficient
$a_{max}[\frac{m}{s^2}]$	1.0	Comfort Class 2
P [N]	280	
$n[\frac{1}{m^2}]$	0.312	$n' = \frac{10.8\sqrt{\xi n}}{S}$
S [m^2]	144	$S = BL$
Ψ [-]	0.68	Linear interpolation

Considering the data listed in Table 5.2 and Table 5.1, the modulus of the load generated by walking pedestrian according to Hivoss guidelines is equal to:

$p = 3.56 N/m^2$	For TC1
------------------	---------

$p = 59.4 N/m^2$	For TC2
------------------	---------

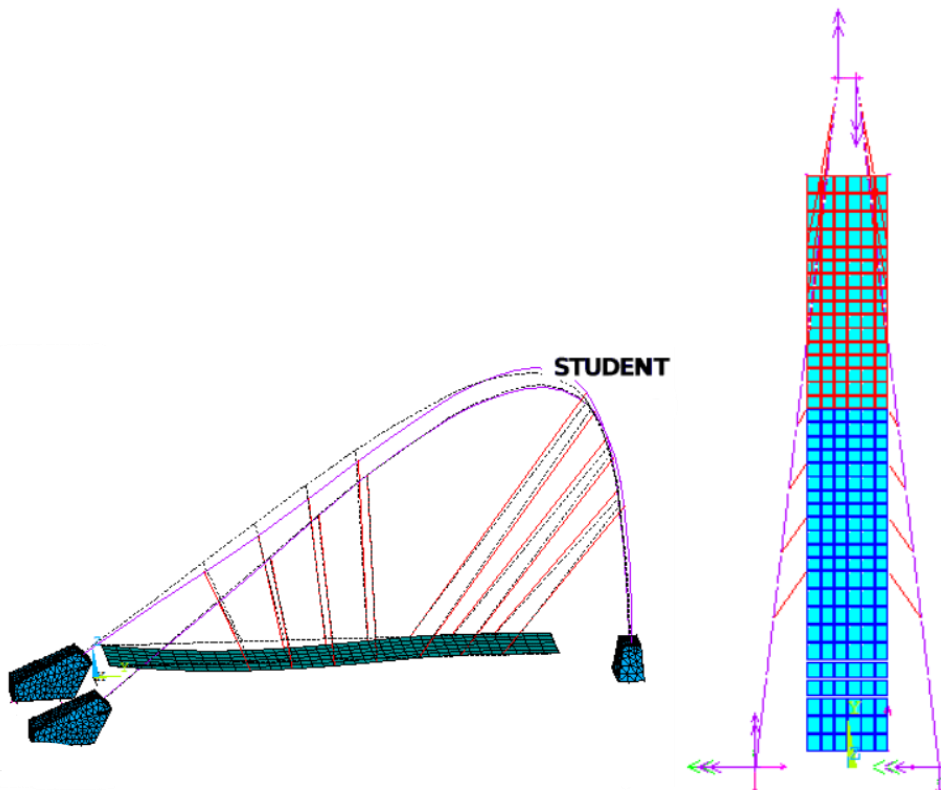


Figure 5.10: Analysed modal shape of the footbridge in a); applied distributed load for the case of the walking pedestrians in accordance with modal shape displacement b).

Concentrated vertical loads applied on each node of the deck grid were computed by multiplying the distributed load by the influence area of each node. Moreover, as suggested by Hivoss guidelines, the direction of distributed loads follows the modal shape displacement (Figure 5.10).

5.4.1 Harmonic analysis for walking pedestrians: results

It is necessary to calculate accelerations from displacements because Ansys only outputs displacements for this type of analysis and the evaluation of comfort level is established as a function of the maximum limit acceleration. Let's look at the most basic scenario of a single degree of freedom (SDOF) system being affected by a harmonic force. Its behaviour is described by the equation of motion:

$$\ddot{x}(t) + 2\xi\omega_1\dot{x}(t) + \omega_1^2x(t) = \frac{F}{K}\omega_1^2\sin(\omega t)$$

Where:

- $\ddot{x}(t), \dot{x}(t), x(t)$ are acceleration, velocity and displacement;
- ξ is the damping coefficient;
- ω_1 is the fundamental frequency of the SDOF;
- F is the amplitude of the force;
- k is the stiffness of the SDOF;
- ω is the frequency of the harmonic force.

The solution of the equation is:

$$x(t) = e^{-\xi\omega_1 t} \left(A \cos(\omega_1 t \sqrt{1 - \xi^2}) + B \sin(\omega_1 t \sqrt{1 - \xi^2}) \right) + x_p(t)$$

Ansys provides displacements for the steady state response, which in this case is $x_p(t)$, a specific integral of the motion equation. Analytical results for the SDOF system under harmonic load are as follows:

$$x_p(t) = \frac{F}{k} N(\beta) \sin(\omega t - \Phi)$$

Where:

- $N(\beta) = 1/\sqrt{(1 - \beta^2)^2 + 4\xi^2\beta^2}$ is the magnification factor;
- $\beta = \omega/\omega_1$ is the frequency ratio;
- $\Phi = \arctan\left(\frac{2\xi\beta}{1 - \beta^2}\right)$ is the phase angle between the excitation and the response.

Therefore, it is sufficient to differentiate twice the analytical expression for displacements with respect to time in order to obtain the system's acceleration. Both the square of the exciting frequency and displacements are related to acceleration.

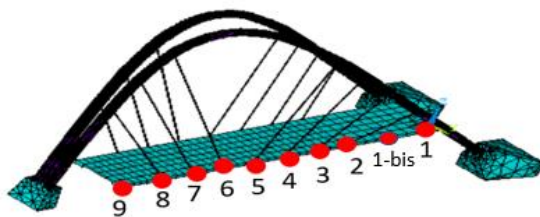
$$\ddot{x}_p(t) = -\frac{F}{K} \omega^2 N(\beta) \sin(\omega t - \Phi)$$

The maximum accelerations of the nodes in the footbridge under consideration will be obtained using this approach. This result can be extended to multi degrees of freedom (MDOF) systems.

The analytical solution $x_p(t)$, which projects the entire complex solution onto the imaginary axis of the "Argand's plane," is obtained by using the complex exponential.

$$\ddot{x}_p(t) = -\frac{F}{K} \omega^2 e^{i(\omega t - \Phi)}$$

Nodes for which results are recorded are showed in Figure 5.11. The nodes selected are the same of the experimental tests in order to have a comparison with them, a node 1 bis is added for a better understanding of the 10 m span.



Node	x	y	z
1	2.25	0	1.51
1-bis	2.25	5	1.51
2	2.25	10	1.51
3	2.25	13	1.51
4	2.25	16	1.51
5	2.25	19	1.51
6	2.25	22	1.51
7	2.25	25	1.51
8	2.25	28	1.51
9	2.225	32	1.51

Figure 5.11: Position of nodes for which results have been extracted and reported here

Following this solution approach, Ansys gives displacements results in term of real, imaginary and amplitude values of displacements (Figure 5.12).

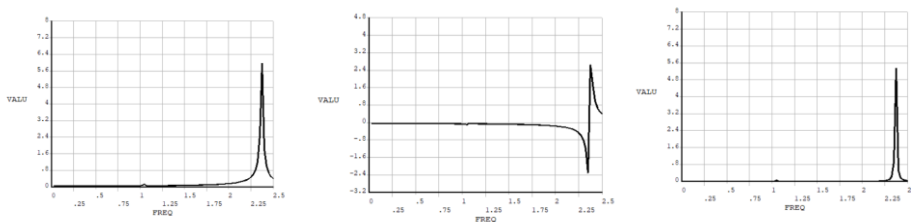


Figure 5.12: Resonance curves of a) amplitude, b) real part and c) imaginary part of vertical displacements for node 2 (x=10 m) for the case of walking pedestrians at a frequency $f=2.3$ Hz.

The numerical values of displacements and accelerations computed for each of the nodes are listed in for Table 5.3 TC1 and Table 5.4 for TC2.

Table 5.3: Max displacement and acceleration at selected nodes for TC1

Points	Displ. [mm]	Acc. [m/s^2]
1	0	0
1-bis	1.3	0.27
2	1.7	0.35
3	1.3	0.27
4	0.7	0.14
5	0.11	0.023
6	0.11	0.023
7	3.5E-02	0.006
8	3.5E-02	0.007
9	0	0

Table 5.4: Max displacement and acceleration at selected nodes for TC2

Points	Displ. [mm]	Acc. [m/s^2]
1	0	0
1-bis	2.1	0.4381
2	5	1.0431
3	5	1.0431
4	5	1.0431
5	2.3	0.4798
6	0.43	0.0897
7	0.43	0.0897
8	0.43	0.0897
9	0	0

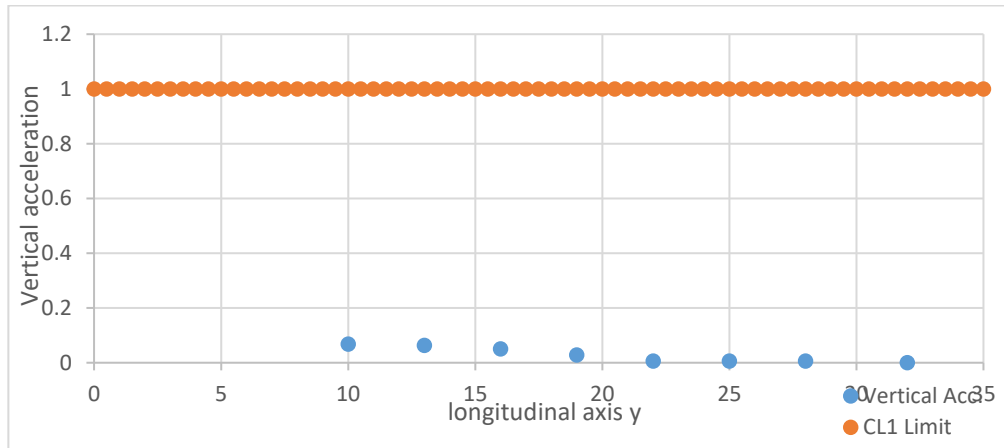


Figure 5.13: Vertical accelerations at selected nodes along the footbridge for TC1

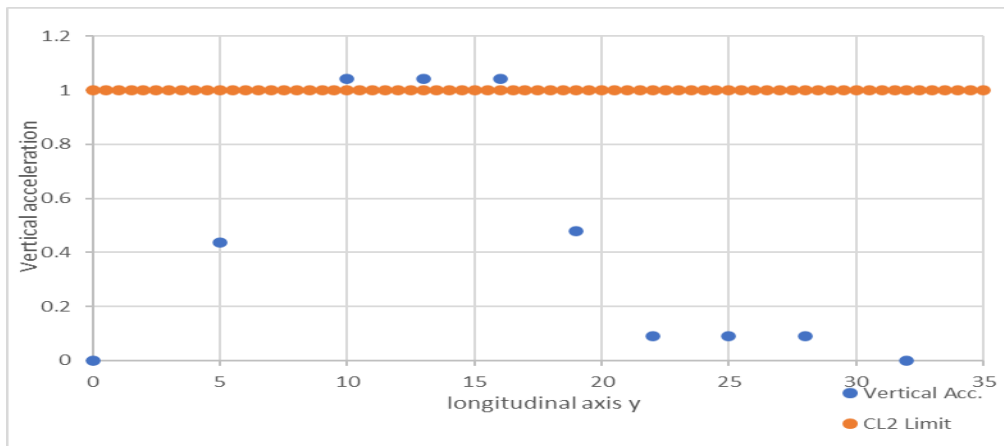


Figure 5.14: Vertical accelerations at selected nodes along the footbridge for TC2

The peak of the response of appears when the load has the frequency equal to the eigenfrequency of the structure. Since the acceleration limit for comfort class 1 is equal to 0.5 m/s^2 , Table 5.3 shows that for the TC1 (Traffic Class 1=15 people) the degree of comfort is acceptable whichever the position of the receiver is on the deck of the footbridge (Figure 5.13). The maximum value of displacements for TC2 is equal to 5 mm (corresponding to node 2). As a consequence, the acceleration generated by the passage of 29 people over the footbridge according to Hivoss is equal to 1.04 m/s^2 . Since the acceleration limit for comfort class 2 is equal to 1 m/s^2 , accelerations slightly exceed the limit degree of comfort of CL2. These results (Figure 5.14) shows the difference in term of stiffness between the first part related to the 10m span and the last part of the footbridge. Not only hanger spacing brings a critical behaviour in

the first part of the structure but also the arches development along the footbridge, as a matter of facts the first part shows more flexible behaviour due to the prevalent bending contribution while the last part where the main contributions is given by axial stiffness of the arch.

5.5 Running pedestrian' analysis: Hivoss

The procedure of Hivoss guidelines for the running pedestrians differs from that for walking pedestrians first for the critical interval of frequencies $1.9 \leq f_s \leq 3.5 \text{ Hz}$. A second difference concerns the load model. In the case of the running pedestrian it is expressly specified that “the proposed load model is a single load $P(t,v)$ which is moving across the bridge with a certain velocity v of the joggers. The single load $P(t,v)$ is defined as:

$P(t, v) = P \cos(2\pi f_s t) n' \psi$	
--	--

Parameters related to this load model and used in the harmonic analysis according to Hivoss guidelines are presented in Table 5.5.

Table 5.5: Parameters for the computation of the modulus of the concentrated load according to Hivoss guidelines for the case of n running pedestrian.

Parameter	Value	Note
$d[\frac{P}{m^2}]$	0.0069	Traffic class 1
$f_i = f_s$	2.31	Eigenfrequency in the critical interval
ξ [%]	0.6	Damping coefficient
$a_{max}[\frac{m}{s^2}]$	0.5	Comfort Class 1
P [N]	1250	
$n[\frac{1}{m^2}]$	1	$n' = n$
S [m^2]	144	$S = BL$
Ψ [-]	1	Linear interpolation

The computed value of the load modulus is:

$P = 1250 N$

5.5.1 Harmonic analysis for running pedestrian: results

The solution is given in terms of amplitude and real and imaginary parts of displacements. The resonance curves for the node 2 that presents the maximum displacement are depicted in Figure 5.15.

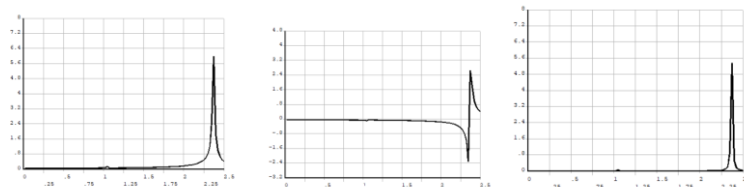


Figure 5.15: Resonance curves of a) amplitude, b) real part and c) imaginary part of vertical displacements for node 2 ($x=10m$) for the case of running pedestrian.

Table 5.6: Max displacements and accelerations at selected nodes

Points	Displ. [mm]	Acc. [m/s^2]
1	0	0
1-bis	0.44	0.0917
2	0.5	0.1043
3	0.5	0.1043
4	0.46	0.0959
5	0.29	0.0605
6	0.0334	0.0069
7	0.17	0.0354
8	0.2	0.0417
9	0	0

Maximum vertical displacement and acceleration for each point is listed in Table 5.6, all the acceleration obtained are in the maximum degree of comfort (Figure 5.16). For a single running pedestrian either displacement or acceleration are not relevant for CL1, moreover it can be seen that the response of the footbridge shows higher results in the first part related to the 10 m span than the last one.

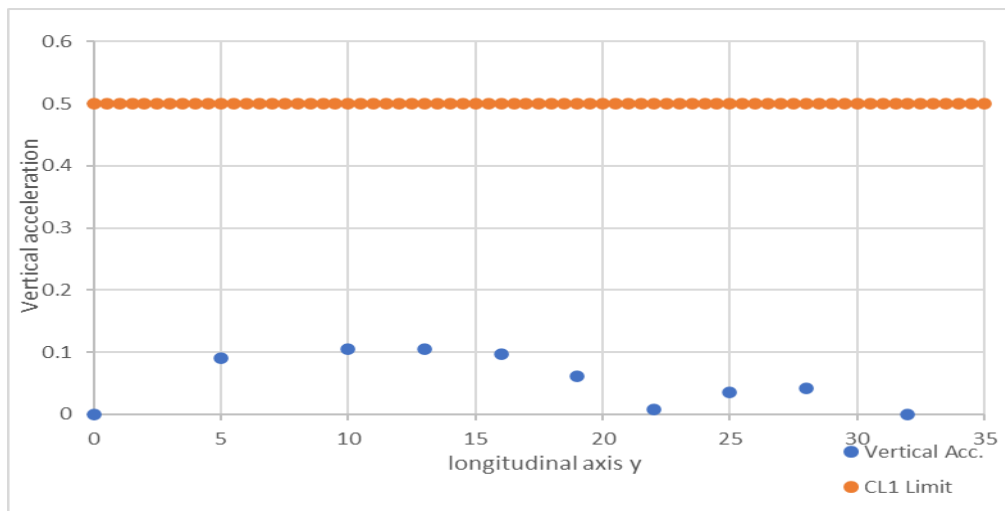


Figure 5.16: Vertical acceleration at selected nodes along the footbridge

5.6 Running Human's analysis: RealRun1

The Matlab code RealRun1 generates a text file that Ansys uses as input to carry out a transient analysis, as already mentioned in section 5.2. Every time a runner's foot makes contact with the footbridge, the pedestrian load must be updated because it changes over time. The frequency of contact between the runner's feet and the structure has been set to 2.3 Hz in order to compare findings acquired using RealRun1 and those achieved by adopting HiVoSS recommendations. In light of the discussion in Chapter 1, it is possible to relate the frequency of contact between the runner and the structure to a speed of the runner equal to 2.2 m/s. Since the length L of the footbridge deck is equal to 32 m, the time required to cross the bridge is 14.54 s. The pedestrian enters the footbridge from the left in Figure 5.11. Hence, his first contact point on the footbridge has the coordinates reported in Table 5.7.

Table 5.7: First contact point between the running pedestrian and the footbridge

X [m]	Y [m]	Z [m]
0	0.9	1.151

Contact point was chosen in in order to have almost the same position of the harmonic load used in the harmonic analysis once in the complete run. The pedestrian's trajectory is rectilinear and, for the entire time history, the coordinate x does not change. Depending on the preferred modelling approach between the two Setra models, the load time history can be selected. The Rayleigh damping model is described in the previous section; the damping coefficient ξ is equal to the one prescribed by Hivoss guidelines while α and β (coefficients of Rayleigh damping) are:

$$\alpha = 0.0425 \quad \beta = 0.0283 * 10^{-2}$$

Utilizing the Newmark's method of the constant average acceleration, the numerical integration of equations of motion has been carried out in Ansys. Table 5.8 lists the coefficients of the algorithm that must be entered into Ansys.

Table 5.8: Values of Newmark's parameters

Newmark's Parameter	Value
α	1/4
δ	1/2
γ	0

Parameters α and δ correspond to the constant average acceleration while γ ensures the unconditional stability of the numerical method. Ansys computes results of the transient analyses in terms of displacements, accelerations, velocities, stresses, strains, etc. as a function of time.

5.6.1 Transient analysis: Setra sinus model results

Plots and data on displacements and accelerations that were directly taken from Ansys over time interval of 24 s will be shown in this part (Table 5.9). These findings were obtained by utilizing the sinus load model that was previously published in section 5.3 of Setra and discussed there. Adopting the same step frequency, the pedestrian's duration on the footbridge ranges from 0 to 14.54 s while until 24 s, the footbridge is unloaded and in free vibration regime.

Table 5.9: Max displacement and acceleration at selected nodes

Points	Displ. [mm]	Acc. [m/s^2]
1	0	0
1bis	0.35	0.42
2	0.48	0.61
3	0.48	0.6
4	0.41	0.52
5	0.29	0.4
6	0.027	0.22
7	2.54e-02	0.5
8	8.5e-03	0.46
9	0	0

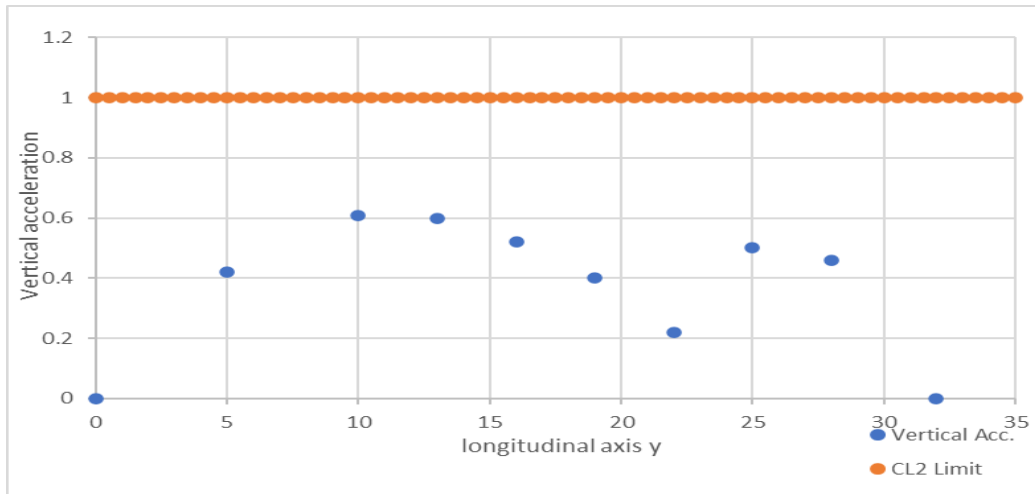


Figure 5.17: Vertical acceleration at selected nodes along the footbridge for transient analysis

The maximum value of the acceleration generated by one running pedestrian over the footbridge is 0.61 m/s^2 , above the threshold of comfort class 1 (0.5 m/s^2), but still guaranteeing a medium degree of comfort ($a_{max} < 1 \text{ m/s}^2$) (Figure 5.17). Figure 5.18, Figure 5.19, and Figure 5.20 left show how flexible the first part of the deck is; not only does it exhibit greater deflection than the last part (Table 5.9), but it also exhibits lower acceleration damping than the final three nodes (Figure 5.20 right and Figure 5.21), supporting the result obtained from the Hivoss Harmonic Result for walking pedestrian. These findings were in line with how the hanger spacing was planned and how the arches shaped along the footbridge, showing that the first section of the footbridge exhibits more flexible behaviour due to the predominate bending contribution than the last section, where the main contributions are provided by the axial stiffness of the arch.

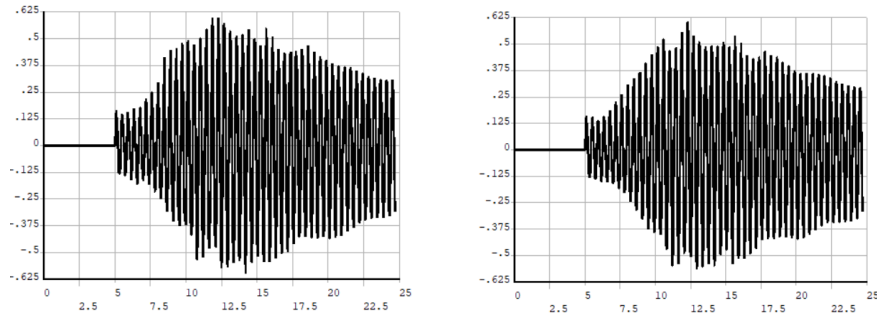


Figure 5.18: Vertical acceleration m/s^2 of node 1-bis (left) and of node 2 (right) during time 0-24s

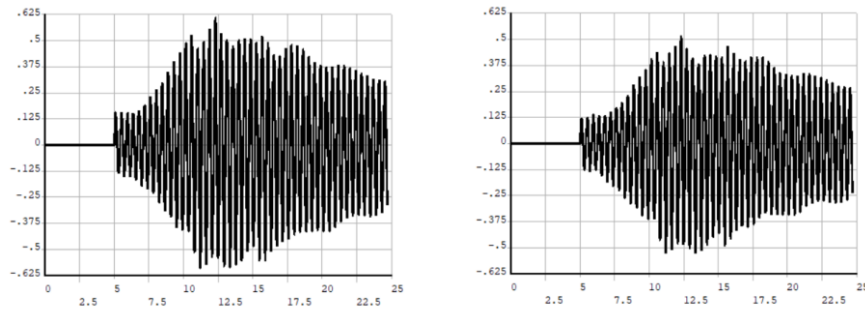


Figure 5.19: Vertical acceleration m/s^2 of node 3 (left) and 4 (right) during time 0-24s

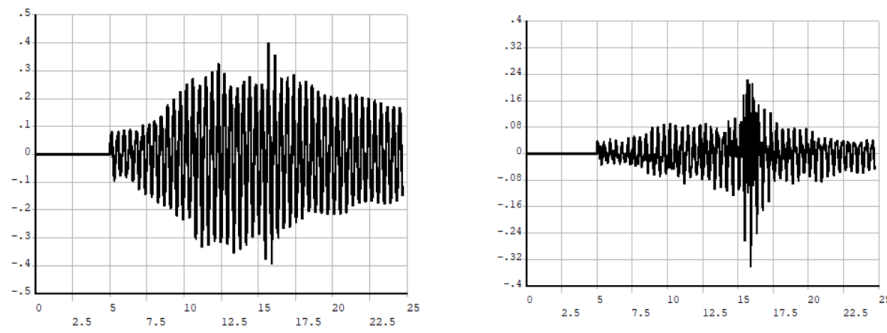


Figure 5.20: Vertical acceleration m/s^2 of node 5 (left) and 6 (right) during time 0-24s

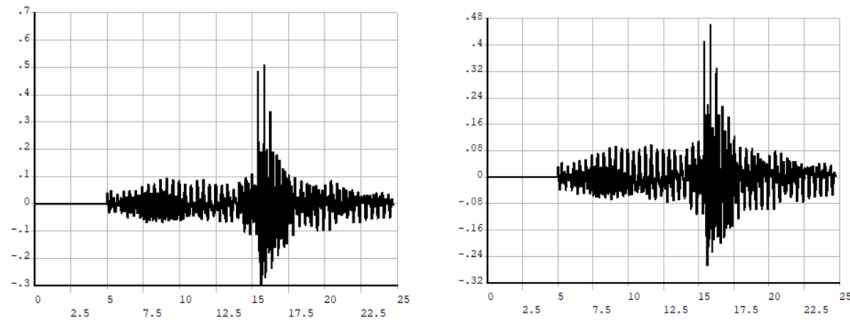


Figure 5.21: Vertical acceleration m/s^2 of node 7 (left) and 8 (right) during time 0-24s

5.6.2 Transient analysis: Setra Fourier model results

Plots and data on displacements and accelerations that were directly taken from Ansys (Table 5.10) over a time interval of 24 s will be shown in this part from the qualitative point of view the behaviour of nodes stays like the one presented above.

Table 5.10: Max displacement and acceleration on selected nodes

Points	Displ. [m]	Acc. [m/s^2]
1	0	0
1-bis	0.36	0.44
2	0.49	0.62
3	0.48	0.6
4	0.42	0.55
5	0.29	0.41
6	0.027	0.28
7	2.57e-02	0.5
8	8.9e-03	0.48
9	0	0

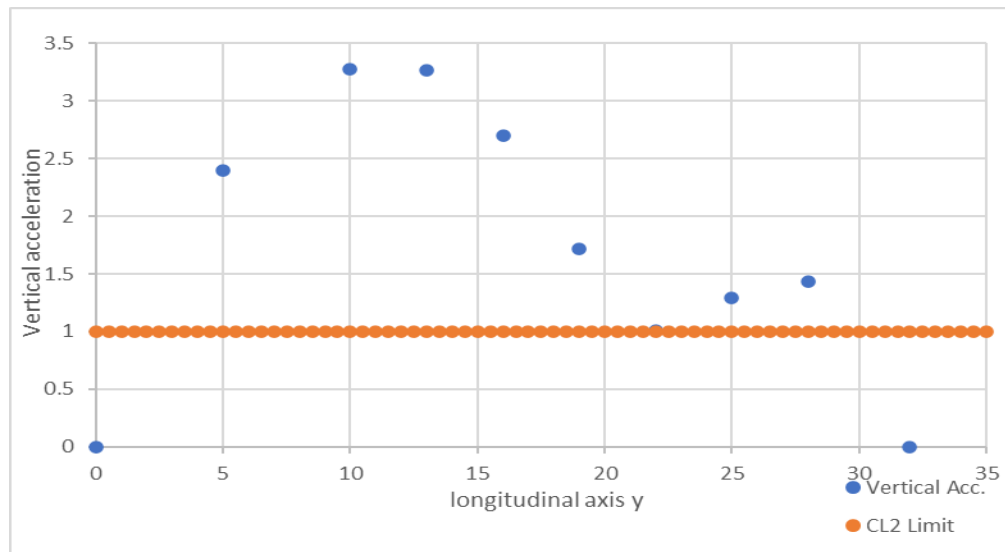


Figure 5.22: Vertical acceleration at selected nodes along the footbridge for transient analysis of 6 running pedestrians

The maximum value the acceleration generated by one running pedestrian over the footbridge is 0.62 m/s^2 on point 2, above the threshold for ensuring comfort class 1 (0.5 m/s^2), but still guarantying a medium degree of comfort ($a_{max} < 1 \text{ m/s}^2$). These results are similar to the one for the sinus model (Table 5.9). These outcomes resemble those of the sinus model (Table 5.7). Figure 5.23, Figure 5.24, and Figure 5.25 on the left illustrate the flexibility of the initial portion of the deck, which not only exhibits substantial deflection (Table 5.10) in comparison to the last part but also exhibits reduced acceleration damping than the last three nodes (Figure 5.25 right and Figure 5.26). These findings were coherent with both the hanger spacing and the different inclination of arches ends along the footbridge, showing that the first footbridge span is more flexible, due to the predominant bending contribution, than the last portion, where the main contributions are provided by the axial stiffness of the arch.

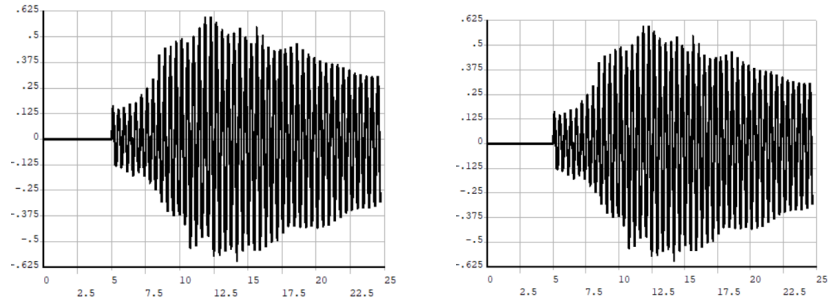


Figure 5.23: Vertical acceleration m/s^2 of node 1-bis (left) and 2 (right) during time 0-24s

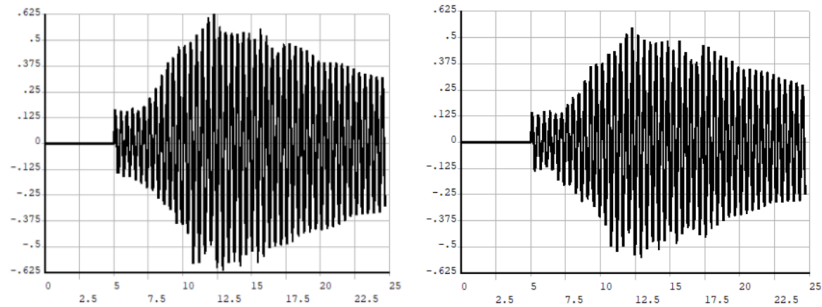


Figure 5.24: Vertical acceleration m/s^2 of node 3 (left) and 4 (right) during time 0-24s

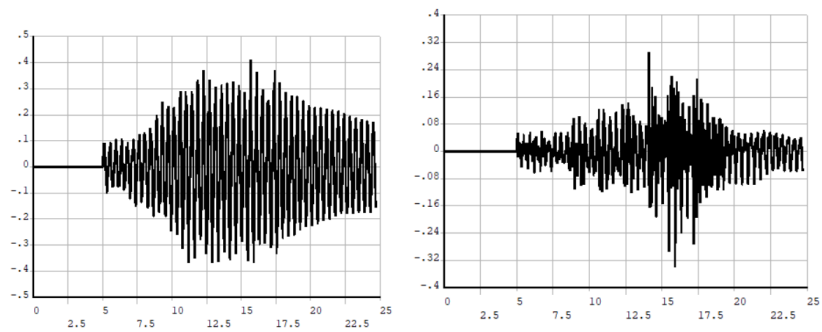


Figure 5.25: Vertical acceleration m/s^2 of node 5 (left) and 6 (right) during time 0-24s

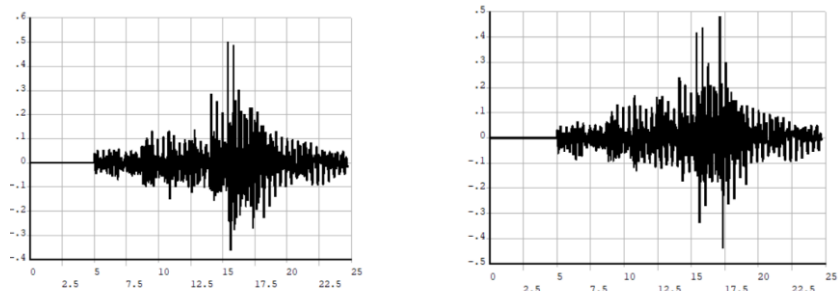


Figure 5.26: Vertical acceleration m/s^2 of node 7 (left) and 8 (right) during time 0-24s

5.6.3 Transient analysis: Sinus model results for 6 pedestrians

In this section, the numerical results in term of displacements and accelerations are presented for a group of 6 pedestrian with synchronized running (Table 5.11). The pedestrians are arranged in two lines of three people and the results are compared to the ones of the experimental campaign (Table 5.12) carried on by A. Banas [30] [5].

Table 5.11: Numerical values of vertical displacement and acceleration on selected points

Points	Displ. [m]	Acc. [m/s^2]
1	0	0
1-bis	0.04	2.4
2	0.097	3.28
3	0.094	3.27
4	0.082	2.7
5	0.054	1.72
6	0.016	1.006
7	0.008	1.29
8	0.0067	1.43
9	0	0

Table 5.12: Experimental extreme values of acceleration [m/s^2] for walking and running pedestrians [5]

N. of people	March	Run
6	0.93	0.45
9	1.84	0.68
12	1.19	0.70

The numerical maximum value of the acceleration generated by six synchronized running pedestrians over the footbridge is $3.28 m/s^2$, well above the threshold of medium comfort class ($a_{max} < 2.5 m/s^2$). In terms of acceleration, the transient

analysis of the FE model largely overestimates the experimental results. In the experimental campaign, pedestrians are not perfectly synchronized and, due to inter-variability, do not maintain the same velocity and step frequency of the ideal pedestrian used in the transient analysis. In addition, the frequency excitation used in on-site tests is not close to any of the bridge's natural vibrations. Even though it is not a perfect representation of the real case of running pedestrians, the transient analysis describes the structure's response at a frequency of excitation equal to the third modal shape of the structure ($f=2.3$ Hz), pointing out the amplification effect of runners perfectly synchronised. In the experimental results, increasing the number of pedestrians did not increase the acceleration level; instead, its reduction was seen, due to the effect of phase differences and lack of synchronization among runners. Conversely, in the transient analysis the reaction increases with an expanding group of synchronized pedestrians (Table 5.12).

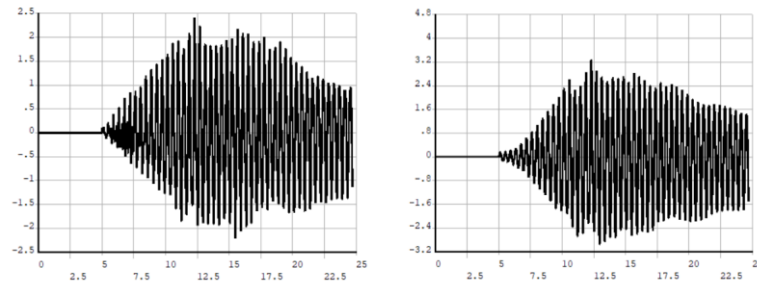


Figure 5.27: Vertical acceleration m/s^2 of node 1-bis (left) and 2 (right) during time 0-24s

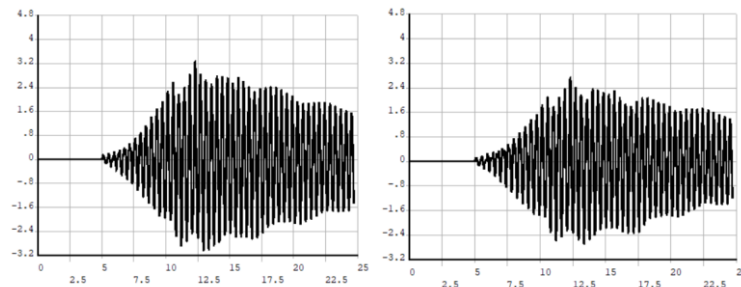


Figure 5.28: Vertical acceleration m/s^2 of node 3 (left) and 4 (right) during time 0-24s

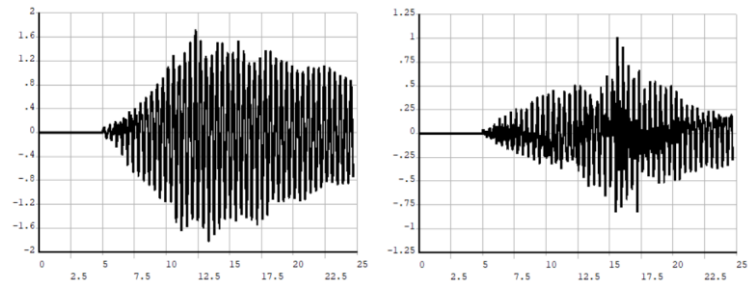


Figure 5.29: Vertical acceleration m/s^2 of node 5 (left) and 6 (right) during time 0-24s

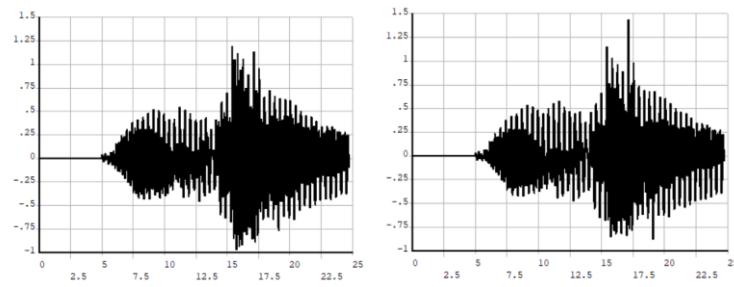


Figure 5.30: Vertical acceleration m/s^2 of node 7 (left) and 8 (right) during time 0-24s

6 CONCLUSIONS

The dynamic behaviour of a footbridge under the influence of running and walking pedestrians has been studied in this thesis. The arch-suspended footbridge (located in Bydgoszcz, Poland) is 32m long, with a not uniform spacing of the hangers, leaving a free span of 10m at one of the two sides and the highest point of the arches is 20 m from the deck level. Previous experimental tests were investigated, under different conditions, including human-induced load, impulse load, and excitations caused by a vibration exciter. The experimental campaign also identified modal properties.

A series of three FE models of the footbridge, produced within the framework of the ANSYS APDL code, have been developed in order to simulate the experimental outcomes with numerical analyses. The first FE model included a beam element for the deck, while the second model adopted shell elements to overcome the assumption of a rigid cross-section and to better model the connection between deck and hangers. With the exception of the third experimental modal shape, which exhibited a poor match and a significant error in terms of frequency, both models had similar modal shapes close to those found during the experimental campaign. Additionally, the models displayed stiffer behaviour in comparison to the actual footbridge, as shown by the fast-rising frequencies for higher modes. For these reasons, the third FE model includes the concrete blocks under the ends of the arches, thermal uniform load on the hangers to simulate the effects of pretension, and springs at the base of the concrete blocks to account for the interaction between the soil and the structure. This led to the

identification of the torsional mode that didn't have a properly match with the third experimental modal shape in the first two models. The identified natural frequencies of the third models have an error lower than 5% with respect to experimental values. The modal shapes correlation, in terms of MAC index, is highly satisfactory.

Based on the third FE model, validated against the experimental results, dynamic analyses under walking and running pedestrians have been carried out, according to Hivoss and Setra Guideline. The first analysis according to the Hivoss guideline was performed with weak traffic classes TC1(very weak) and TC2 (weak), considering a step frequency $f_s = 2.31$ Hz, equal to the first vertical natural frequency of the footbridge. The acceleration of all the selected points, corresponding to the one used in the experimental campaign, showed that the main critical part of the structure was the one related to the 10 m span. The accelerations of the nodes corresponding to the critical portion of the footbridge are slightly beyond the threshold of CL2 for the harmonic analysis of walking pedestrians, but are under the limit of CL1 for a single running pedestrian.

A more complete load model that takes into account the peaks of accelerations due to impulsive effects when the pedestrian hits the deck for the first time and consider more than one harmonic of the load. For this reason, a previously derived Matlab code, named RealRun1, has been adopted to compute the two mathematical models of the loads transmitted by a running pedestrian of Setra Guideline, the Setra sinus model and the Setra fourier model. RealRun1 produces a text file describing the time history of the force induced by a runner moving along a rectilinear trajectory, with imposed starting node (central node of the deck), velocity (2.2 m/s), step frequency (2.31 Hz equal to the modal shape frequency under consideration) and weight (81.5 kg that is the average weight of the pedestrian in the experimental analysis). The text file represents the input file for a transient analysis with Ansys.

The two transient analyses, one for each force model, validated the findings of the Hivoss technique on the fact that the 10 m span is the most critical portion of the structure. In this work, Realrun1 was improved to enable analysis of six pedestrians running simultaneously at the same speed. Similarly to the experimental tests, the

pedestrians were arranged in two rows of three. The footbridge accelerations were higher in the transient analysis than in the experimental data. The experimental campaign's pedestrians are not really synchronized and are unable to maintain the same velocity and step frequency of the pedestrian used in the transient analysis. In addition, the frequency excitation used in on-site tests was not close to any of the bridge's natural frequencies. The transient analysis shows that the acceleration increases as the number of synchronized pedestrians increases, while the experimental data show that a larger number of runners does not enhance the acceleration level but rather causes it to decrease. This is because it is difficult to synchronize several pedestrians.

The model updating and the numerical analyses showed that for structures where an experimental campaign is performed, an accurate model can be obtained and validated, allowing to perform numerical tests, that could partially substitute further experimental tests. This approach is less time consuming and efficient. In addition, the FE model can be used for studying a variety of solutions that can be applied in the real structure. It should be added that, once the footbridge has been constructed, it is recommended to conduct dynamic field tests, especially if the frequencies determined from the numerical model at the design stage are similar to the human-induced loading. The identified dynamic parameters can be further used to update the numerical model. Then, the updated numerical model can be employed to carry out the extensive numerical analyses focused on the response of structures under different dynamic loads, including wind and earthquakes.

BIBLIOGRAPHY

- [1] P. Dallard, A. J. Fitzpatrick, A. Flint, S. Le Bourva, A. Low, R.M. Ridsdill-Smith, M. Willford, “The London Millennium Footbridge,” *The Structural Engineer* 79, no. 22, pp. 17-33, 2001.
- [2] M. Mimram, “Passerelle Solférino Paris,” 2001.
- [3] T. P. Andriacchi, J. A. Ogle, J.O. Galante, “Walking speed as basis for normal and abnormal gait measurements,” *Journal of Biomechanics* 10, pp. 261-268, 1977.
- [4] T. S. Keller, A. M. Weisberger, J. L. Ray, S. S. Hasan, R. G. Shiavi, D. M. Spengler, “Relationship between vertical ground reaction force and speed during walking,slow jogging and running,” *Clinicla Biomechanics* 11, pp. 253-259, 1996.
- [5] Anna Banas and Robert Jankowski, “Experimental and Numerical Study on Dynamics of Two Footbridges with Different Shapes of Girders,” *applied sciences*, 29 June 2020.

- [6] HiVoSS (Human induced Vibrations of Steel Structures), Design of Footbridges – Guideline, 2008.
- [7] SETRA, Technical guide, Footbridges, Assessment of vibrational behaviour of footbridges under pedestrian loading; Ministère des Transports, de l'Équipement, du Tourisme et de la Mer, République Française, October 2006.
- [8] ISO, “Bases for Design of Structures-Serviceability of Buildings Against vibrations,” International Standardization Organization, Geneva, Switzerland, 1992.
- [9] N. Messenger, “Moving the human machine: understanding the mechanical characteristics of normal human walking,” *Physics Education* 29, pp. 352-357, 1994.
- [10] E. Ayyappa, “Words about words: the terminology of human walking,” *Monograph of the American Academy of Orthotists and Prosthetists Gait Society*, Vols. 1-2, 1994.
- [11] J. Perry, “Gait Analysis: Normal and Pathological Function,” *Thorofare*, 1992.
- [12] V. T. Inman, H. J. Ralston, F. Todd, “Human walking, Williams & Wilkins,” 1981.
- [13] J. Perry, “Gait Analysis: Normal and Pathological Function,” *Thorofare*, 1992.
- [14] C. L. Vaughan, B. L. Davis, J. C. O’ Connor, “Dynamics of Human Gait,” *Kiboho Publishers*, 1999.

- [15] V. Racic, A. Pavic, J. M. W. Brownjohn,, “Experimental identification and analytical modelling of human walking forces: Literature review,” *Journal of Sound and Vibration*, no. 326, pp. 253-259, 2009.
- [16] F. W. Galbraith, M. V. Barton, “Ground loading from footsteps,” *Journal of the Acoustic Society of America*, pp. 1288-1292, 1970.
- [17] S. Zivanovic, A. Pavic and P.Reynold, “Vibration serviceability of footbridges under human-induced excitation: A literature review,” *Journal of sound and vibration* , vol. 279, no. 1-2, pp. 1-74, 2005.
- [18] J. M. W. Brownjohn, A. Pavic, P. Omenzetter, “A spectral density approach for modelling continuous vertical forces on pedestrian structures due to walking,” *Canadian Journal of Civil Engineering* 31, pp. 65-77, 2004.
- [19] P. E. Eriksson, “Vibration of Low-Frequency Floors- Dynamic Forces and Response Prediction, PhD Thesis,” *Unit for Dynamics in Design*, 1994.
- [20] R. W. Clough, J. Penzien, “Dynamics of Structures,” *McGraw-Hill*, 1993.
- [21] E. Lai, M.G. Mulas, “Uncoupled approaches for walking-induced vertical vibration of a lively footbridge,” *Insights and Innovation in Structural Engineering*, 2016.
- [22] P. Dallard, T. Fitzpatrick, A. L. A. Flint, R. Ridsdill-Smith, M. Willford and M. Roche, “pedestrian-induced lateral vibration,” *Journal of Bridge Engineering*, vol. 6, no. 6, pp. 412-417, 2001.
- [23] H. K. M. S. H. Grundmann, “Dynamic calculations of footbridges,” *Bauingenieur* 68, pp. 215-225, 1993.

- [24] A. McRobie, G. Morgenthal, «Risk management-induced dynamics of footbridges,» *Proceedings of the International Conference on the Design and Dynamic Behaviour of Footbridges*, 20-22 November 2002.
- [25] P. Dallard, T. Fitzpatrick, A. Flint, A. Low, R. Ridsdill-Smith, “Problems and solutions,” *The Structural Engineer*, vol. 79, no. 8, pp. 15-17, 2001.
- [26] T. Fitzpatrick, P. Dallard, S. Le Bourva, A. Low, R. Ridsdill-Smith, M. Willford, “The Millennium Bridge,” The Royal Academy of Engineering, London, June 2001.
- [27] T. Fitzpatrick, R. R. Ridsdill-Smith, “Stabilising the London Millennium Bridge,” *Ingenia*, June 2001.
- [28] E. T. Ingólfsson, C. T. Georgakis, J. Jönsson, “Pedestrian-induced lateral vibrations: A literature review,” *Engineering Structures* 45, 2012.
- [29] C. Cremona, “Dynamic investigations of the Solferino footbridge,” *Proceedings of IOMAC '09, 3rd International Operational Modal Analysis Conference*, Portonovo, Italy, 4th-6th May 2009.
- [30] A. Banas, Private communications via e-mail, May-September 2022.
- [31] Heylen, W.; Lammens, S.; Sas, P., “Modal Analysis Theory and Testing,” Leuven, Belgium, 2007.
- [32] T. Rossing and N. Fletcher, “Principles of Vibration and Sound,” New York, NY, USA, 2004.
- [33] De Silva, C.W., “Vibration and Shock Handbook,” Taylor & Francis Inc., Boca Roca, USA, 2005.

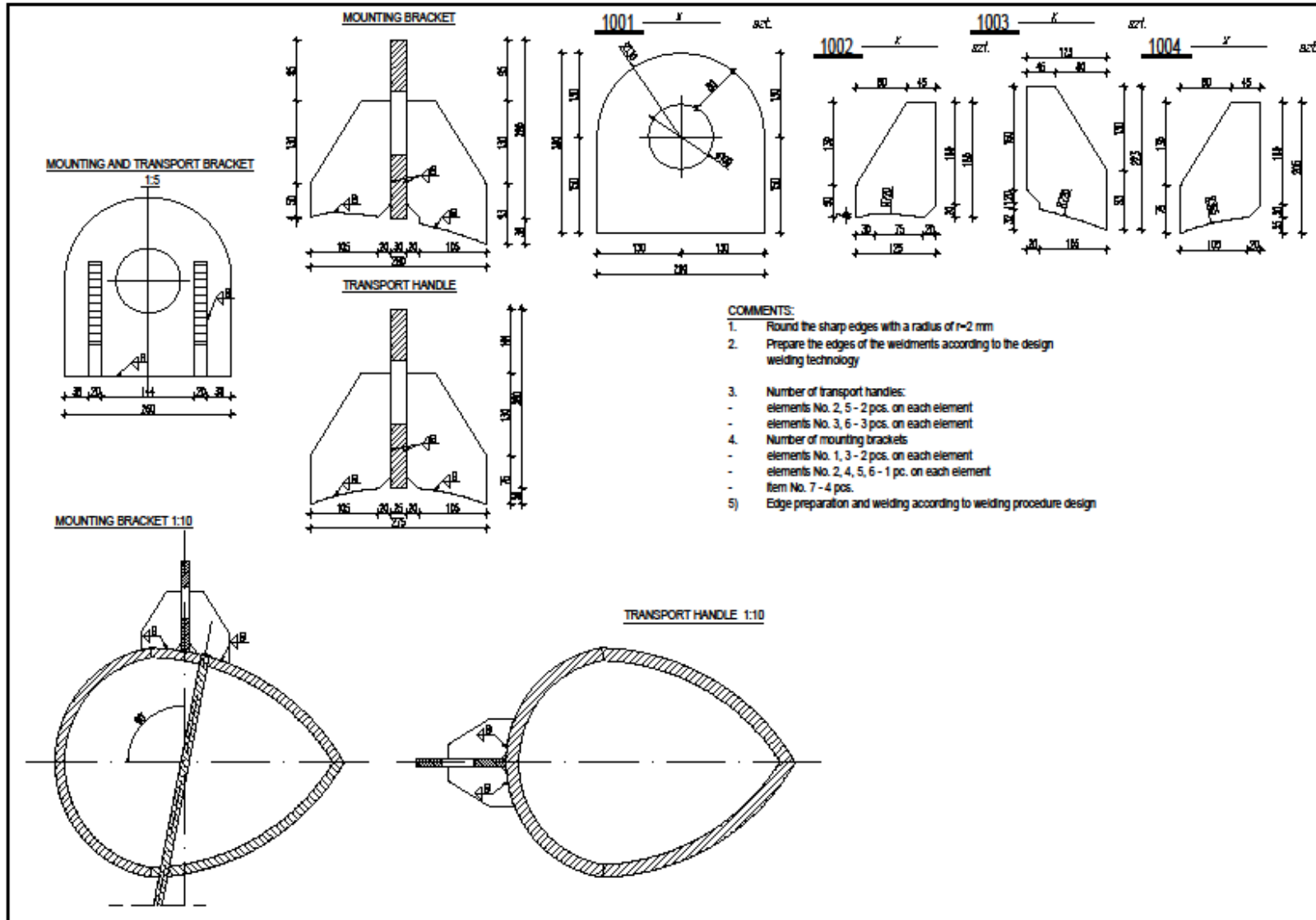
- [34] Clough, R.W.; Penzien, J., Dynamics of Structures, NJ, USA: Pearson Education: Upper Saddle River, 1975.
- [35] Bianchi, G.; Sorrentino, R., Electronic Filter Simulation & Design, NY, USA: McGraw-Hill Education: New York, 2007.
- [36] ANSYS, “Inc., ANSYS Mechanical APDL Element References Release 15.0,” November 2013.
- [37] A. M. A. Documentation, “Theory Reference , Chapter 15, Analysis Procedure, Release 17.1”.
- [38] P.J. Moore, Analysis and Design of foundations for vibrations, Boston: University of Melbourne, 1985, pp. 309-341.
- [39] Pisani M., Dynamic analysis of a steel footbridge under running pedestrian, Milano, 2017.
- [40] V. Racic, A. Pavic, J. M. W. Brownjohn, Experimental identification and analytical modelling of human walking forces: Literature review, Journal of Sound and Vibration 326, 2009, pp. 1-49.
- [41] T. S. Keller, A. M. Weisberger, J. L. Ray, S. S. Hasan, R. G. Shiavi, D. M. Spengler, Relationship between vertical ground reaction force and speed during walking, slow jogging and running, Clinica Biomechanics 11, 1996, pp. 253-259.
- [42] S. Živanović, A. Pavic, P. Reynolds, “Vibration serviceability of footbridges under human-induced excitation: a literature review,” *Journal of Sound and Vibration*, pp. 1-74, 2005.

- [43] V. Racic, J.B. Morin, Data-driven modelling of vertical dynamic excitation of bridges induced by people running, 2014: Mechanical Systems and Signal Processing 43.

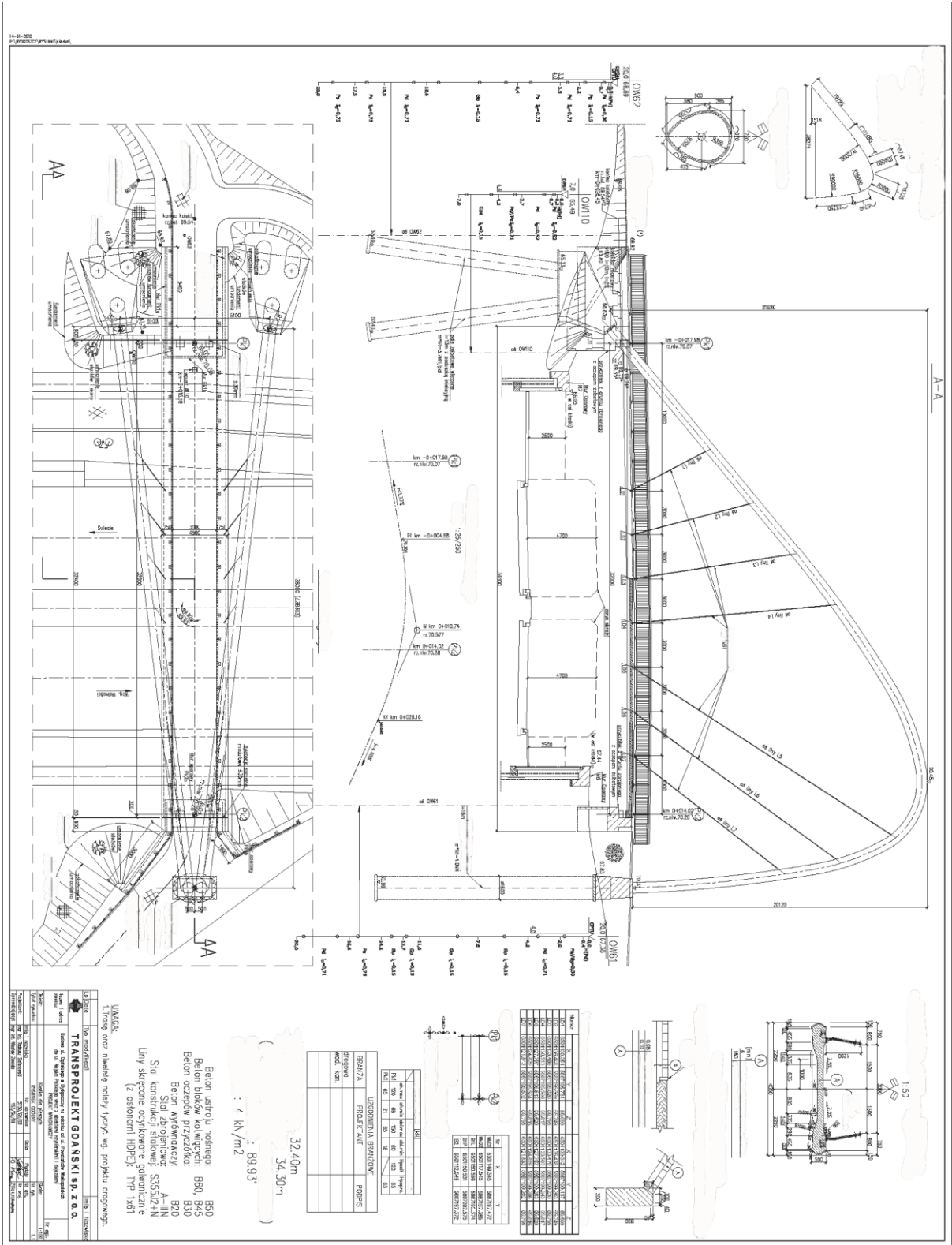
APPENDIX A

Appendix A contains some structural details of the studied structure. The reported drawing is subdivided in four windows. Window A contains the arches details in term of sections and materials. Window B shows the link between the arc and the rods. Window C shows the link between the link the deck and the rods. Window D shows the general details of the structure and the soil indexes -

NUMERICAL MODELLING VS ON-SITE TESTING OF AN ARCH-SUSPENDED FOOTBRIDGE



NUMERICAL MODELLING VS ON-SITE TESTING OF AN ARCH-SUSPENDED FOOTBRIDGE



APPENDIX B

As described in paragraph 3.1, Ansys Mechanical APDL was adopted to model the footbridge. In this section, the model derivation from the practical point of view is presented. As already stated, the use of APDL involves the need to generate the model and perform the analyses through a code written in text file format and following the rules of the Ansys parametric language. Some code examples of this language are presented in the following. The first part of every Ansys code must be the so-called Pre-Processor phase. The Pre-Processor is the phase in which the user sets in place material properties, constitutive laws, geometry of the structure, loads and boundary conditions. In Ansys, meshing is inside the Pre-Processor and do not need a separated phase. If loads and boundary conditions are not defined in the Pre-Processor phase, they can be defined in the Solution part of the code. This phase is the one in which the user defines all the rules to run the analysis and the possible initial conditions. Different options can be chosen static, modal, harmonic, transient, spectrum or buckling analysis. For all of them other options can be selected concerning, for instance, computation method, number of iterations and so on. All the results can be visualized trough the last part of the code, called General Post-Processing Phase. To plot and list results for element or nodal solutions, commands are available too. Anyway, visualization of results is easier if done through the GUI and, for this reason, the /POST1 command (necessary to enter this phase using the parametric language) was not inserted in the case at study.

Sample of one Ansys Input file

```

/PREP7                                ! Enter the Preprocessor
ET,1,BEAM188,,1,3,2,,,
                                        ! KEYOPT(2)=1=Section is assumed to
                                        !be rigid (classical beam theory)
                                        ! KEYOPT(3)=3=shape functions: CUBICHE
                                        ! KEYOPT(4)=2=shear stress output=torsion
                                        ! and flexure related

ET,2,LINK180,,1,,,,
to be rigid                            ! KEYOPT(2)=1=Section is assumed

ET,3,MASS21,1,,2
                                        ! KEYOPT(1)=1=Interpret real constants as
                                        !volumes and rotary inertias/density
                                        !(Density must be input as a material property)
                                        ! KEYOPT(3)=2=3-D mass without rotary inertia

!! ----- Definition of real constant SETS ----- !!

R,2,0.02016                            ! Volume of lumped masses on longitudinal
                                        !edge of the footbridge
R,3,0.004473                            ! Volume of lumped masses on transversal
                                        !edge of the footbridge (V1=V6)
R,4,0.008946                            ! Volume of lumped masses on transversal
edge of the footbridge (V2=V3=V4=V5)
R,7,0.014553                            ! Volume of lumped masses on transversal
                                        ! edge of the footbridge (V7=V12)

...
...
...
SECTYPE,1,BEAM,HREC,LATBEAM,0          !Definition of deck's lateral beam
                                        !section

SECDATA,0.15,0.20,0.01,0.01,0.01,0.01
SECOFFSET,CENT                          !Beam origin will be offset to the
                                        !section CENTER OF GRAVITY

```

```
...
...
...
!! Definition of tapered sections for archs elements !!
...
...
...
SECTYPE,17,BEAM,L
SECDATA,0.3,0.55,0.02,0.02
SECOFFSET,USER,0.09,0.01

SECTYPE,18,BEAM,L
SECDATA,0.307,0.537,0.02,0.02
SECOFFSET,USER,0.09,0.01

SECTYPE,170,TAPER
SECDATA,17,2.68071,4.654,-2.23
SECDATA,18,2.78021,5.176,-1.851
...
...
...
!!Definition of cable elements !!

SECTYPE,41,LINK
SECDATA,0.000490625                                !Section of cables linking deck and
                                                    !archs, D=0.025 m
SECCONTROL,0,1                                    !KEYOPT(0)=0=value of added
                                                    !mass per unit length
                                                    !KEYOPT(1)=1=tension only behaviour

...
...
...
!!!Definition of Steel (isotropic)!!!

MP,DENS,1,8000                                     !Density [kg/m^3]
MP,EX,1,210000000000                               !Young's modulus [KN/m^2]
MP,NUXY,1,0.3
```

E,43,49

E,49,55

E,55,61

...

...

...

!! -- Definition of mass elements to take into account wood deck covering -- !!

TYPE,3

MAT,7

!! Masses for equal inter-axes between transversal beams!!

!! Edge masses!!

REAL,2

E,13

E,19

E,25

...

...

...

!Definition of supports at beam ends

D,2,UZ,0,,,,UX,UY,,ROTY,ROTZ,

D,3,UZ,0,,,,UX,UY,,ROTY,ROTZ,

D,4,UZ,0,,,,UX,UY,,ROTY,ROTZ,

...

...

...

!Definition of constraints between arches and deck!

CP,1,UX,241,2000

CP,2,UY,241,2000

CP,3,UZ,241,2000

...

...

...

!!!!BEGIN SOLUTION!!!!

```

/SOLU
!Non linear Static Analysis!

ANTYPE,STATIC
nlgeom,on                !large displacement on!
pstres,on                !include prestress effect!
nropt,full
OUTRES,ALL,ALL
solcontrol,on,on
KBC,o                    !KBC,o=Loads are linearly
                        !interpolated (ramped) !

ematwrite,yes
!----- load steps non linear analysis -----

!----- load step 1 -----
g=9.81                    !Definition of gravity acceleration!
ACEL,,g                  !ACEL generate, in absence of other
                        !loads, g positive in opposite to positive
                        ! direction of Z.!
                        !So it is not correct to write -g !

!!Definition of Pretension!!

INISTATE,SET,MAT,2
INISTATE,DEFINE,,,,,305580000

INISTATE,SET,MAT,3
INISTATE,DEFINE,,,,,295080000

INISTATE,SET,MAT,4
INISTATE,DEFINE,,,,,284580000

INISTATE,SET,MAT,5
INISTATE,DEFINE,,,,,298580000

INISTATE,SET,MAT,6
INISTATE,DEFINE,,,,,292580000

TIME,10                    ! we need to give a value of time at each

```



```
DELTIM,1,0.001,1
```

```
ematwrite,yes
```

```
solve
```

```
!----- load step 2 -----
```

```
...
```

```
...
```

```
...
```

```
!----- load step 3 -----
```

```
...
```

```
...
```

```
...
```

```
!----- modal analysis
```

```
/solu
```

```
antype,modal
```

```
ematwrite,yes
```

```
upcoord,1,0,on
```

```
pstres,on
```

```
modopt,lanb,100,0.1,10
```

```
mexpand,,0.1,10
```

```
psolve,eiglanb
```

```
finish
```

```
/solu
```

```
upcoord,1,0,on
```

```
expass,on
```

```
psolve,eigexp
```

```
finish
```

```
save
```

```
finish
```

!load step (two load step cannot have

! the same value of time)!

! It is the duration of a substep. With

! this value of time, we will have at

!least 10 substeps!

